

Powderhorn Ranch Geoenvironmental Atlas

Jeffrey G. Paine, Edward W. Collins,
Tiffany L. Caudle, and Lucie Costard

Bureau of Economic Geology

Scott W. Tinker, Director
Jackson School of Geosciences
The University of Texas at Austin
Austin, Texas 78713-892



BUREAU OF
ECONOMIC
GEOLOGY



December 2018

A Report Partly Funded by a
Texas Coastal Management Program
Grant Approved by the Texas Land
Commissioner Pursuant to National
Oceanic and Atmospheric Administration
Award No. NA16NOS4190174.

Final Report Prepared for the
General Land Office under
Contract No. 17-186-000-9823.

QAe8581

Page intentionally blank

Powderhorn Ranch Geoenvironmental Atlas

by

Jeffrey G. Paine, Edward W. Collins, Tiffany L. Caudle, and Lucie Costard

Bureau of Economic Geology
John A. and Katherine G. Jackson School of Geosciences
The University of Texas at Austin
University Station, Box X
Austin, Texas 78713

Corresponding author
jeff.paine@beg.utexas.edu
(512) 471-1260
TBPG License No. 3776

A Report Partly Funded by a Texas Coastal Management Program Grant Approved by the Texas Land Commissioner Pursuant to National Oceanic and Atmospheric Administration Award No. NA16NOS4190174

Report Prepared for the General Land Office under Contract No. 17-186-000-9823

December 2018



Page intentionally blank

Contents

Overview	1
Topography and 2016 Airborne Lidar Survey	4
Water Wells and Windmills	6
Geology and Geophysics	8
Shoreline Types, Retreat Vulnerability, and Historical Movement	18
Sandy Slopes	23
Spits	23
Bay-margin Marshes or Tidal Flats	23
Historical Shoreline Movement	25
Hurricanes and Tropical Storms	27
Wetlands Status and Trends	32
Status of Wetlands and Aquatic Habitats, 2008	34
Historical Trends in Wetland and Aquatic Habitats	37
Acknowledgments	41
References	41
Appendix A: Water Wells, Windmills, and Geophysical logs	44
Appendix B: Time-domain Electromagnetic Induction Soundings	64

Tables

1. Wetland codes and descriptions	34
2. Water-regime symbols and descriptions	35
3. Areal extent of mapped wetland and aquatic habitats, 2008.	37
4. Total area of major habitats, including uplands, in 1956, 1979, and 2008.	40

Figures

1. Map of the Matagorda Bay system showing the location of Powderhorn Ranch	1
2. Map of Powderhorn Ranch	2
3. TPWD announcement of the acquisition of Powderhorn Ranch	3
4. BEG's Chiroptera lidar system used for the Powderhorn Ranch topographic survey	4
5. High-resolution digital elevation model (DEM) of Powderhorn Ranch	5
6. Location of water wells and windmills on Powderhorn Ranch	6
7. Windmill at Powderhorn Ranch used for livestock	7
8. Measuring water depth in a water well before geophysical logging.	7
9. Quaternary geologic units of the Texas Coastal Plain	8
10. Pimple mounds on sandy Ingleside barrier system deposits on Powderhorn Ranch	9
11. Geologic map of Powderhorn Ranch	10
12. Exposure of Pleistocene Ingleside barrier system sand and mud with soil features	11
13. Location of logged wells and TDEM soundings on Powderhorn Ranch	12
14. Geophysical logging at water well PH19 along Powderhorn Lake	13
15. Equipment laid out for TDEM sounding POC-02	13
16. Gamma activity log for well PH05 and its geologic interpretation	14
17. Well log cross section oriented southwest to northeast across Powderhorn Ranch	15
18. Subsurface electrical conductivity model constructed from TDEM sounding POC-04.	16
19. Thickness of the Ingleside barrier system sand	17
20. Distribution of principal shoreline types in the Copano, San Antonio, and Matagorda Bay systems	18
21. Shoreline types on Powderhorn Ranch along Matagorda Bay and Powderhorn Lake	19
22. Shoreline susceptibility to non-storm wave activity.	20
23. Shoreline susceptibility to storm surge and storm waves	21
24. Shoreline susceptibility to relative sea-level rise	22
25. Bulkhead and riprap along the Matagorda Bay shoreline at the ranch house	23
26. Sandy slope with a narrow, sandy beach along the Matagorda Bay shoreline	24
27. Sandy and shelly spit along the Matagorda Bay shoreline.	24
28. Bay-margin marsh and tidal flat along the Powderhorn Lake shoreline	25

29. Net shoreline movement rates between the 1930s and 2015	27
30. Estimated inundation areas and depths from storm surge during Hurricane Carla.....	29
31. Estimated inundation areas and depths from storm surge during Hurricane Beulah.....	30
32. Hurricane Harvey (2017) debris line along Matagorda Bay	31
33. Hurricane Harvey debris line along Matagorda Bay	31
34. Hurricane Harvey washover deposits on a bay-margin marsh along Matagorda Bay	32
35. Hurricane Harvey debris and Harvey-related erosion above riprap.....	32
36. Areal distribution of major habitats on Powderhorn Ranch in 2008.....	36
37. Areal extent of selected habitats in the Powderhorn Ranch area in 2008.....	37
38. Maps showing distribution of major wetland and aquatic habitats in 2008, 1979, and 1956 in the Powderhorn Ranch area	39
39. Areal distribution of habitats in Powderhorn Ranch in 1956, 1979, and 2008.....	40
40. Areal distribution of emergent marsh habitats in Powderhorn Ranch in 1956, 1979, and 2008	41
A1. Natural gamma and apparent conductivity logs from water well PH01	46
A2. Natural gamma and apparent conductivity logs from water well PH02	47
A3. Natural gamma and apparent conductivity logs from water well PH03	48
A4. Natural gamma and apparent conductivity logs from water well PH04	49
A5. Natural gamma and apparent conductivity logs from water well PH05	50
A6. Natural gamma and apparent conductivity logs from water well PH06	51
A7. Natural gamma and apparent conductivity logs from water well PH07	52
A8. Natural gamma and apparent conductivity logs from water well PH08	53
A9. Natural gamma and apparent conductivity logs from water well PH09	54
A10. Natural gamma and apparent conductivity logs from water well PH10	55
A11. Natural gamma and apparent conductivity logs from water well PH11	56
A12. Natural gamma and apparent conductivity logs from water well PH12	57
A13. Natural gamma and apparent conductivity logs from water well PH13	58
A14. Natural gamma and apparent conductivity logs from water well PH14	59
A15. Natural gamma and apparent conductivity logs from water well PH15	60
A16. Natural gamma and apparent conductivity logs from water well PH16	61

A17. Natural gamma and apparent conductivity logs from water well PH17 62

A18. Natural gamma and apparent conductivity logs from water well PH18 63

A19. Natural gamma and apparent conductivity logs from water well PH19 64

B1. Subsurface electrical conductivity model constructed from TDEM sounding POC-01..... 66

B2. Subsurface electrical conductivity model constructed from TDEM sounding POC-02..... 67

B3. Subsurface electrical conductivity model constructed from TDEM sounding POC-03..... 68

B4. Subsurface electrical conductivity model constructed from TDEM sounding POC-04..... 69

B5. Subsurface electrical conductivity model constructed from TDEM sounding POC-05..... 70

B6. Subsurface electrical conductivity model constructed from TDEM sounding POC-06.....71

B7. Subsurface electrical conductivity model constructed from TDEM sounding POC-07..... 72

B8. Subsurface electrical conductivity model constructed from TDEM sounding SNE-03..... 73

Overview

Powderhorn Ranch, located along Matagorda Bay and Powderhorn Lake in Calhoun County, Texas, is a 7,022 ha property that has been purchased for the state of Texas through a partnership among the Texas Parks and Wildlife Foundation, The Nature Conservancy (TNC), Texas Parks and Wildlife Department (TPWD), and The Conservation Fund (figs. 1, 2, and 3). The environmental and conservation significance of Powderhorn Ranch is immense. It is one of the largest remaining tracts of native coastal prairie and is destined to become a state park and wildlife management area. It encompasses diverse coastal environments that include 18 km of bay frontage, tallgrass prairies, fresh and saltwater wetlands, and live oak woodlands established on a Pleistocene barrier island complex (the Ingleside barrier system). According to TNC, the ranch offers year-round habitat for shorebirds, wading birds, and waterfowl and critical fall-out areas for migrating birds. This geoenvironmental atlas compiles diverse geologic, topographic, hydrologic, geophysical, and biological data sets and serves as a foundation providing planners, managers, conservationists, and visitors information on the geologic, geomorphic, coastal habitat, and coastal hazard (susceptibility to waves, storms, and relative sea-level rise) characteristics of Powderhorn Ranch.

Data compiled for this atlas include high-resolution topography from an airborne lidar survey of the ranch conducted in July 2016, 7.5-minute quadrangle-scale geologic mapping from 2015 through 2018, wetland status and trends mapping based on aerial photographs from 1956 to 2008, historical shoreline movement from the 1930s through 2015, interpretations of shoreline susceptibility to wave action, storm surge, and relative sea-level rise, inundation depths observed during historic hurricanes Carla (1961) and Beulah (1967), and near-

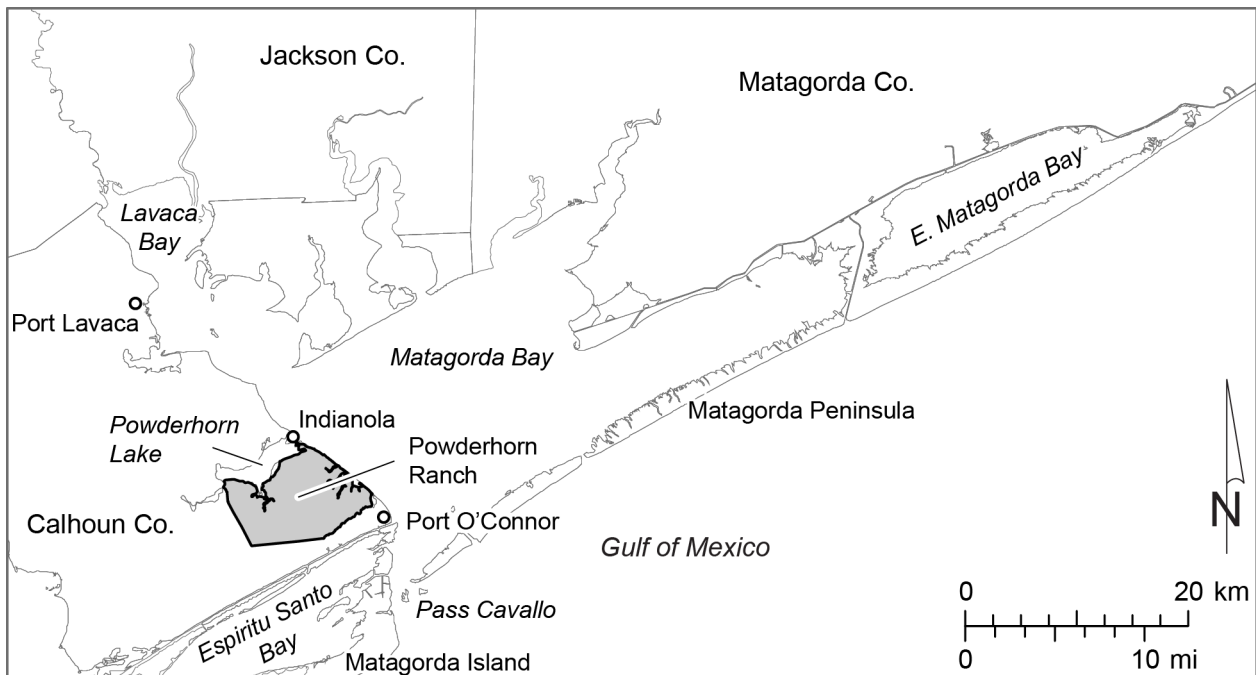


Figure 1. Map of the Matagorda Bay system showing the location of Powderhorn Ranch, a 7,022 ha parcel acquired for the State of Texas in 2014 by a coalition led by the Texas Parks and Wildlife Foundation.

surface geophysical measurements that included logs of 19 water wells and 8 time-domain electromagnetic induction soundings on or adjacent to the ranch. The purpose of this atlas is to convey the current knowledge of the surface and near-surface environment at Powderhorn Ranch to the public so that the best and most complete data can be used to influence development and management decisions that will ensure responsible stewardship and future use of the ranch.

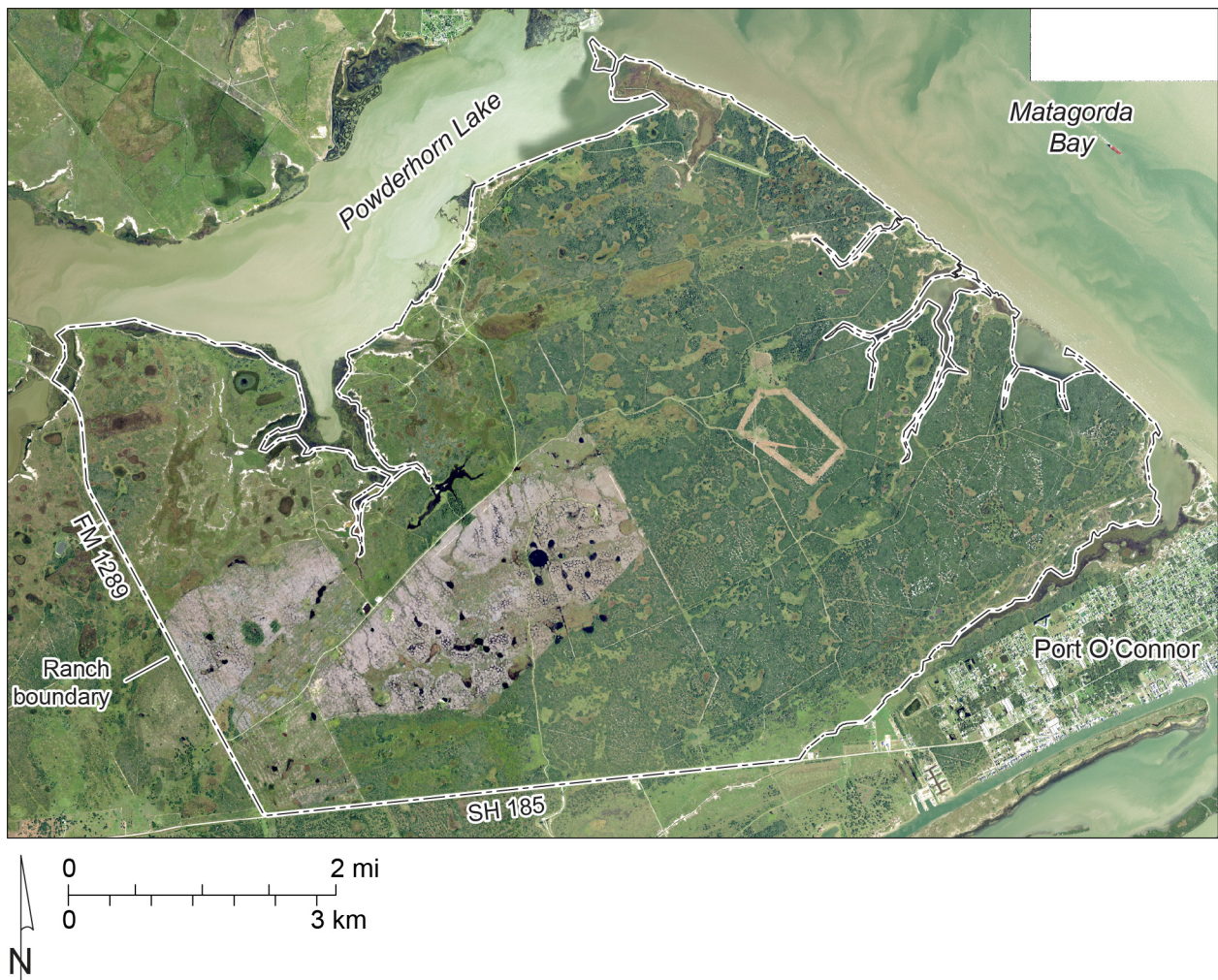


Figure 2. Map of Powderhorn Ranch, Powderhorn Lake, Matagorda Bay, and Port O'Connor, Calhoun County, Texas. Aerial imagery is from the 2016 National Agriculture Imagery Program obtained through the Texas Natural Resources Information System.

Powderhorn Ranch Becomes Largest Conservation Investment in Texas History

Donations used for Landmark \$37.7 Million Acquisition

HOUSTON — A multi-partner coalition including the Texas Parks and Wildlife (TPW) Foundation today announced the purchase of the 17,351-acre Powderhorn Ranch along the Texas coast in Calhoun County. The acquisition will conserve a spectacular piece of property that is one of the largest remaining tracts of unspoiled coastal prairie in the state. At \$37.7 million it is the largest dollar amount ever raised for a conservation land purchase in the state and represents a new partnership model of achieving conservation goals in an era of rapidly rising land prices. In years to come, Powderhorn Ranch is expected to become a state park and wildlife management area.

Figure 3. Texas Parks and Wildlife Department (TPWD) announcement of the acquisition of Powderhorn Ranch, August 2014.

Topography and 2016 Airborne Lidar Survey

Powderhorn Ranch is a low-relief area typical of the Texas coastal plain. Standard topographic maps show elevations at 5-ft intervals, which is insufficiently detailed to accurately map surficial geologic units, delineate wetlands, and forecast inundation areas and depths related to elevated bay and Gulf of Mexico water levels caused by frequent tropical cyclones.

For this atlas, Bureau of Economic Geology (BEG) researchers acquired lidar data along the western shore of Matagorda Bay July 5-8, 2016. Data were collected using the Chiroptera airborne system (fig. 4) from Airborne Hydrography AB. The topographic lidar scanner operates at a wavelength of 1 μm , a pulse rate as high as 400 kHz, and an incident angle (from vertical) of 28 to 40 degrees. It can operate to a maximum height of about 1,500 m, allowing the system to rapidly scan large areas with a range accuracy of about 2 cm over a flat target. GPS data from base stations at the Calhoun County Airport near Port Lavaca and at Powderhorn Ranch were used to improve positioning accuracy. Flight elevation was between 450 to 580 m for all flights and laser pulse rate was 240 kHz, providing sufficient point density to allow creation of a high-resolution digital elevation model (DEM) with a 1-m grid cell size (fig. 5). These data were used to establish ground elevations for water wells and associated geophysical logs, geophysical soundings, and wetland and upland habitat, to identify surficial geologic units and delineate their boundaries, and to estimate water inundation areas and depths for historic hurricanes Carla and Beulah. These data can be



Figure 4. BEG's Chiroptera lidar system used for the Powderhorn Ranch topographic survey.

used to model inundation areas and depths for future storms with arbitrary storm-surge heights.

Topographically, Powderhorn Ranch consists of a series of generally coast-parallel ridges oriented ENE-WSW that reach elevations above 5 m, separated by parallel swales at lower elevations (fig. 5). The average elevation of the ranch is about 3 m. The lowest elevations, between sea level and less than 1 m above sea level, occur around drainages that connect the swales to Matagorda Bay and Powderhorn Lake. Most prominent among these lows are the northwestern part of the ranch along Powderhorn Lake and its tributaries, the northern tip of the ranch at the junction between Matagorda Bay and Powderhorn Lake, an area along Matagorda Bay where several prominent swales reach the bay, and along the southeastern margin of the ranch toward Port O'Connor.

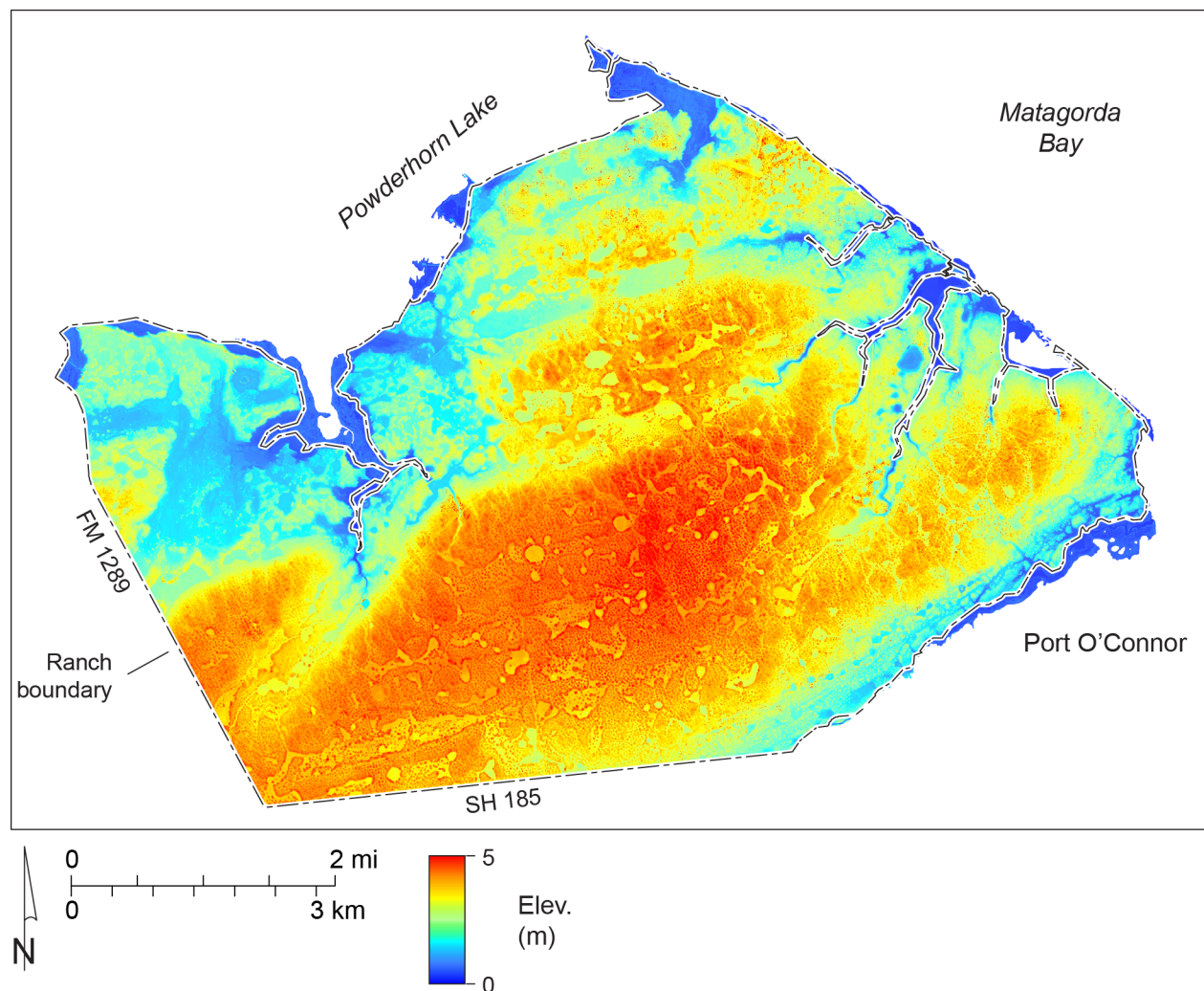


Figure 5. High-resolution (1-m grid cell size) digital elevation model (DEM) of Powderhorn Ranch created from the July 2016 BEG airborne lidar survey.

Water Wells and Windmills

Numerous water wells and windmills (figs. 6 to 8) were documented during geologic and geophysical investigations at Powderhorn Ranch. The locations of these wells were determined using GPS (Appendix A), their water depths and well depths were measured, samples from most of the wells were tested for total dissolved solids concentration (TDS), and 19 of the wells were geophysically logged. The water well at the ranch house is a water-supply well and was not entered. Wells PH01 through PH19 are cased with PVC, are generally capped or open to the surface, and range in depth from 59 to 97 m. Water depths in these wells range from 1.0 to 5.8 m below the ground surface. Deeper water depths are found in wells at higher surface elevations. Estimates of TDS concentration range from fresh (191 mg/L) to moderately saline (3230 mg/L), but these values are measured without purging stagnant water from the well and may differ substantially from true ground-water values. Most of the water wells were drilled adjacent to oil or gas well drilling pads to support drilling activities and were left for other uses. Water levels, well depths, and water salinities were not measured at the windmills.

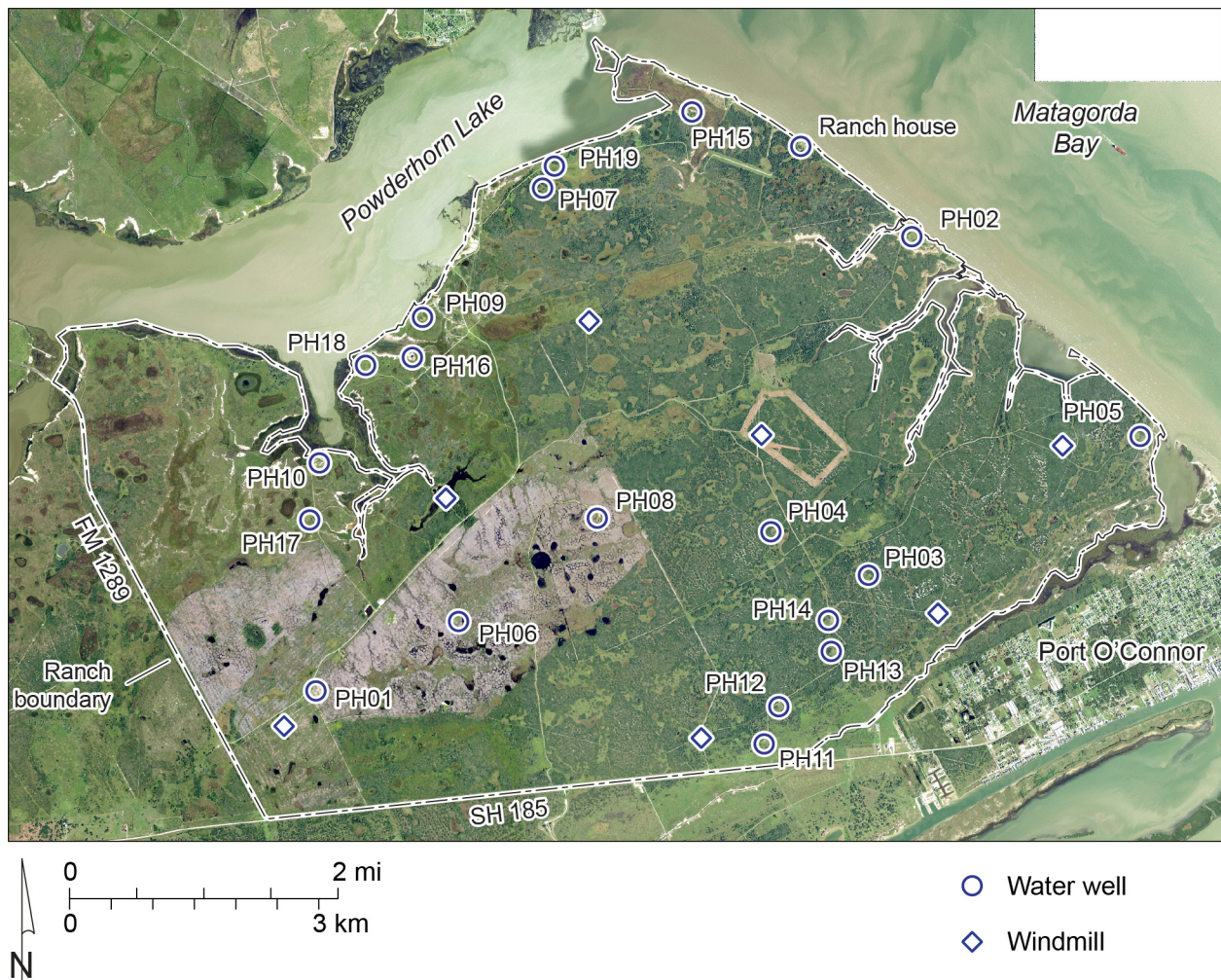


Figure 6. Location of water wells and windmills on Powderhorn Ranch. Water wells PH01 through PH19 were logged with geophysical instruments to produce natural gamma and electrical conductivity logs that can be used in subsurface lithologic and ground-water studies (Appendix A).



Figure 7. Windmill at Powderhorn Ranch used for livestock.



Figure 8. Measuring water depth in a PVC-cased water well before geophysical logging.

Geology and Geophysics

The Texas Coastal Plain is underlain by a complex assemblage of fluvial, deltaic, estuarine, and marine-influenced deposits that make up two Pleistocene formations (fig. 9): the younger Beaumont Formation and the older Lissie Formation (Hays and Kennedy, 1903; Sellards and others, 1932; Price, 1934, 1958; Metcalf, 1940; Doering, 1956; Aronow, 1971). These two formations record depositional, erosional, and weathering events associated with more than 20 full or partial glacial-interglacial cycles recorded in ice and sediment cores worldwide (Shackleton and Opdyke, 1973, 1976; Imbrie and others, 1984; Lorius and others, 1985; Robin, 1985; Lisiecki and Raymo, 2005). These strata have previously been mapped at a regional scale (1:250,000) as part of the Geologic Atlas of Texas series published by the BEG, and also have been mapped at 1:125,000 scale as part of the Environmental Geologic Atlas of the Texas Coastal Zone published by the BEG.

Two geologic units are mapped at Powderhorn Ranch on the 1:250,000-scale Geologic Atlas of Texas map (Brown and others, 1975). Most of the ranch is shown to be underlain by Beaumont Formation barrier island and beach deposits (map unit Qbb) consisting mostly of fine-grained sand with scarce shell. The surface is slightly higher than the surrounding deposits and is characterized by numerous pimple mounds and relict beach ridges. Pimple mounds (fig. 10), which are low mounds of sand that can be tens of meters in diameter and a meter or more high, are common on Powderhorn Ranch. The map unit is interpreted

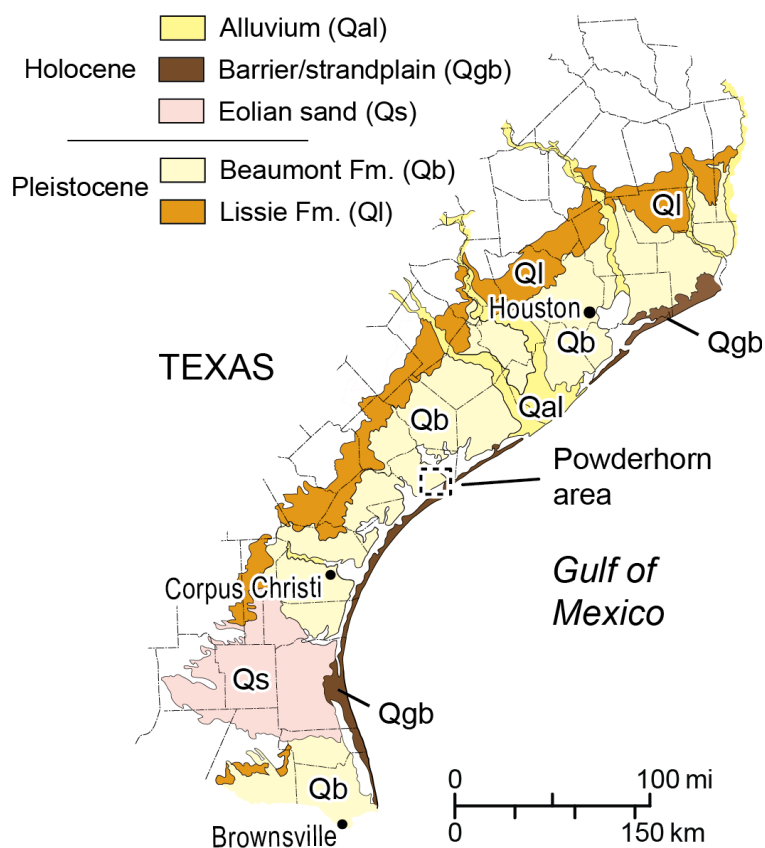


Figure 9. Quaternary geologic units of the Texas Coastal Plain. Modified from the Geologic Atlas of Texas.

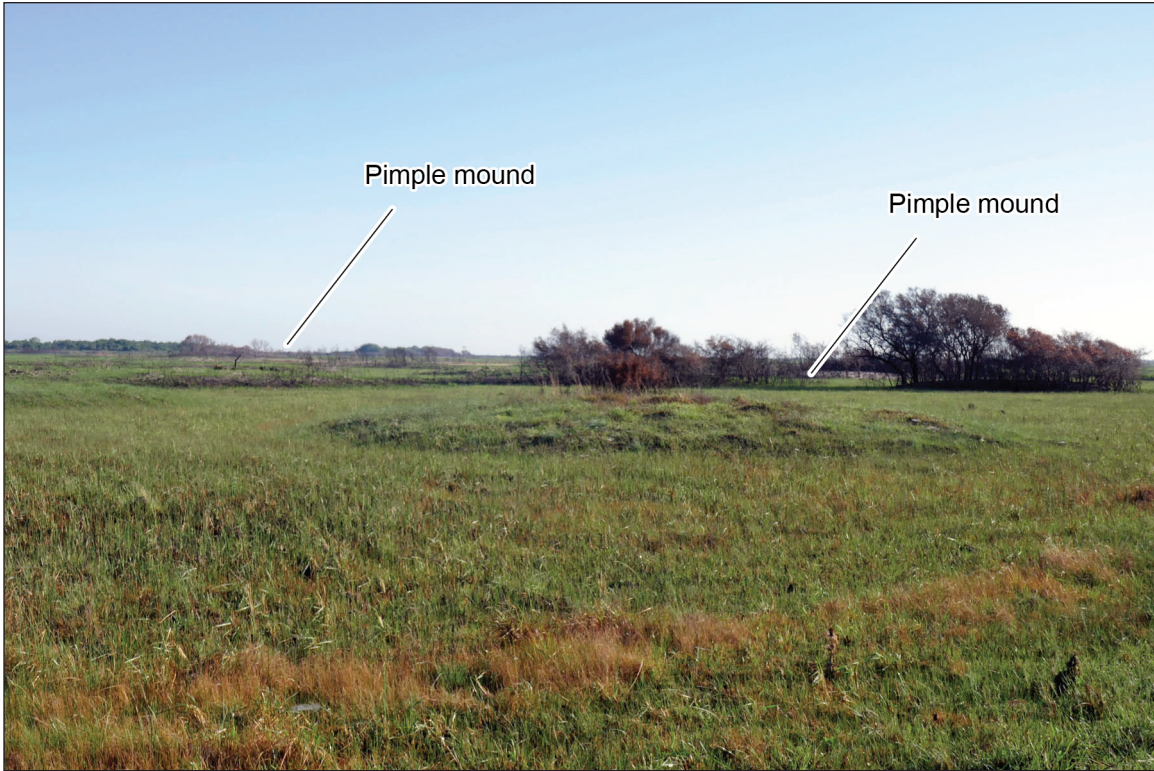


Figure 10. Pimple mounds on sandy Ingleside barrier system deposits on Powderhorn Ranch.

as part of the Ingleside barrier system and is less than 20 m thick (Brown and others, 1975). The Ingleside system is a series of late Pleistocene barrier island and strandplain segments that extends discontinuously from south of Corpus Christi Bay to Matagorda Bay. Powderhorn Ranch is the northernmost segment of four that are separated by Corpus Christi Bay, Aransas Bay, and San Antonio Bay. Minor alluvial units (Qal) are mapped on Powderhorn Ranch along Powderhorn Lake and Matagorda Bay (Brown and others, 1975). At a somewhat finer scale, the Environmental Geologic Atlas (McGowen and others, 1976) depicts Powderhorn Ranch as mostly tree- or grass-covered sand in a barrier-strandplain system. Mud-filled swales are mapped between beach-ridge complexes.

High-resolution, lidar-derived topographic maps, recent aerial imagery, field studies, and surface and borehole geophysical measurements have been used to conduct new geologic mapping in the Powderhorn Ranch area at the 7.5-minute quadrangle (1:24,000) scale (Paine and Collins, 2016a,b; Paine and Collins, 2017a,b,c,d). These maps have been merged to create a geologic map of Powderhorn Ranch (fig. 11). Principal geologic units include Pleistocene strata of the Beaumont Formation (sandy deposits of the Ingleside barrier system ridge complexes, sandy and muddy deposits of the intervening swales, and clayey or sandy fluvial and deltaic deposits landward of the Ingleside barrier in the northwest part of the mapped area). Holocene units include bay margin sand and mud, sand and clay alluvial deposits along drainages, sandy and muddy tidal flat deposits, sandy and shelly beaches and spits along the Matagorda Bay and Powderhorn Lake shorelines, ephemeral lake basin

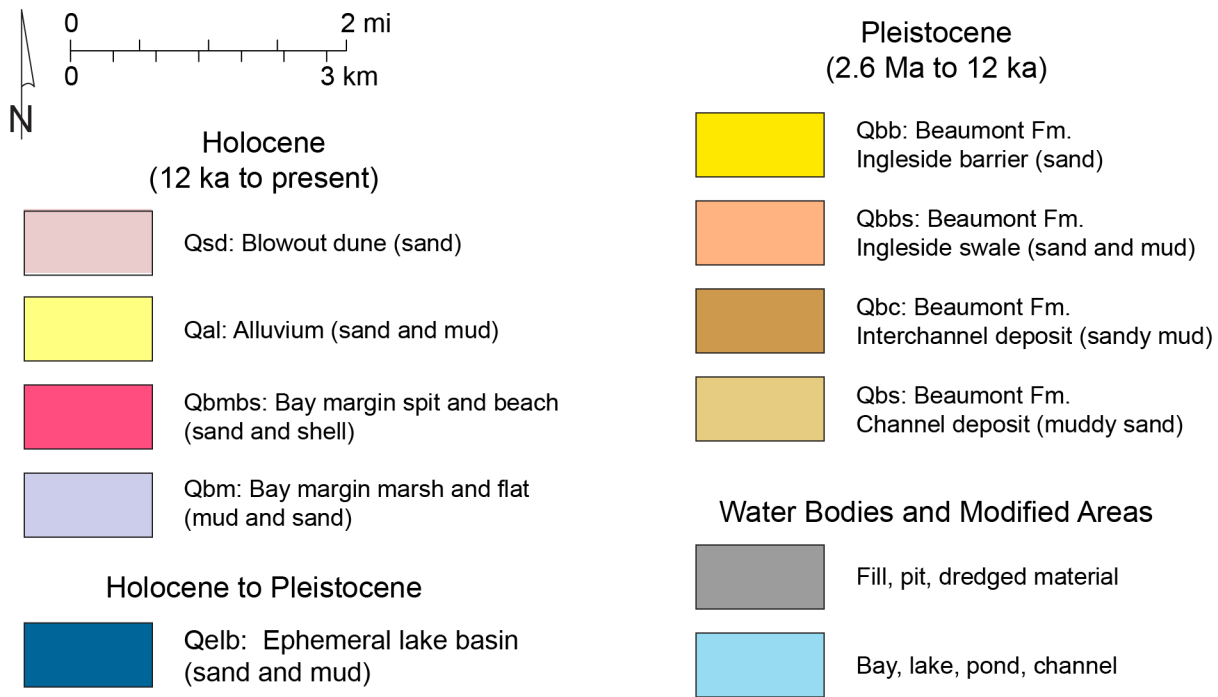
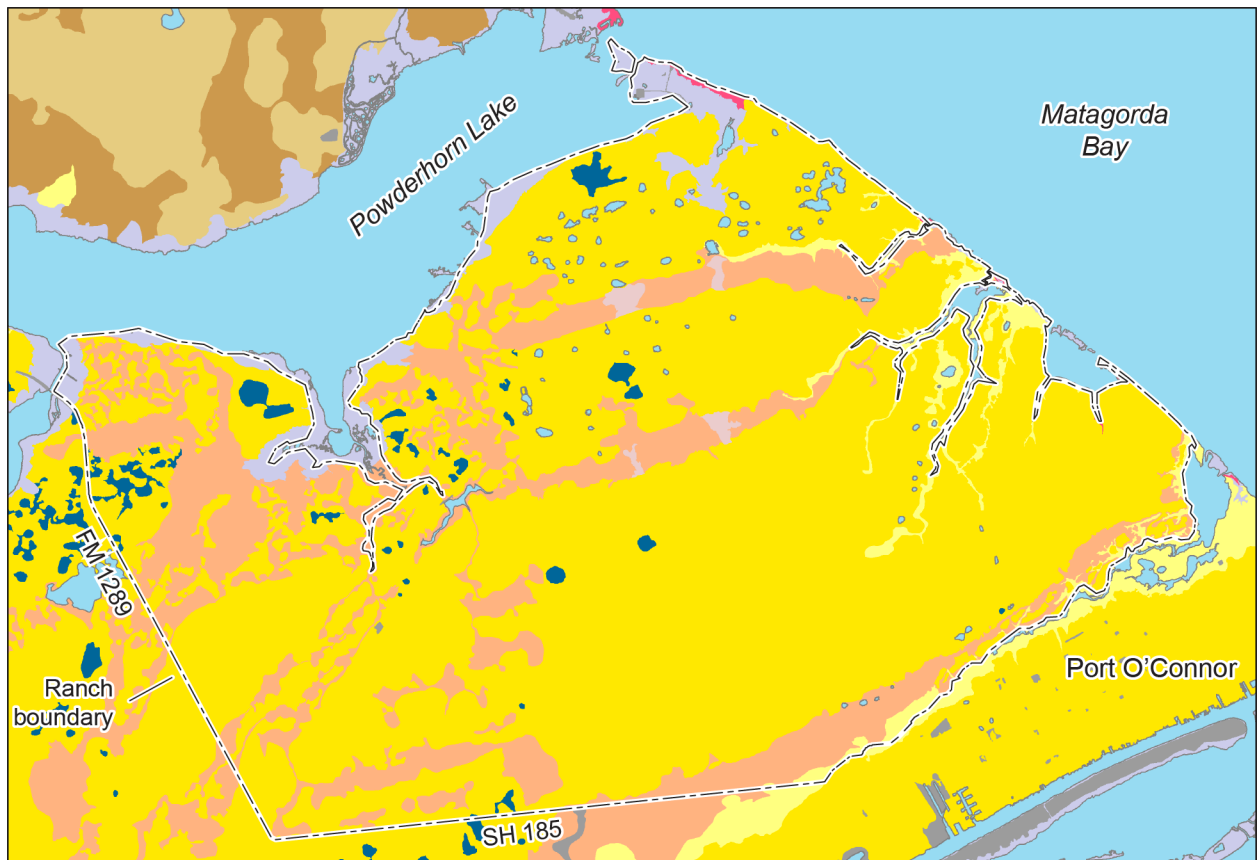


Figure 11. Geologic map of Powderhorn Ranch. Modified from Paine and Collins (2016a,b; Paine and Collins, 2017a,b,c,d).

sand and mud deposits, and wind-blown sands in widespread sheet deposits and local dunes.

Eroding low bluffs along Matagorda Bay and Powderhorn Lake expose the shallowest of these deposits. Along Matagorda Bay, Ingleside barrier and lagoonal sands and muddy sands have well-developed soil horizons and common piping features (fig. 12). These strata are overlain by a sheet of well-sorted, wind-blown sand with little soil development. Optical luminescence dates obtained on the Ingleside deposits yielded ages of 72 to 83 ka (plus or minus about 15 ka). The younger eolian sheet sands yielded ages of 4.9 to 6.5 ka (plus or minus about 1 ka). Dates are pending for additional samples collected along Matagorda Bay in 2018. The Ingleside dates are consistent with deposition during the last interglacial sea-level highstand series between 80 and 120 ka (oxygen isotope stage 5).

Given the low relief and limited exposures on the Texas coastal plain in general and Powderhorn Ranch specifically, other approaches must be used to gather information about the shallow subsurface lithologic and hydrologic conditions. Geophysical methods used at Powderhorn Ranch to explore below the surface included (a) borehole geophysical logging of 19 water wells (figs. 13 and 14; Appendix A) that revealed detailed information about the vertical changes in lithology and water quality to maximum well depths ranging from 59 to 97 m (figs. A1 to A19) and (b) 8 time-domain EM soundings (figs. 13 and 15; Appendix B)



Figure 12. Exposure of Pleistocene Ingleside barrier system sand and mud with soil features (iron staining and concretions, well-developed peds, and pedogenic carbonate nodules) overlain by Holocene eolian sheet sand along Matagorda Bay. Piping features are common in these sand-rich strata.

that provided generalized electrical conductivity profiles to maximum depths of 132 to more than 200 m (figs. B1 to B8).

Borehole logging at Powderhorn Ranch included natural gamma and electrical conductivity logs (Appendix A). Gamma logs record the natural radioactivity (gamma rays) emitted by strata surrounding the well and are used to examine lithologic variations. Pleistocene Beaumont Formation strata in the shallow subsurface beneath Powderhorn Ranch consist of a series of more- and less-clay rich units whose sharp or gradational contacts can be determined from gamma logs. Clays tend to contain minerals having higher gamma-ray count rates, whereas sands tend to contain minerals having low gamma-ray count rates.

A gamma log from well PH05 (figs. 13 and 16) illustrates how gamma activity varies from the ground surface to the bottom of the well at about 87 m. The low count rates (about 10 counts/s) at the left of the log correspond to sandy strata; the higher count rates (about 30 counts/s) at the right of the log correspond to clayey strata. The patterns evident in the log include both gradual changes in count rates (interpreted as a gradual change in clay

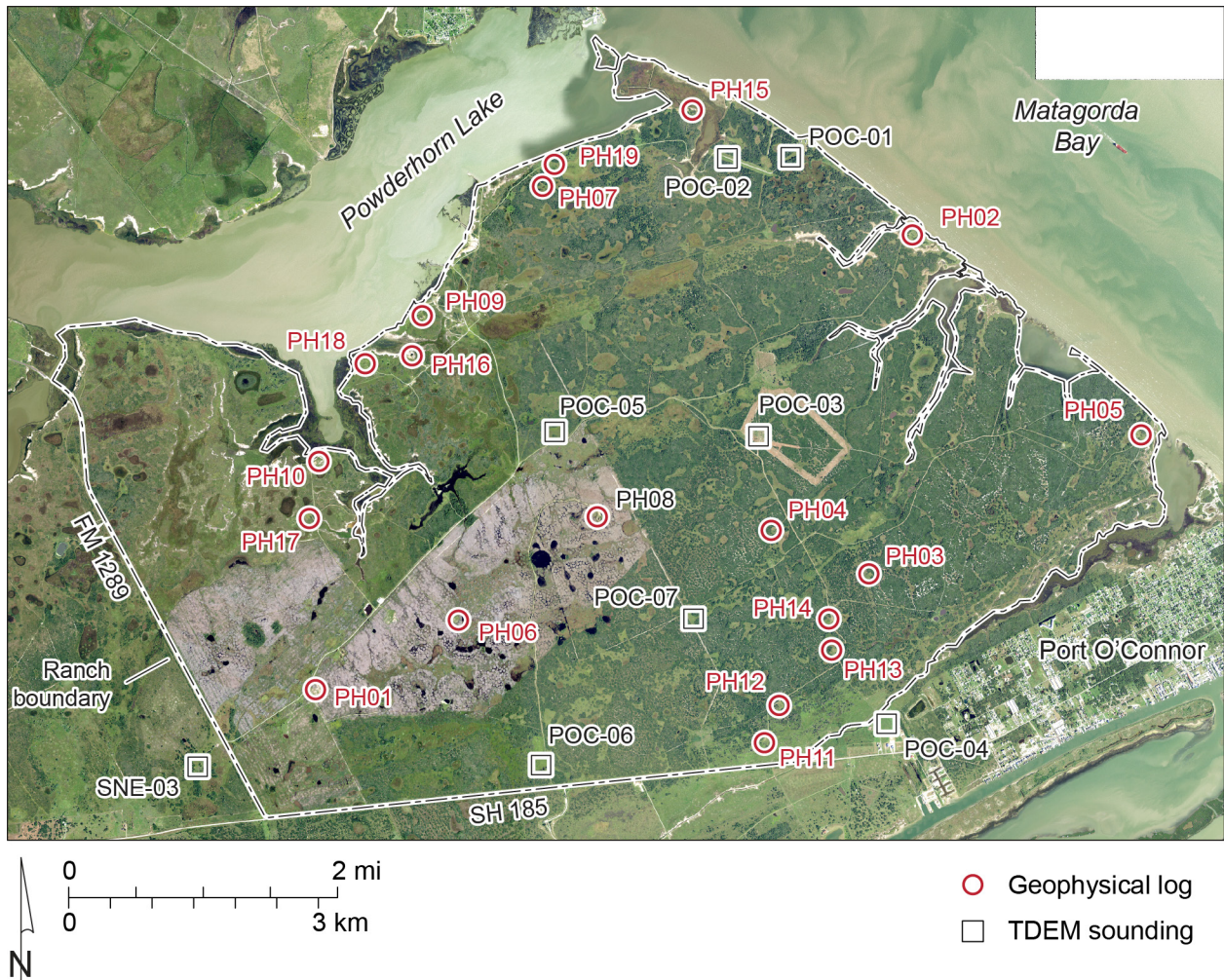


Figure 13. Location of logged wells (Appendix A) and time-domain electromagnetic induction (TDEM) soundings on Powderhorn Ranch (Appendix B).



Figure 14. Geophysical logging at water well PH19 along Powderhorn Lake, May 16, 2018.



Figure 15. Equipment laid out for TDEM sounding POC-02 (fig. 13), November 11, 2015.

content) as well as abrupt changes in count rates (interpreted as sharp boundaries between depositional units. The gamma log for well PH05 can be interpreted to show a series of depositional units that transition from fluvial environments (point bar and flood plain) below 30 m depth, to a coarsening-upward deltaic environment between 20 and 30 m depth, and finally marine-influenced environments (bay or estuarine and barrier island) in the upper 20 m. The sandy unit above 10 m depth is the Ingleside barrier system. Similar patterns occur in many of the Powderhorn Ranch wells (Appendix A).

Electrical conductivity logs also respond to lithologic changes. All other factors being equal, measured electrical conductivity is higher for clayey strata than it is for sandy strata.

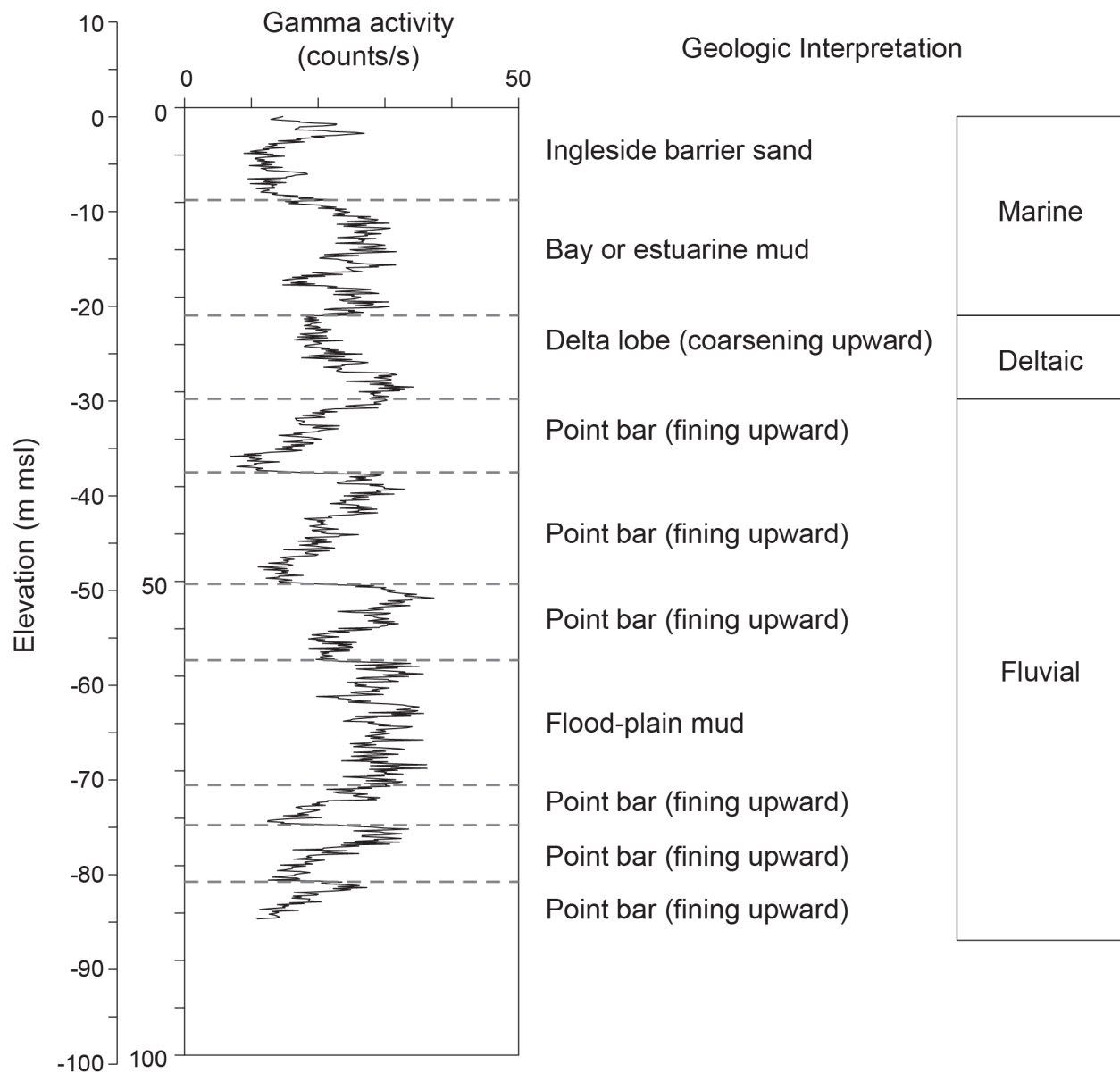


Figure 16. Gamma activity log for well PH05 (figs. 13 and B-5) and its geologic interpretation.

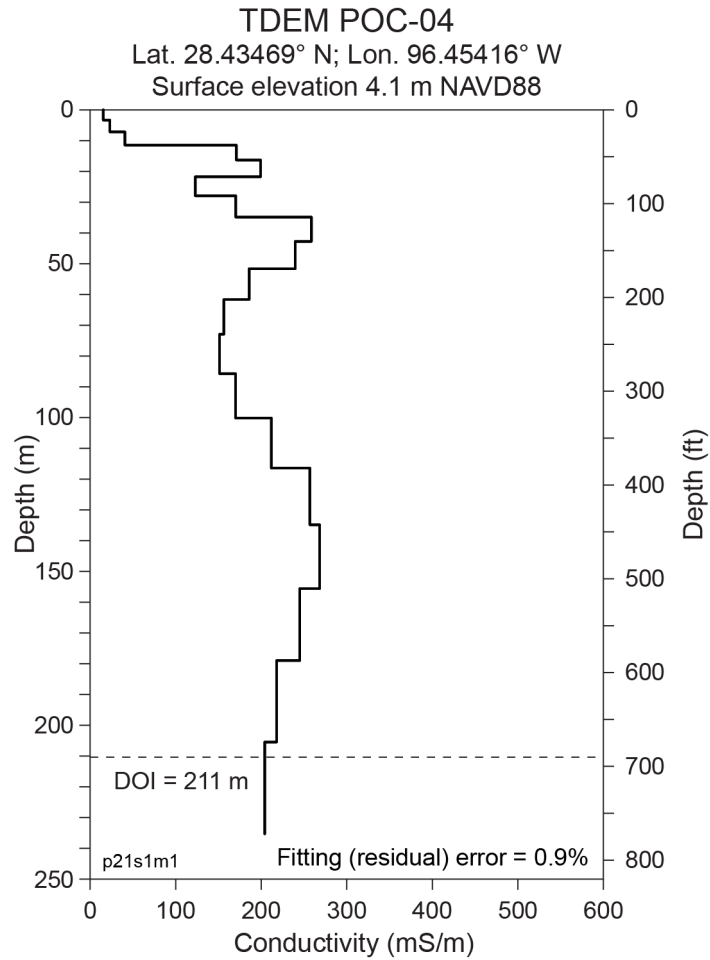


Figure 18. Subsurface electrical conductivity model constructed from TDEM sounding POC-04 (fig. 13).

The information from well logs and TDEM soundings can be combined to determine the thickness of the Ingleside barrier system sands across Powderhorn Ranch. These data indicate that the Ingleside barrier system sands are 8 to 11 m thick (fig. 19).

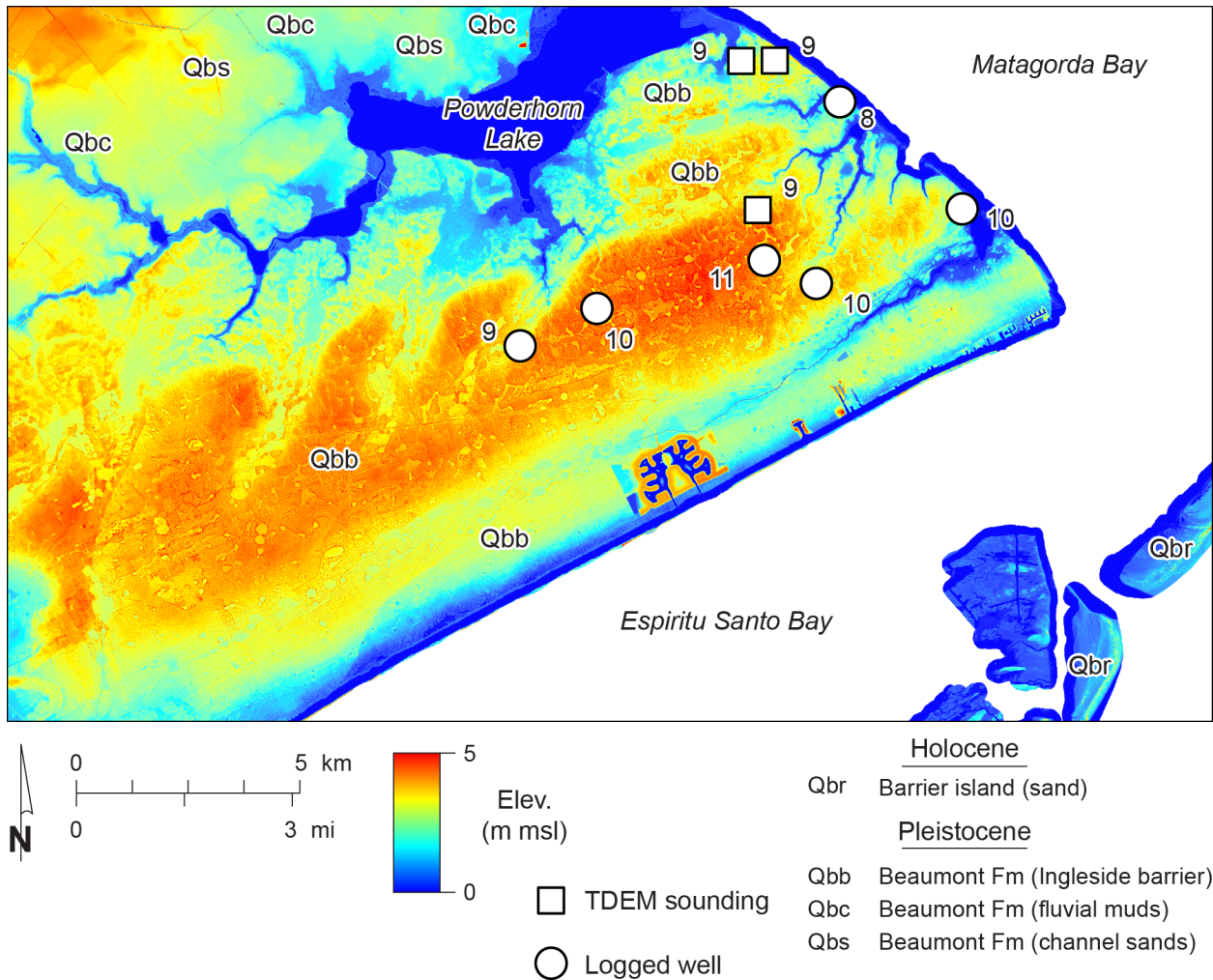


Figure 19. Thickness of the Ingleside barrier system sand determined from selected geophysical logs and TDEM soundings on and near Powderhorn Ranch. Thicknesses are superimposed on topography from a 3-m grid cell lidar survey conducted by the U.S. Geological Survey in 2011.

Shoreline Types, Retreat Vulnerability, and Historical Movement

Shorelines are the dynamic boundary between land and water. Bay shorelines on the middle Texas coast have been grouped into 11 types that are distinguished by a combination of elevation, slope, depositional environment, material and consolidation level, and vegetation or habitat (fig. 20; Paine and others, 2016). From highest to lowest elevation, these types are: high and low bluff, sandy slope, fan delta, beach, spit, tidal pass, flood-tidal delta marsh or tidal flat, deltaic marsh, back-barrier marsh or tidal flat, and bay-margin marsh or tidal flat. Together, these shoreline types extend for about 1,065 km among the middle Texas bay systems.

Powderhorn Ranch has more than 20 km of bay or lake shoreline, including 8.4 km along Matagorda Bay and about 12 km along the southeastern shore of Powderhorn Lake. Common shoreline types at Powderhorn Ranch are sandy slopes, spits and beaches, and bay-margin marshes or tidal flats (fig. 21). Each of these shoreline types differs in material composition, elevation, slope, degree of consolidation, and vegetation cover and responds differently to the major causes of shoreline retreat and land loss, including non-storm wave action, storm surge and storm wave action, and relative sea-level rise (figs. 22 to 24). Most

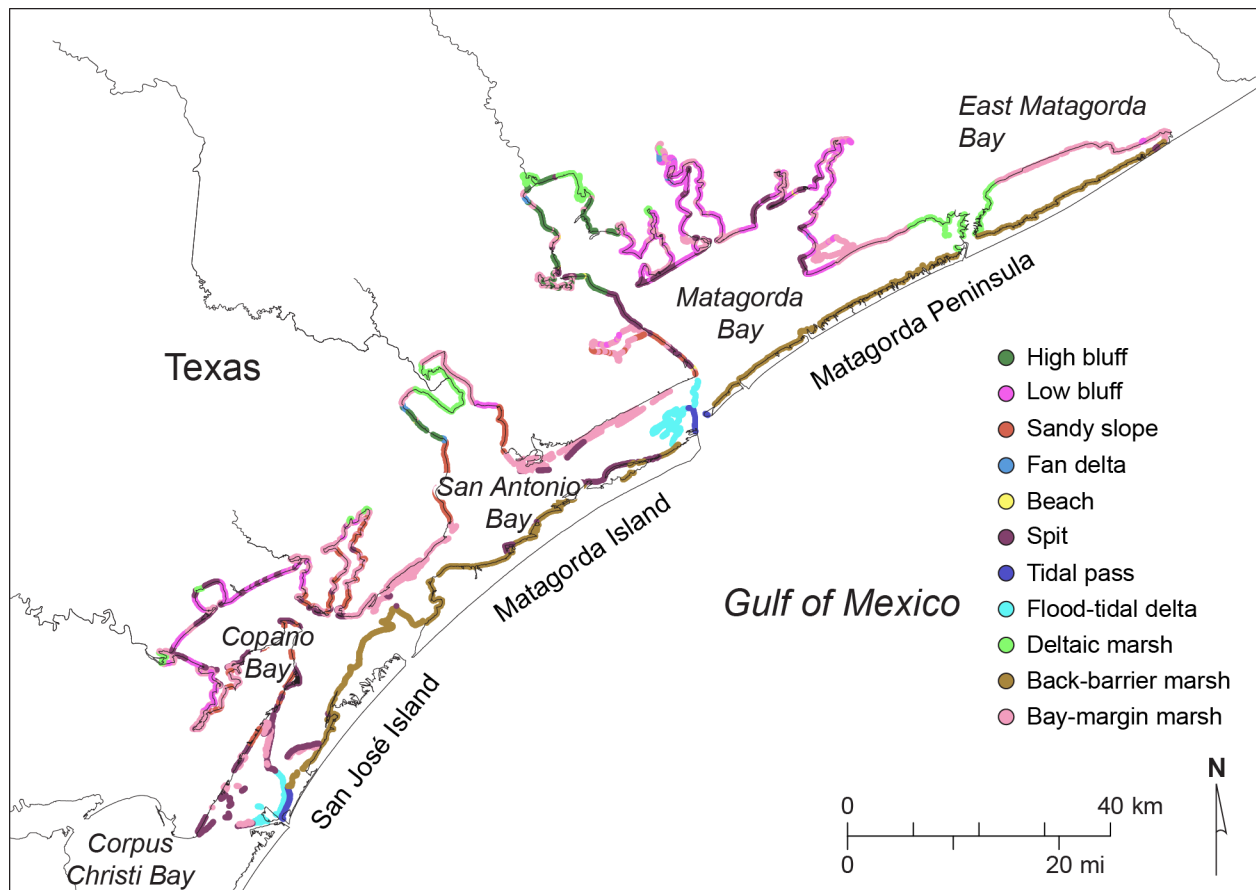


Figure 20. Distribution of principal shoreline types in the Copano, San Antonio, and Matagorda Bay systems (Paine and others, 2016).

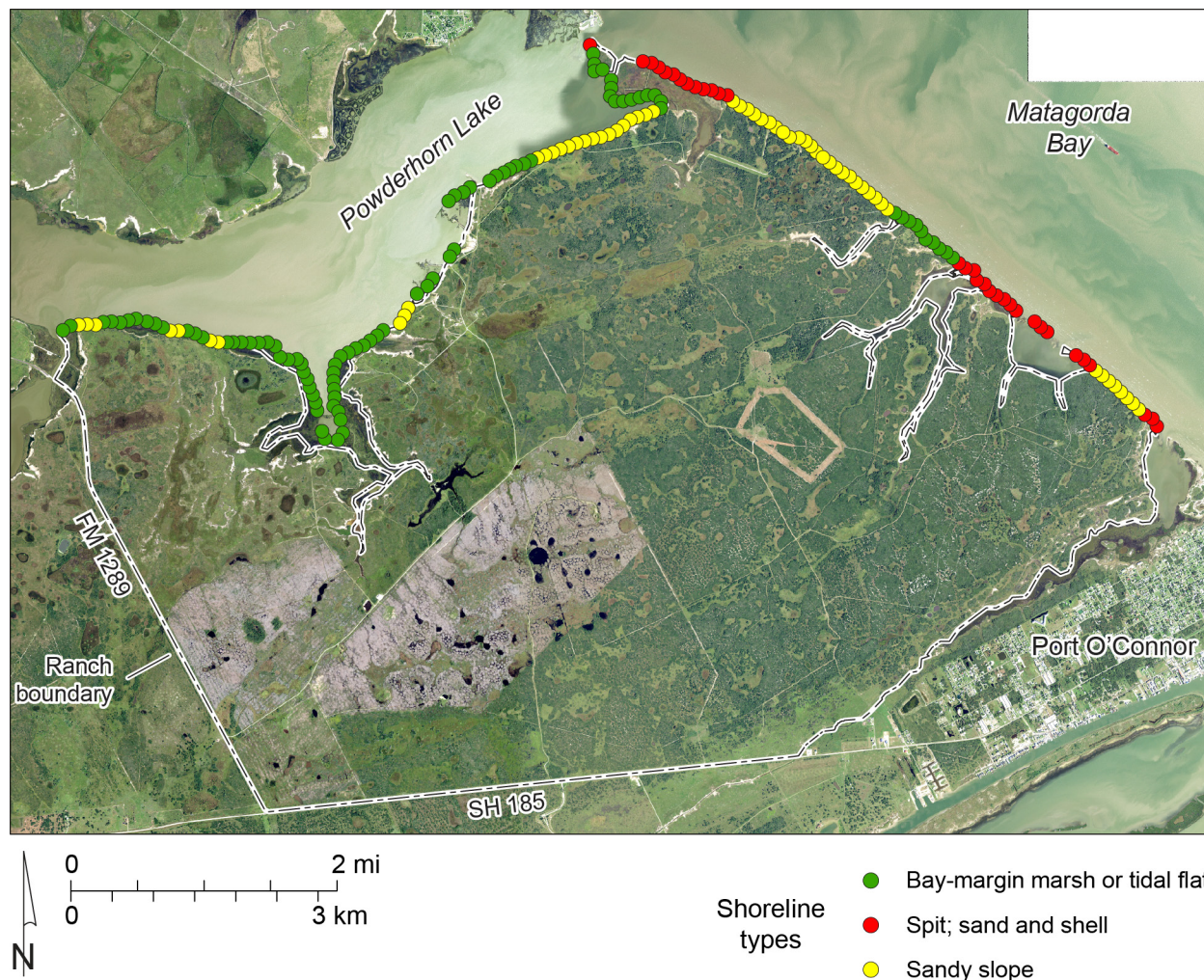


Figure 21. Shoreline types on Powderhorn Ranch along Matagorda Bay and Powderhorn Lake.

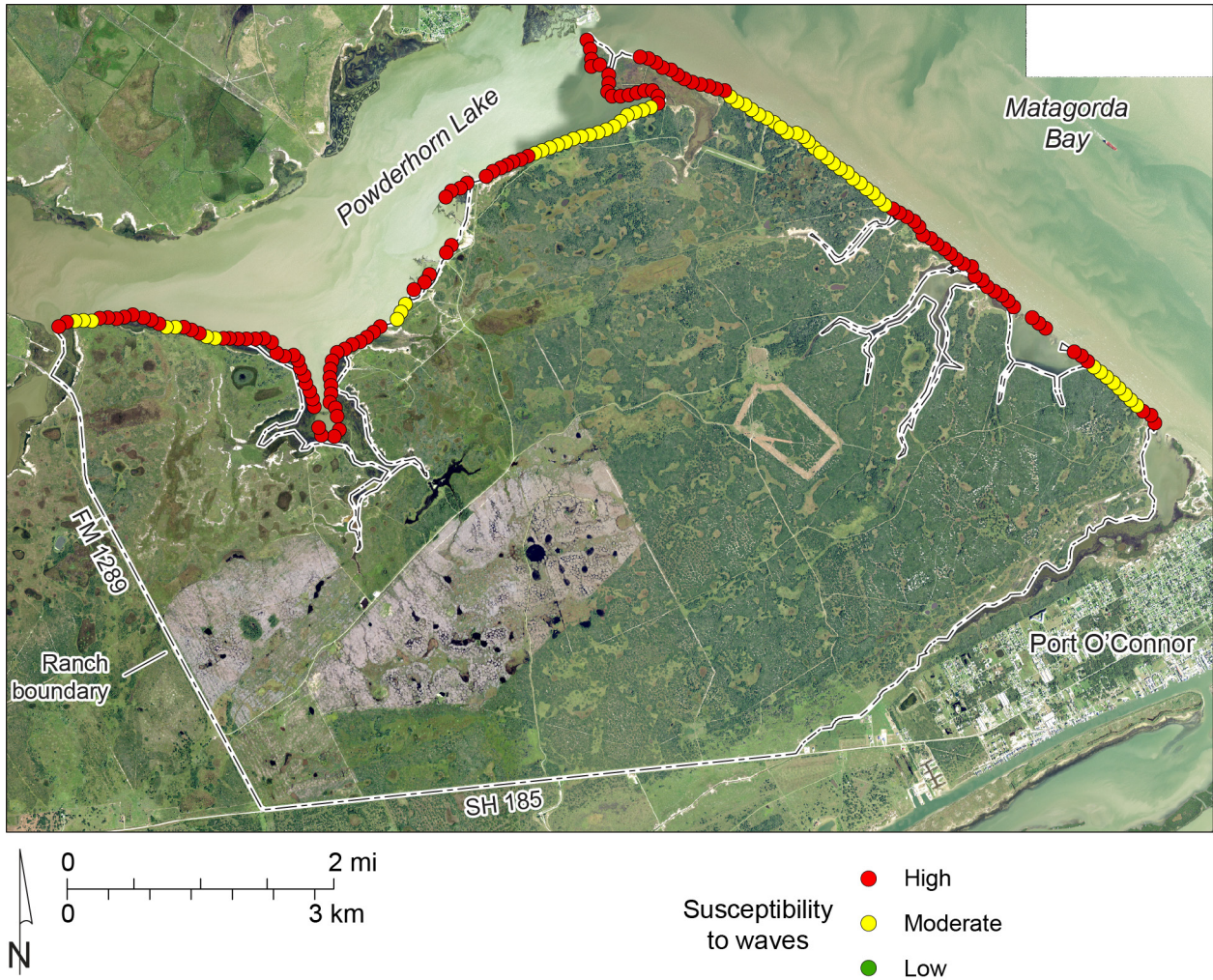


Figure 22. Shoreline susceptibility to non-storm wave activity on Powderhorn Ranch along Matagorda Bay and Powderhorn Lake.

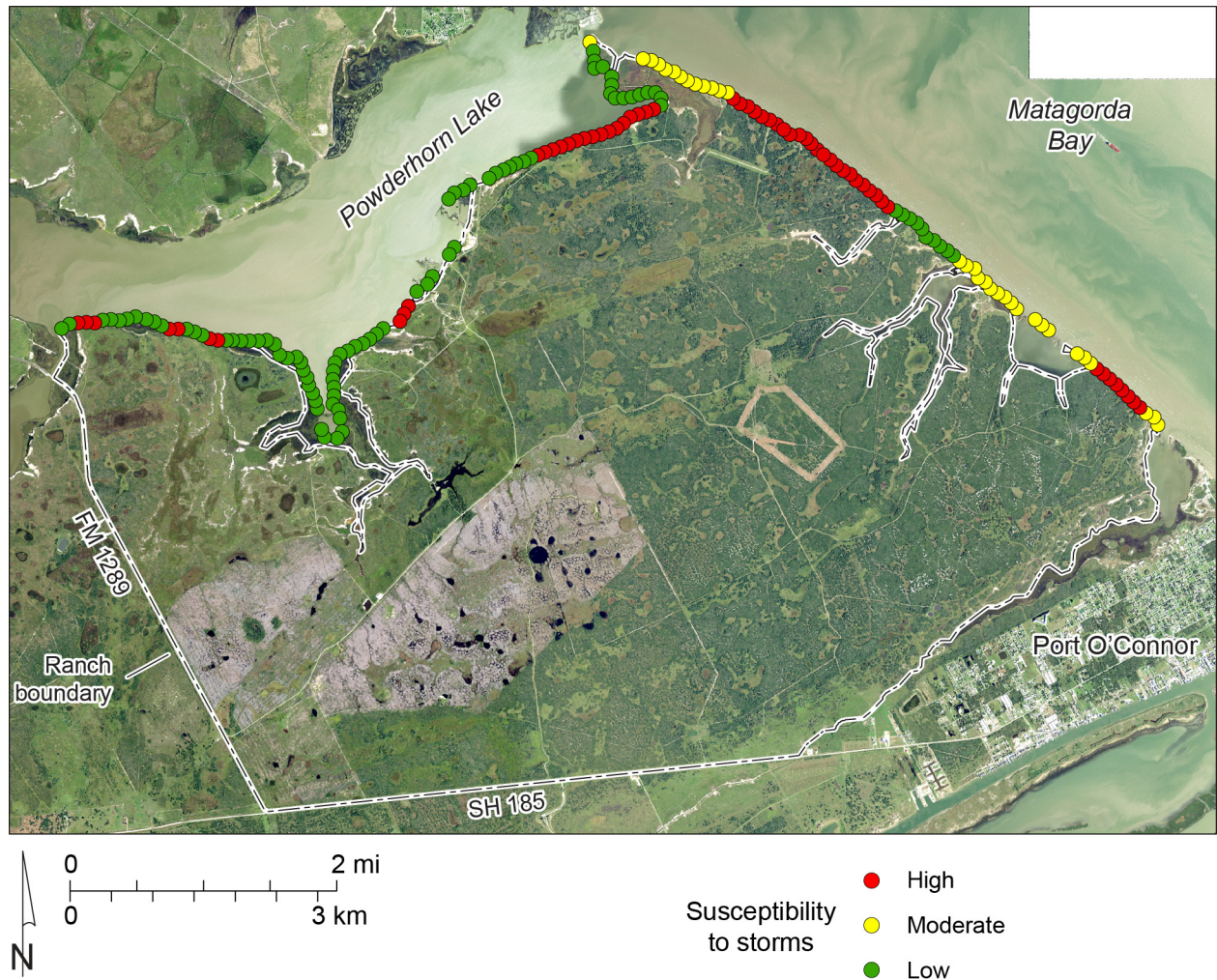


Figure 23. Shoreline susceptibility to storm surge and storm waves on Powderhorn Ranch along Matagorda Bay and Powderhorn Lake.

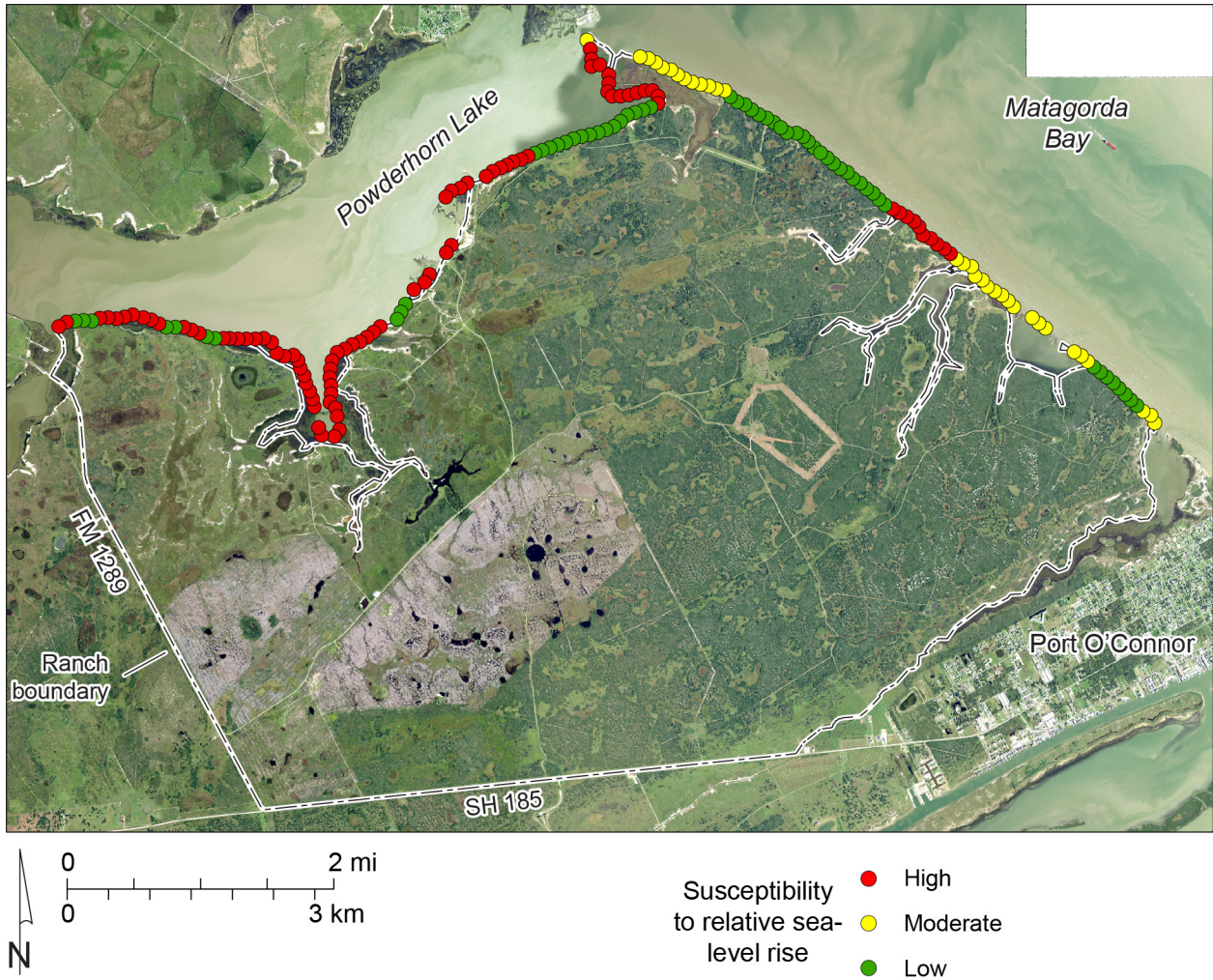


Figure 24. Shoreline susceptibility to relative sea-level rise on Powderhorn Ranch along Matagorda Bay and Powderhorn Lake.



Figure 25. Bulkhead and riprap along the Matagorda Bay shoreline at the ranch house.

of the shoreline along Matagorda Bay and Powderhorn Ranch remains in its natural state. Only near the ranch house has a bulkhead and flanking riprap been emplaced (fig. 25).

Sandy Slopes

Sandy or clayey sand slopes occur along about a third of the Powderhorn Ranch shoreline and are located where low to moderate sandy Ingleside bluffs intersect the shoreline along Matagorda Bay and along Powderhorn Lake near where it joins Matagorda Bay (fig. 21). Sandy slopes are composed of unconsolidated to semiconsolidated sand to muddy sand that can be partly stabilized by upland grasses and shrubs (fig. 26). Elevations on the slopes landward of the shoreline range from 1 to 3 m above sea level. Some of the sandy slopes are fronted by narrow sandy beaches or marshes. Sandy slopes are highly susceptible to shoreline retreat caused by storm surge and storm waves (fig. 23) and moderately susceptible to erosion from non-storm wave activity (fig. 22), but are relatively insensitive to short-term relative sea-level rise (fig. 24) given their higher elevation.

Spits

Spits are low, elongate, and unconsolidated sandy and shelly beaches that form along eroding bay shorelines by longshore drift and lateral migration (fig. 27). At Powderhorn Ranch, they comprise about 18 percent of the total shoreline length and are found across



Figure 26. Sandy slope with a narrow, sandy beach along the Matagorda Bay shoreline of Powderhorn Ranch.



Figure 27. Sandy and shelly spit along the Matagorda Bay shoreline of Powderhorn Ranch.

small embayments where topographic swales and drainages reach Matagorda Bay and where Matagorda Bay intersects Powderhorn Lake (fig. 21). Because of their low elevation and unconsolidated state, they are highly susceptible to erosion from non-storm wave action and are moderately susceptible to retreat caused by relative sea-level rise and storm-related surge and waves.

Bay-margin Marshes or Tidal Flats

Bay-margin marshes and tidal flats are the most common shoreline type at Powderhorn Ranch, constituting half of the total shoreline length (fig. 21). They are most common in the lower-energy environment along Powderhorn Lake. Bay-margin marshes and tidal flats have low elevation, minimal slope, muddy sand or sandy mud substrate, and dominant marsh vegetation with interspersed tidal flats (fig. 28). These shorelines are highly susceptible to erosion by non-storm waves and to land loss by submergence related to relative sea level rise. They have a low susceptibility to erosion related to storm surge and storm waves because they are inundated before storm passage.



Figure 28. Bay-margin marsh and tidal flat along the Powderhorn Lake shoreline of Powderhorn Ranch.

Historical Shoreline Movement

Two major shoreline change studies that include the Powderhorn Ranch shorelines have been conducted. The first study used shoreline positions from 1800s topographic charts and from aerial photographs taken between the 1930s and 1950s to examine historical shoreline change rates for the Matagorda Bay area (McGowen and Brewton, 1975). More recently, BEG researchers determined Matagorda Bay shoreline positions from a 2015 airborne lidar survey and analyzed historical shoreline change rates from the 1930s to 2015 (Paine and others, 2016).

In the recent study, shoreline movement at Powderhorn Ranch was determined at 180 measurement points spaced at 100-m intervals along the Matagorda Bay and Powderhorn Lake shoreline (fig. 29). Overall, net shoreline movement rates range from retreat at 3.6 m/yr to advance at 1.8 m/yr, averaging retreat at 0.8 m/yr. Translated to area, these data suggest that Powderhorn Ranch land loss averages 1.6 ha/yr for a total estimated land loss of 136 ha from 1930 to 2015.

Net retreat rates are higher along Matagorda Bay than they are along Powderhorn Lake. The Matagorda Bay shoreline has greater exposure to non-storm wave activity during frontal passage and storm surge and storm wave effects during frequent tropical cyclones. Net shoreline movement rates averaged 1.5 m/yr of retreat; the shoreline retreated at all but one of the 73 measurement points on Matagorda Bay. Along Powderhorn Lake, net shoreline movement rates averaged 0.3 m/yr of retreat.

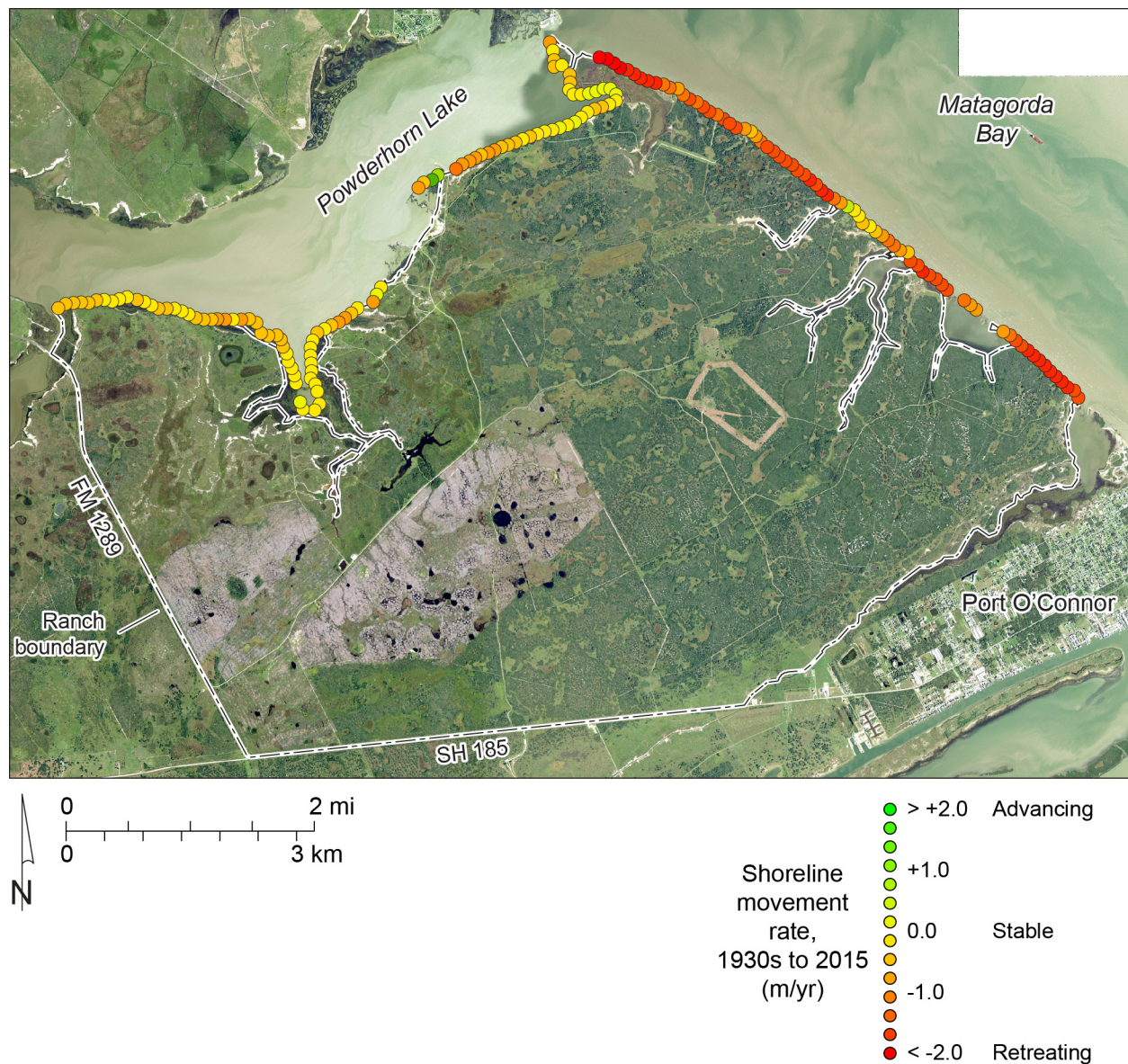


Figure 29. Net shoreline movement rates between the 1930s and 2015 along the Matagorda Bay and Powderhorn Lake shorelines of Powderhorn Ranch. Data from Paine and others (2016).

Hurricanes and Tropical Storms

Tropical cyclones (hurricanes and tropical storms) are frequent visitors to the Texas coast, bringing strong winds, high water, and large waves to bear on the coastal environment. Tropical cyclones include tropical storms (sustained winds between 62 and 118 km/hr) and hurricanes that are classified following the Saffir/Simpson system (Simpson and Riehl, 1981). Category 1 hurricanes have sustained winds of 119 to 143 km/hr; Category 2: 154 to 177 km/hr; Category 3: 178 to 209 km/hr; Category 4: 210 to 249 km/hr; and Category 5: greater than 249 km/hr. In general, minimum central pressures decrease as the categories increase, as does pressure- and wind-driven storm surge. Two critical parameters that influence the erosion potential of a tropical cyclone are surge height and surge duration: the longer sea level is elevated above normal during storm passage, the greater the potential for erosion along the shoreline and redistribution of eroded sediment. Historical records (data from NOAA and Roth, 2010) indicate that 65 hurricanes and 60 tropical storms have struck the Texas coast between 1850 and 2017, an average of four hurricanes and four tropical storms per decade.

At Powderhorn Ranch, principal hurricane hazards include wind damage, wave erosion along the Matagorda Bay and Powderhorn Lake shorelines, and inundation caused by storm surge. Two great hurricanes illustrate the inundation potential of these storms. Hurricane Carla, classified as a Category 4 hurricane with sustained winds of more than 230 km/hr, made landfall near Port O'Connor in September 1961. Maximum still-water elevations were reported to be 4.5 m at Port O'Connor east of Powderhorn Ranch and 6.7 m at Port Lavaca west of Powderhorn Ranch (U.S. Army Corps of Engineers, 1962). Assuming a surge elevation of about 5.2 m at Powderhorn Ranch, subtracting ground-surface elevations determined from the 2016 airborne lidar survey from the Carla surge elevation yields an inundation map that suggests that nearly all of Powderhorn Ranch was inundated to water depths ranging from near 0 m to about 5 m along the low-lying shore, swale, and drainage areas (fig. 30).

Hurricane Beulah, another major hurricane that made landfall near the mouth of the Rio Grande in September 1967, produced surge heights in Matagorda Bay reported at 1.6 m at Port O'Connor and 2.1 m near Port Lavaca (U.S. Army Corps of Engineers, 1968). At Powderhorn Ranch, subtracting lidar-derived ground elevations from an estimated surge height of 1.8 m yields a map showing inundation areas along Powderhorn Lake and within the swales and drainages along Matagorda Bay (fig. 31). Most of Powderhorn Ranch remained above surge flooding.

Hurricane Harvey, a Category 4 storm that made landfall near Rockport, Texas, in August 2017, produced surge heights of about 1 m at Port O'Connor and 2.2 m at Port Lavaca. Debris lines recording inundation extent were mapped along Matagorda Bay and Powderhorn Lake during field investigations in January 2018 (figs. 32 and 33). Washover deposits composed of sand, shell, and storm debris were common along the Matagorda Bay shoreline (fig. 34). Significant Harvey-related erosion occurred along the Matagorda Bay shoreline, including sandy bluff retreat above riprap near the ranch house (fig. 35).

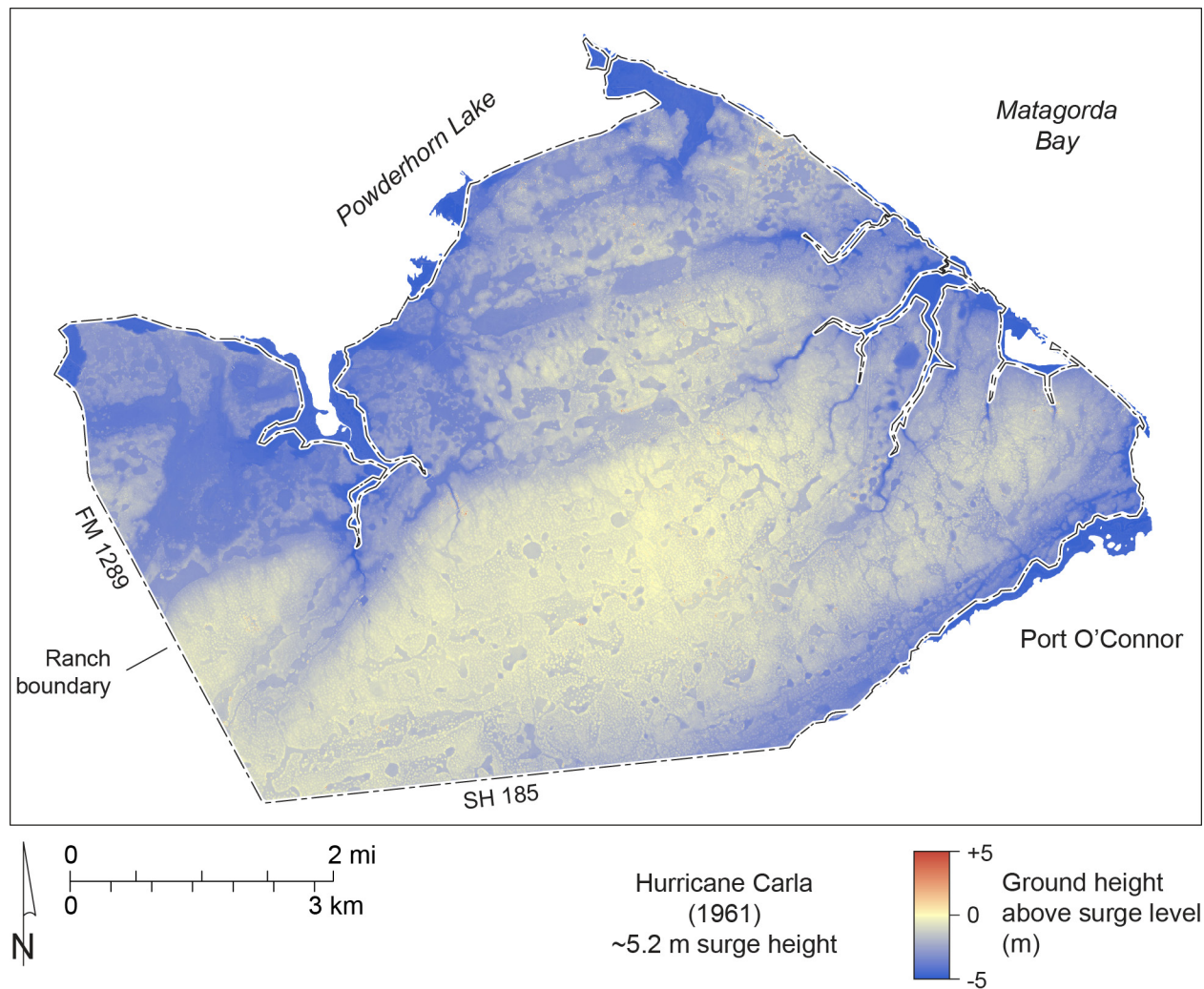


Figure 30. Estimated inundation areas and depths from storm surge during Hurricane Carla (September 1961). Storm surge height estimated from U.S. Army Corps of Engineers (1962).

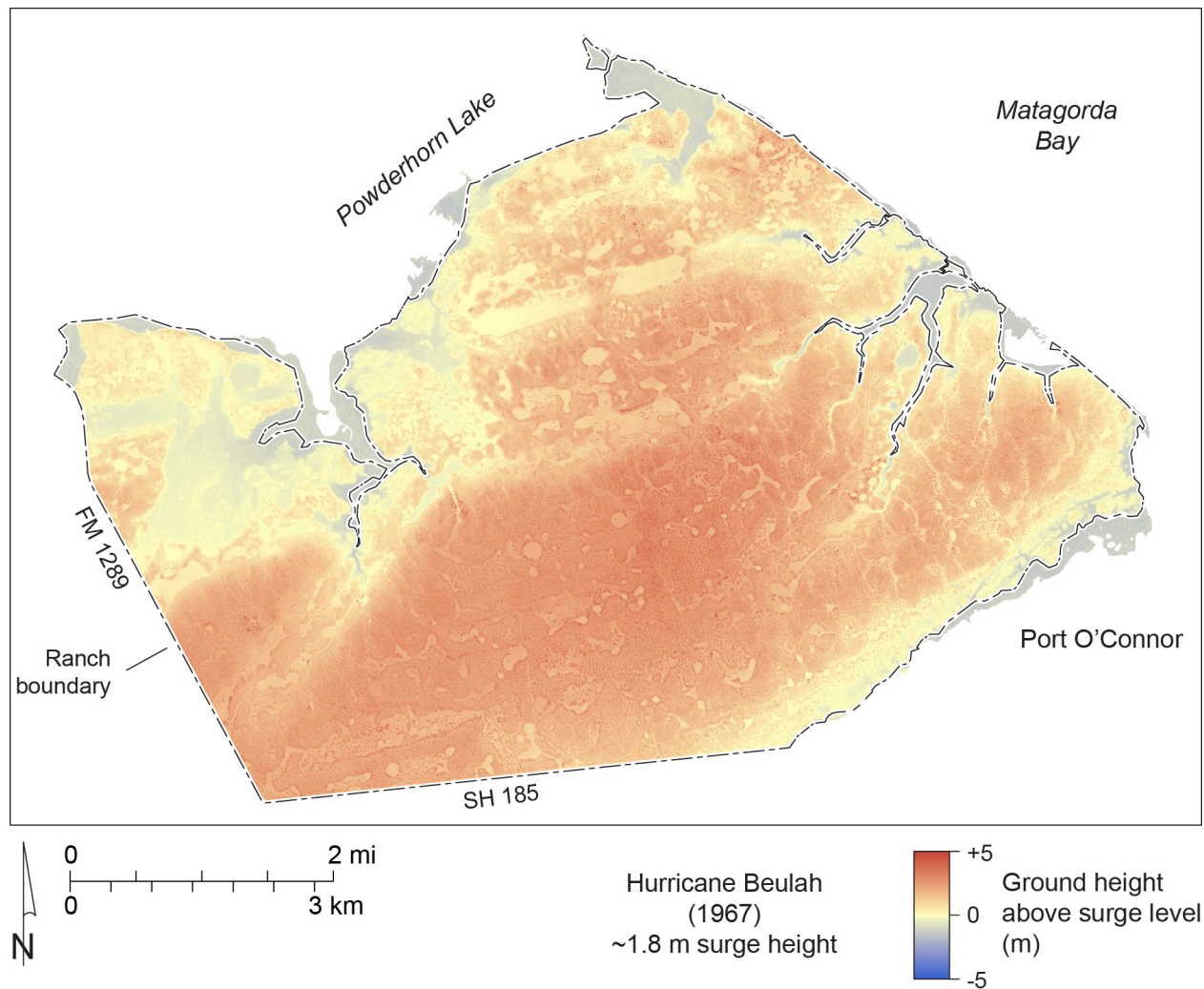


Figure 31. Estimated inundation areas and depths from storm surge during Hurricane Beulah (September 1967). Storm surge height estimated from U.S. Army Corps of Engineers (1968).



Figure 32. Hurricane Harvey (2017) debris line along Matagorda Bay on Powderhorn Ranch. Storm-eroded low bluffs are visible in the background.



Figure 33. Hurricane Harvey debris line along Matagorda Bay at Powderhorn Ranch.



Figure 34. Hurricane Harvey washover deposits on a bay-margin marsh along Matagorda Bay at Powderhorn Ranch.



Figure 35. Hurricane Harvey debris and Harvey-related erosion above riprap along Matagorda Bay at Powderhorn Ranch.

Wetlands Status and Trends

The BEG has undertaken coast-wide studies of the status and trends of wetlands and aquatic habitats along the Texas portion of the Gulf of Mexico. Coastal wetlands provide many vital functions including water quality enhancement by filtering runoff, flood protection and recharge through their action as natural sponges, buffers that reduce erosive forces from storm surges, high quality habitat that supports fish and shellfish production, migratory waterfowl, and many other species, and recreational opportunities. Wetland and aquatic habitats are essential components of inland and barrier island environments along the Texas coast. These valuable resources are highly productive biologically and chemically and are part of an ecosystem in which a variety of flora and fauna depend. Scientific investigations of wetland distribution and abundance through time are prerequisites to effective habitat management. They provide critical information for the preservation and protection of wetland functions and uses, and could guide mitigation/restoration projects. Moreover, studies of habitat status and trends contribute information to be incorporated in valuation studies of wetlands, that is, the types and areal extents of different wetlands from which ecosystem services can be quantified. Based on these studies, the BEG produced a series of GIS datasets and reports designed to determine the status and historical trends of wetlands and associated aquatic habitats.

The study of status and trends are based on wetlands interpreted and mapped on recent and historical aerial photographs. The most recent status of wetlands for the Powderhorn Ranch area was determined by mapping wetlands on color-infrared (CIR) photographs taken in 2008 (Tremblay and Calnan, 2010). Historical wetland distribution was based on 1956 black-and-white and 1979 CIR photographs.

The U.S. Fish and Wildlife Service (USFWS, 1983, unpublished digital data of wetland maps) mapped historical wetland distribution using methods established through the National Wetlands Inventory Program. Habitats were interpreted on the historical aerial photographs then transferred to 1:24,000-scale base maps using a zoom transfer scope. The maps were digitized and entered into a GIS. Sources of error for the mapping of historical wetlands includes the interpretation of wetland units, lack of field checking wetland boundaries, the transfer of mapped boundaries from aerial photographs to hardcopy maps, and digitization and registration of the historical maps. The BEG obtained the 1956 and 1979 wetland map GIS files from USFWS and partly revised them to be more consistent with wetlands interpreted on the 2008 photographs (Tremblay and Calnan, 2010).

The 2008 photographs were digital images with a 1 m pixel resolution and registered to U.S. Geologic Survey Digital Orthophoto Quadrangles (DOQ's). Mapping of the wetland and aquatic habitats was done by interpreting and delineating habitats onscreen in a GIS at a scale of 1:5,000. This allowed for more detailed mapping. The current maps were used to make comparisons with the historical mapping to determine habitat trends (Tremblay and Calnan, 2010).

The wetland mapping by the USFWS and BEG follows the classification determined by Cowardin and others (1979) in *Wetlands and Deepwater Habitats of the United States*.

Wetlands are classified by system (marine, estuarine, riverine, palustrine, lacustrine), subsystem (reflective of hydrologic conditions), and class (descriptive of vegetation and substrate). The systems represented in the Powderhorn Ranch area include estuarine, palustrine, and lacustrine (table 1). The 1979 and 2008 maps were also classified by subclass (subdivisions of vegetated classes only), water regime (table 2), and special modifiers. The 1956 wetlands were mapped only down to class.

A wetland trend analysis was completed by examining the distribution of wetland habitats as mapped in 1956, 1979, and 2008. Wetland classes were emphasized in the trend analysis over water regime and special modifiers, in part because habitats were only mapped to the class level on the 1950s photography. Also water regime classification can be influenced by local or shore-term events such as precipitation (1950s Texas drought) and tidal cycles.

The estuarine system consist of many types of wetland habitats. Estuarine subtidal unconsolidated bottom (E1UBL 2008), or open water (E1OW 1956 and 1979), occurs in the bays and adjacent salt and brackish marshes. Unconsolidated shore (E2US 2008) includes tidal flats (E2FL 1956 and 1979) and bay beaches (E2BB 1979). The emergent areas around estuarine waters consist of low and high marshes (E2EM) that contain a variety of salt-tolerant and brackish-tolerant plants. Estuarine habitats extend landward to a point where salinity decreases to 0.5 ppt. The mapping of the boundaries between estuarine and palustrine systems is subjective based upon proximity to estuarine water bodies and vegetation types. A pond or emergent wetland is typically placed in the palustrine system if it is separated from the estuarine system by an upland break.

Table 1. Wetland codes and descriptions from Cowardin and others (1979). Codes listed below were used in mapping the wetlands in the Powderhorn Ranch area based upon interpretation of 2008 photography. The codes varied in some cases from 1956 and 1979 maps.

NWI code (water regime)	NWI description	Common description
E1AB3	Estuarine, subtidal aquatic bed, rooted vascular	Estuarine seagrass
E1UB (L)	Estuarine, subtidal unconsolidated bottom	Estuarine bay
E2AB1 (P)	Estuarine, intertidal aquatic bed, algal	Algal mat
E2EM1 (N, P)	Estuarine, intertidal emergent, persistent	Estuarine bay marshes, salt and brackish water
E2US (M, N, P)	Estuarine, intertidal unconsolidated shore	Estuarine bay, tidal flats, beaches
L1UB (H)	Lacustrine, limnetic unconsolidated bottom	Lakes
PEM1 (A, C, F)	Palustrine, emergent persistent	Freshwater marshes, meadows, depressions, or drainage areas
PUB (H)	Palustrine, unconsolidated bottom	Pond
U	Upland	Upland

Table 2. Water-regime symbols and descriptions (Cowardin and others, 1979).

Nontidal	
A	Temporarily flooded-Surface water present for brief periods during growing season, but water table usually lies well below soil surface. Plants that grow both in uplands and wetlands are characteristic of this water regime.
C	Seasonally flooded-Surface water is present for extended periods, especially early in the growing season, but is absent by the end in most years. When surface water is absent, the water table is often near the land surface.
F	Semipermanently flooded-Surface water persists throughout the growing season in most years. When surface water is absent, the water table is usually at or very near the land surface.
H	Permanently flooded-Water covers land surface throughout the year in all years.

Tidal	
L	Subtidal-Substrate is permanently flooded with tidal water.
M	Irregularly exposed-Land surface is exposed by tides less often than daily.
N	Regularly flooded-Tidal water alternately floods and exposes the land surface at least once daily
P	Irregularly flooded-Tidal water floods the land surface less often than daily.

Mapped palustrine areas included the following classes: unconsolidated bottom or open water ponds (PUB 2008, POW 1956 and 1979), unconsolidated shore (PFL 1956), aquatic bed (PAB 1979), emergent wetlands (PEM), and scrub-shrub (PSS 1956). The palustrine emergent wetlands are fresh or inland marshes not inundated by tidal waters. Open water bodies with a surface area greater than 8ha are classed as lacustrine unconsolidated bottom (L1UB 2008) or open water (L1OW 1956). Lacustrine and palustrine unconsolidated bottom or open water were combined to represent fresh open water in the status report and trend analysis.

Status of Wetlands and Aquatic Habitats, 2008

In 2008, wetland and aquatic habitats covered 2,359 ha within the Powderhorn Ranch study area (fig. 36; table 3) and 4,959 ha was classified as uplands. The palustrine system is the largest of the wetland systems mapped covering 1,515 ha, 64% of all wetland and aquatic habitats (fig. 37). The mean elevation of palustrine marsh is 2.74 m above NAVD88. All emergent vegetated wetlands (E2EM and PEM) cover 2,111 ha. The estuarine intertidal emergent wetland habitat (E2EM) consists of 615 ha of salt or brackish marshes. This habitat makes up 26% of the study area, excluding the upland unit, with a mean elevation of 0.97 m. Approximately 132 ha of estuarine tidal flats and algal flats (E2US and E2AB) was mapped in the study area. The mean elevation of the tidal flats was 24 cm lower than the estuarine marshes. The total mapped area of palustrine and lacustrine open water (fresh) in Powderhorn Ranch was approximately 28 ha, around 1% of mapped wetland and aquatic habitats in 2008.

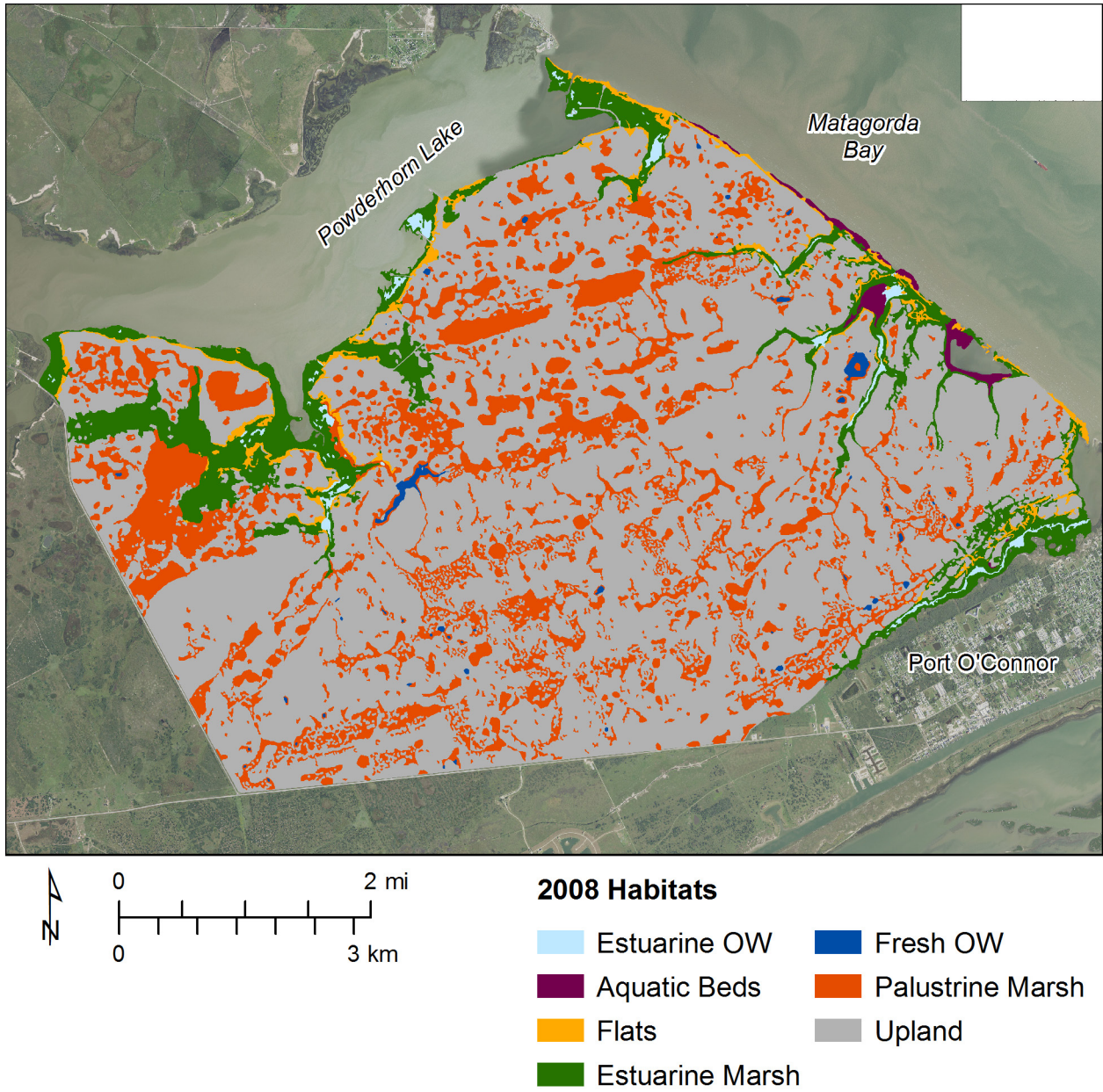


Figure 36. Areal distribution of major habitats on Powderhorn Ranch in 2008. Modified from Tremblay and Calnan (2010).

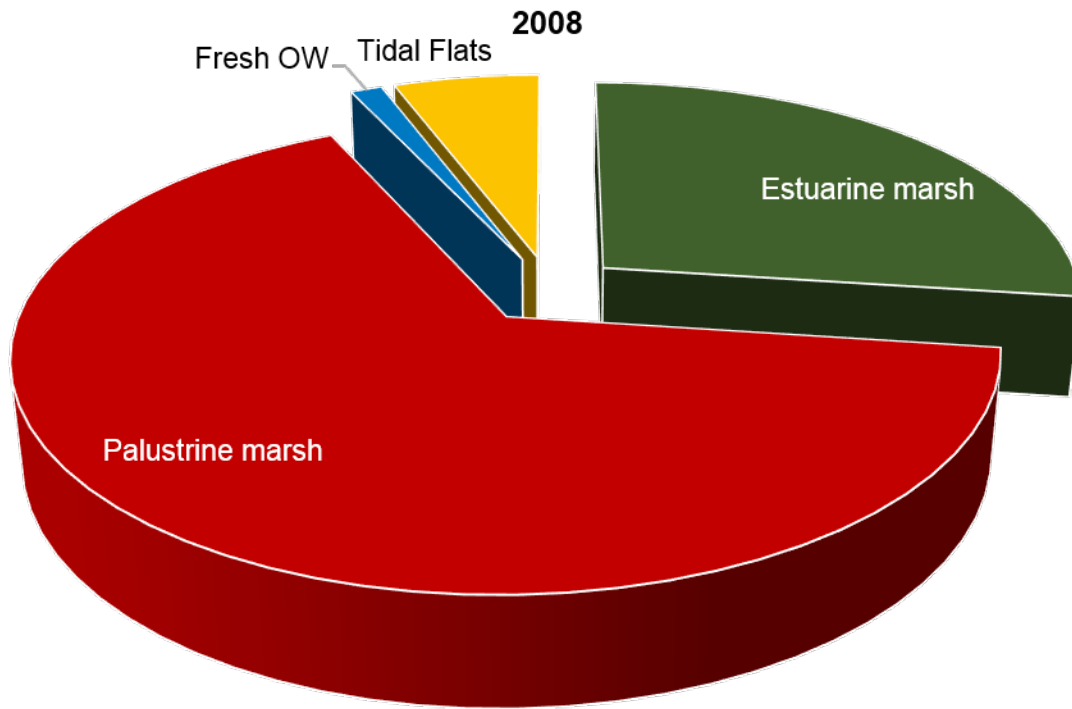


Figure 37. Areal extent of selected habitats in the Powderhorn Ranch area in 2008. Fresh open water (OW) in this figure includes palustrine and lacustrine waters.

Table 3. Areal extent of mapped wetland and aquatic habitats, 2008.

NWI Code	Hectares	Acres	%
E1AB3	39.17	96.79	2
E1UBL	48.25	119.23	2
E2AB1P	0.42	1.04	0
E2EM1N	367.79	908.82	16
E2EM1P	247.18	610.80	10
E2USM	4.04	9.99	0
E2USN	16.52	40.82	1
E2USP	110.90	274.03	5
L1UBH	9.13	22.56	0
PEM1A	871.05	2,152.40	37
PEM1C	520.54	1,286.28	22
PEM1F	104.45	258.11	4
PUB	19.24	47.55	1
Total	2,359	5,828	100

Historical Trends in Wetland and Aquatic Habitats

Broad wetland classes were emphasized over water regimes in analyzing historical trends due to the limitations of the 1956 mapping. The total area of estuarine marshes increased from 580 ha in 1956 to 811 ha in 1979, then decreased to 615 ha in 2008 (figs. 38 and 39; table 4). Palustrine marsh increased from 771 ha in 1956 to 1,448 in 1979, a gain of almost 30 ha/year. The total area of palustrine marsh in 2008 was similar (1,496 ha) to 1979, but the distribution of the habitat differed (fig. 38). Fresh open water areas decreased by approximately half between 1956 (53 ha) and 1979 (27 ha) and remained stable in 2008 (28 ha). A recurring trend in wetland habitat studies along the Texas coast is the loss of tidal flats through time (Tremblay and Calnan, 2010). In the Powderhorn Ranch study area, tidal flats covered 282 ha in 1956 and were reduced to 111 ha in 1979. There was a slight increase of tidal flats to 132 ha in 2008. The overall tidal flat habitat was reduced by 53% between 1956 and 2008 at a rate of 3 ha/yr.

Analysis of trends in wetlands and aquatic habitats in the Powderhorn Ranch area show that there was a slight net increase in marshes from 1956 through 2008. Emergent wetlands (both estuarine and palustrine) increased from 1,352 ha to 2,111 ha, a gain of 759 ha (fig. 40). Marsh area fluctuated through the study time period. The rate of marsh gain from 1956 to 1979 was 39 ha/yr, and from 1979 to 2008 marsh lost 5 ha/yr. The long-term (1956-2008) change rate of marsh was a gain of 15 ha/yr.

Although areas of fresh open water decreased over time, the increase of emergent marsh habitats between 1956 and 1979 may be due to the wetter conditions during the later period. The severe drought that occurred in Texas in the 1950s, peaked in 1956 (Riggio and others, 1987) limiting the extent of marsh habitats. The increase in palustrine marsh into upland habitat between 1956 and 2008 may be due to wetter conditions in the later time periods. The decrease in in estuarine marshes between 1979 and 2008 may be due to relative sea level rise and partly due to interpretational differences between mapping periods (Tremblay and Calnan, 2010).

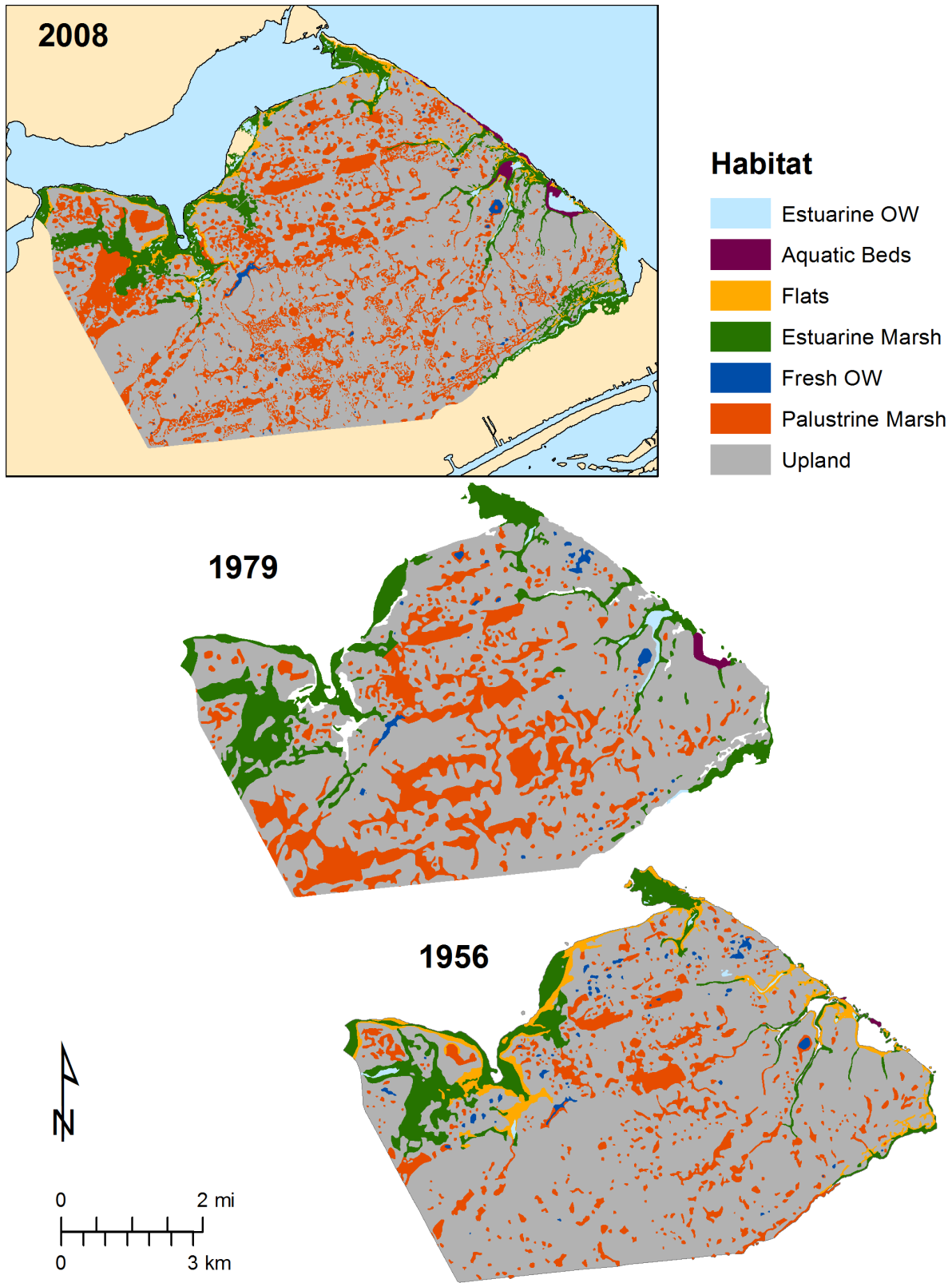


Figure 38. Maps showing distribution of major wetland and aquatic habitats in 2008, 1979, and 1956 in the Powderhorn Ranch area. Modified from Tremblay and Calnan (2010).

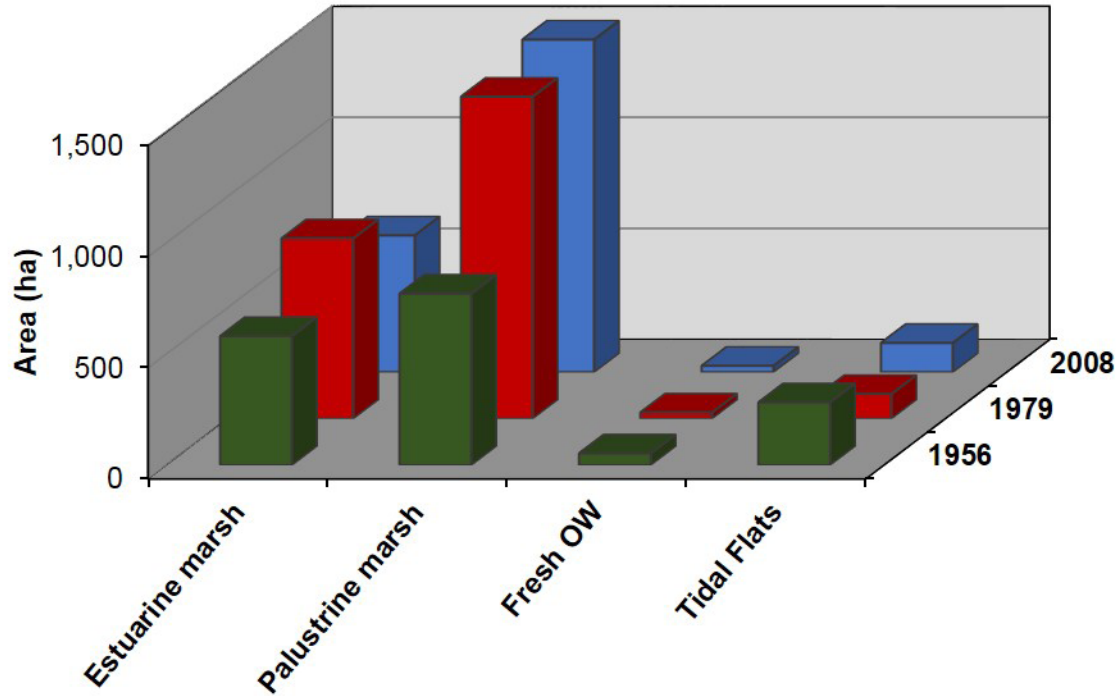


Figure 39. Areal distribution of habitats in Powderhorn Ranch in 1956, 1979, and 2008.

Table 4. Total area (ha and acres) of major habitats, including uplands, in 1956, 1979, and 2008.

Habitat	1956		1979		2008	
	ha	acres	ha	acres	ha	acres
Estuarine marsh	580	1,434	811	2,004	615	1,520
Palustrine marsh	771	1,906	1,448	3,578	1,496	3,697
Fresh OW	53	132	27	68	28	70
Tidal Flats	282	697	111	273	132	326
Uplands	5,291	13,819	4,872	12,039	4,959	12,253

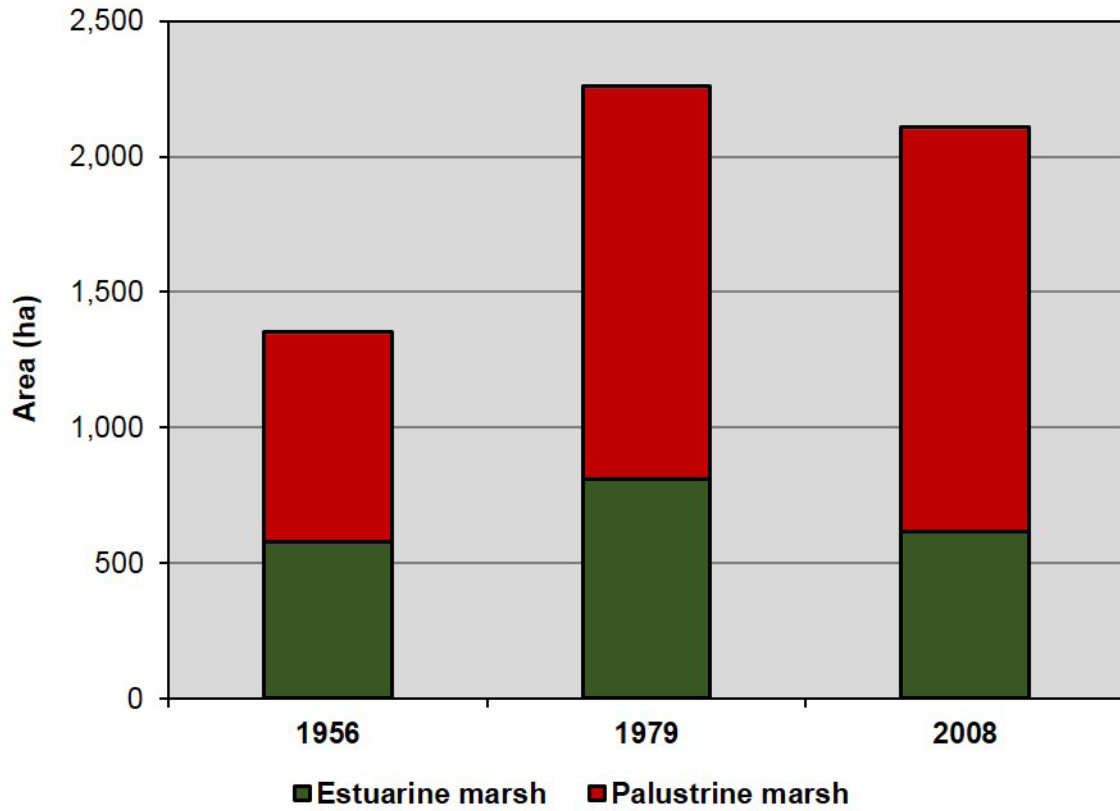


Figure 40. Areal distribution of emergent marsh habitats in Powderhorn Ranch in 1956, 1979, and 2008.

Acknowledgments

This project was partly supported by a Texas Coastal Management Program Grant approved by the Texas Land Commissioner pursuant to National Oceanic and Atmospheric Administration Award No. NA16NOS4190174. Work was completed under Contract No. 17-186-000-9823 from the General Land Office of Texas (GLO). Julie McEntire (GLO) served as project manager. Jeffrey G. Paine served as principal investigator. Daniel Walker (Texas Parks and Wildlife Department) and James Brown (Powderhorn Ranch foreman) facilitated access to Powderhorn Ranch for multiple field visits between 2015 and 2018. BEG staff Aaron Averett, John Hupp, John Andrews, and Kutalmis Saylam acquired and processed topographic data from an airborne lidar survey of Powderhorn Ranch in 2016. Tom Tremblay and Tom Calnan conducted the status and trends study of wetland and aquatic habitats.

References

- Aronow, S., 1971, Nueces River delta plain of Pleistocene Beaumont Formation, Corpus Christi region, Texas: American Association of Petroleum Geologists Bulletin, v. 55, p. 1231-1248.
- Brown, T. E., Brewton, J. L., McGowen, J. H., Proctor, C. V., Aronow, S., and Barnes, V. E., 1975, Geologic Atlas of Texas, Beeville-Bay City Sheet: The University of Texas at Austin, Bureau of Economic Geology, Geologic Atlas Sheet, map scale 1:250,000.
- Cowardin, L.M., Carter, V., Golet, F.C., and LaRoe, E.T., 1979. Classification of wetlands and deepwater habitats of the United States. U.S. Department of Interior, Fish and Wildlife Service, Washington, D.C., USA 131p.
- Doering, J. A., 1956, Review of Quaternary surface formations of Gulf Coast region: American Association of Petroleum Geologists Bulletin, v. 40, p. 1816-1862.
- Freeman, M. D., 2017, History of the Powderhorn property, Calhoun County, Texas: report prepared for Texas Parks and Wildlife Department, 198 p.
- Hayes, C. W., and Kennedy, W., 1903, Oil fields of the Texas-Louisiana gulf coastal plain: U.S. Geological Survey Bulletin 212, 174 p.
- Imbrie, J., Hays, J. D., Martinson, D. G., McIntyre, A., Mix, A. C., Morley, J. J., Pisias, N. G., Prell, W. L., and Shackleton, N. J., 1984, The orbital theory of Pleistocene climate: support from a revised chronology of the marine 180 record: in Milankovitch and Climate, Part I, New York, Springer, p. 269-305.
- Lisiecki, L. E., and Raymo, M. E., 2005, A Pliocene-Pleistocene stack of 57 globally distributed benthic $\delta^{18}O$ records: Paleoceanography, v. 20, 17 p..
- Lorius, C., Jouzel, J., Ritz, C., Merlivat, L., Barkov, N. I., Korotkevich, Y. S., and Kotlyakov, V. M., 1985, A 150,000-year climatic record from Antarctic ice: Nature, v. 316, p. 591-596.
- Metcalf, R. J., 1940, Deposition of Lissie and Beaumont Formations of Gulf Coast of Texas: American Association of Petroleum Geologists Bulletin, v. 24, p. 693-700.
- McGowen, J. H., and Brewton, J. L., 1975, Historical Changes and Related Coastal Processes, Gulf and Mainland Shorelines, Matagorda Bay Area, Texas: The University of Texas at Austin, Bureau of Economic Geology, Special Report SR0003, 72 p.
- McGowen, J. H., Proctor, C. V., Jr., Brown, L. F., Jr., Evans, T. J., Fisher, W. L., and Groat, C. G., 1976, Environmental Geologic Atlas of the Texas Coastal Zone - Port Lavaca Area: The University of Texas at Austin, Bureau of Economic Geology, Environmental Geologic Atlas EA0007, 107 p.
- Paine, J. G., Caudle, T., and Andrews, J. R., 2016, Shoreline movement in the Copano, San Antonio, and Matagorda Bay systems, central Texas coast, 1930s to 2010s: Bureau of Economic Geology, The University of Texas at Austin, Special Report SR0003, 72 p.

- ty of Texas at Austin, Final Report prepared for General Land Office under contract no. 13-258-000-7485, 72 p.
- Paine, J. G., and Collins, E. W., 2016, Geologic map of the Port O'Connor Quadrangle, Texas Gulf of Mexico Coast: Sheet 1: The University of Texas at Austin, Bureau of Economic Geology, Open-File Map, 1:24,000.
- Paine, J. G., and Collins, E. W., 2016, Geologic map of the Port O'Connor Quadrangle, Texas Gulf of Mexico Coast: Sheet 2, Geophysical logs and time-domain electromagnetic induction soundings: The University of Texas at Austin, Bureau of Economic Geology, Open-File Map, 1:24,000.
- Paine, J. G., and Collins, E. W., 2017, Geologic map of the Port Lavaca East Quadrangle, Texas Gulf of Mexico Coast: The University of Texas at Austin, Bureau of Economic Geology, Open-File Map, no. 0233, 1:24,000.
- Paine, J. G., and Collins, E. W., 2017, Geologic map of the Port Lavaca East Quadrangle, Texas Gulf of Mexico Coast, Sheet 2, Digital elevation model, time-domain electromagnetic induction sounding, and frequency-domain electromagnetic induction measurements: The University of Texas at Austin, Bureau of Economic Geology, Open-File Map, no. 0233.
- Paine, J. G., and Collins, E. W., 2017, Geologic map of the Seadrift NE Quadrangle, Texas Gulf of Mexico Coast: The University of Texas at Austin, Bureau of Economic Geology, Open-File Map, no. 0232, 1:24,000.
- Paine, J. G., and Collins, E. W., 2017, Geologic map of the Seadrift NE Quadrangle, Texas Gulf of Mexico Coast, Sheet 2, Digital elevation model geophysical logs, time-domain electromagnetic induction soundings, and frequency-domain electromagnetic induction measurements: The University of Texas at Austin, Bureau of Economic Geology, Open-File Map, no. 0232.
- Price, W. A., 1934, Lissie formation and the Beaumont clay in south Texas: American Association of Petroleum Geologists Bulletin, v. 18, p. 948-959.
- Price, W. A., 1958, Sedimentology and Quaternary geomorphology of south Texas," in Gulf Coast Association of Geological Societies Transactions, v. 8, p. 41-75.
- Riggio, R.R., Bomar, G.W., and Larkin, T.J., 1987, Texas drought: its recent history (1931-1985). Texas Water Commission, LP 87-04, 74p.
- Robin, G. d. Q., 1985, Contrasts in Vostok core — changes in climate or ice volume?: Nature, v. 316, p. 578-579.
- Roth, D., 2010, Texas hurricane history: National Weather Service, Camp Springs, Maryland, 83 p. <http://origin.hpc.ncep.noaa.gov/research/txhur.pdf>
- Simpson, R. H., and Riehl, H., 1981, The hurricane and its impact: Baton Rouge, Louisiana State University Press, 398 p.
- Sellards, E. H., Adkins, W. S., and Plummer, F. B., 1932, The geology of Texas, Volume I: stratigraphy: The University of Texas, Austin, Bulletin 3232, 1007 p.
- Shackleton, N. J., and Opdyke, N. D., 1973, Oxygen isotope paleomagnetic stratigraphy of equatorial Pacific core V28–238: oxygen isotope temperatures and ice volumes on a 105 and 106 year scale: Quaternary Research, v. 3, p. 39-55.
- Shackleton, N. J., and Opdyke, N. D., 1976, Oxygen-isotope and paleomagnetic stratigraphy of Pacific core V28–239: late Pliocene to latest Pleistocene: Geological Society of America Memoir 145, p. 449-464.
- Tremblay, T.A., and Calnan, T.R., 2010. Status and Trends of Inland Wetland and Aquatic Habitats, Matagorda Bay Area. Austin, Texas: University of Texas at Austin, Bureau of Economic Geology Report Prepared for General Land Office Contract 09-046 and National Oceanic and Atmospheric Administration Award NA-08NOS4190458, 71p.

- White, W. A., Calnan, T. R., Morton, R. A., and others, 1989, Submerged Lands of Texas, Port Lavaca Area: Sediments, Geochemistry, Benthic Macroinvertebrates, and Associated Wetlands: The University of Texas at Austin, Bureau of Economic Geology, SLO007, 165 p.
- U. S. Army Corps of Engineers, 1962, Report on Hurricane Carla: 9-12 September 1961: Galveston District, U.S. Army Corps of Engineers, 29 p.
- U. S. Army Corps of Engineers, 1968, Report on Hurricane "Beulah": 8-21 September 1967: Galveston District, U.S. Army Corps of Engineers, 26 p.

Appendix A: Water Wells, Windmills, and Geophysical logs

Water wells and windmills on Powderhorn Ranch (fig. 6). Ground elevations were determined from an airborne lidar survey conducted by the Bureau of Economic Geology in July 2016. Well and water depths are measured from the ground surface. Total dissolved solids (TDS) concentration is estimated from the measured electrical conductivity of samples drawn from the wells during geophysical logging. Wells PH01 through PH19 were geophysically logged using spectral gamma and electromagnetic induction borehole tools (figs. A1 to A19).

Well	Longitude (degrees W)	Latitude (degrees N)	Well Type	Ground elevation (m)	Well depth (m)	Water depth (m)	TDS (mg/L)
PH01	96.52396	28.43960	PVC	3.66	84.1	4.33	829
PH02	96.44973	28.48747	PVC	1.97	92.4	3.95	2500
PH03	96.45591	28.45090	PVC	3.71	61.16	4.98	633
PH04	96.46777	28.45580	PVC	4.32	60.33	5.4	686
PH05	96.42224	28.46530	PVC	2.16	86.8	3.67	1640
PH06	96.50630	28.44681	PVC	4.43	78.61	5.52	1240
PH07	96.49488	28.49355	PVC	2.49	58.81	3.9	847
PH08	96.48898	28.45769	PVC	4.89	62.82	5.76	-
PH09	96.50990	28.47980	PVC	1.83	89.25	3.29	2110
PH10	96.52297	28.46430	PVC	1.59	78.6	2.39	-
PH11	96.46915	28.43289	PVC	2.96	60.43	3.41	905
PH12	96.46721	28.43686	PVC	3.49	61.91	4.92	1000
PH13	96.46067	28.44271	PVC	3.24	60.11	4.48	889
PH14	96.46095	28.44611	PVC	3.64	59.54	4.96	937
PH15	96.47635	28.50143	PVC	2.61	89.04	3.81	407
PH16	96.51126	28.47553	PVC	1.15	61.18	0.99	954
PH17	96.52424	28.45815	PVC	2.51	72.52	2.96	191
PH18	96.51703	28.47479	PVC	1.61	93.4	2.56	3230
PH19	96.49339	28.49593	PVC	2.26	96.54	3.67	2650
-	96.46307	28.49750	Supply	3.33	-	-	-
-	96.46868	28.46638	Windmill	4.26	-	-	-
-	96.43181	28.46447	Windmill	3.20	-	-	-
-	96.47683	28.43371	Windmill	3.49	-	-	-
-	96.48955	28.47906	Windmill	2.93	-	-	-
-	96.50754	28.46020	Windmill	2.53	-	-	-
-	96.44753	28.44666	Windmill	2.47	-	-	-
-	96.52795	28.43593	Windmill	4.06	-	-	-

PH01
Elevation: 3.66 m NAVD88 (BEG 2016 lidar survey)
Lat. 28.43960° N; Lon. 96.52396° W

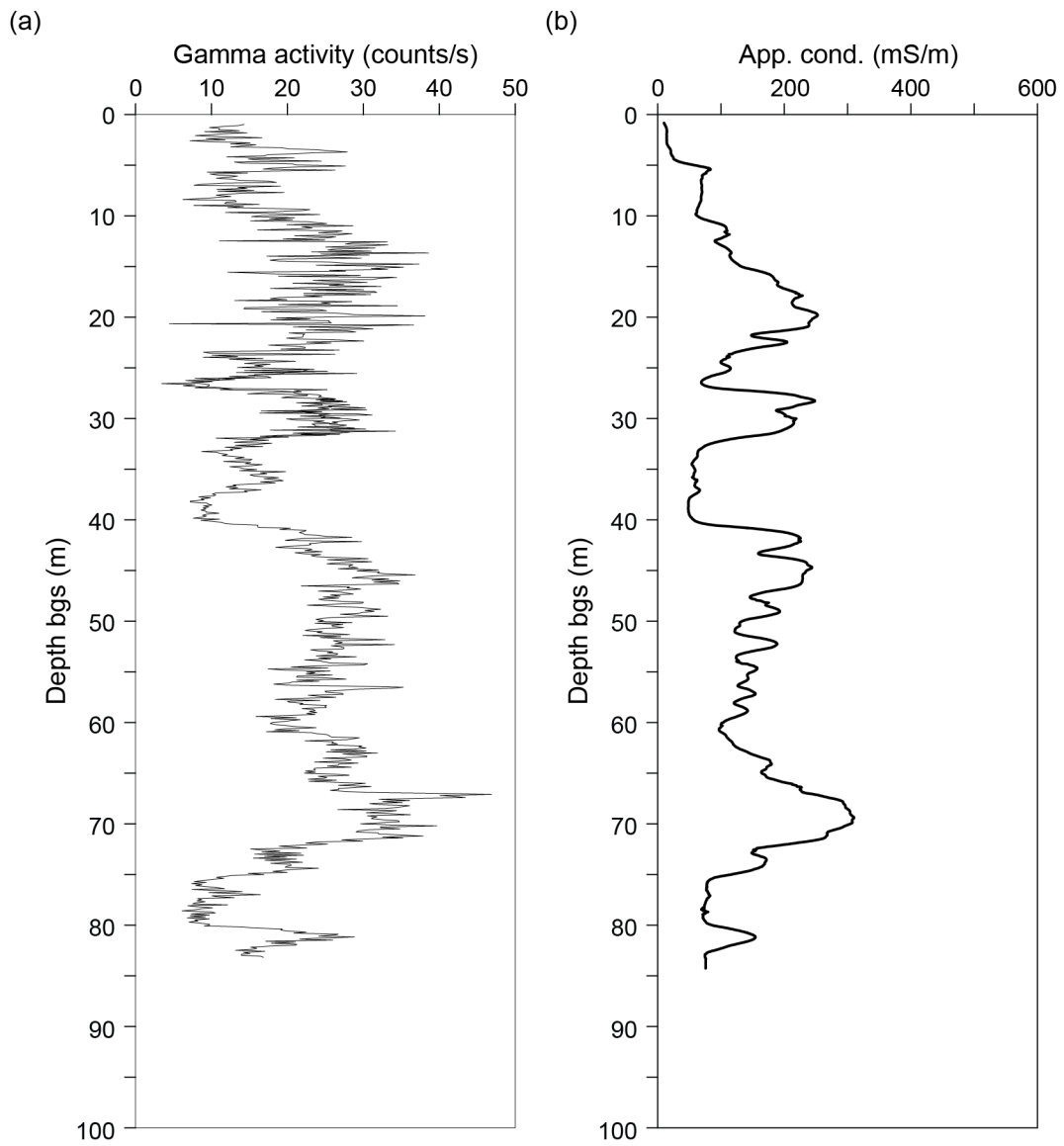


Figure A1. Natural gamma and apparent conductivity logs from water well PH01 (fig. 13). The well was logged on February 16, 2016 and January 11, 2018.

PH02
Elevation: 1.97 m NAVD88 (BEG 2016 lidar survey)
Lat. 28.48747° N; Lon. 96.44973° W

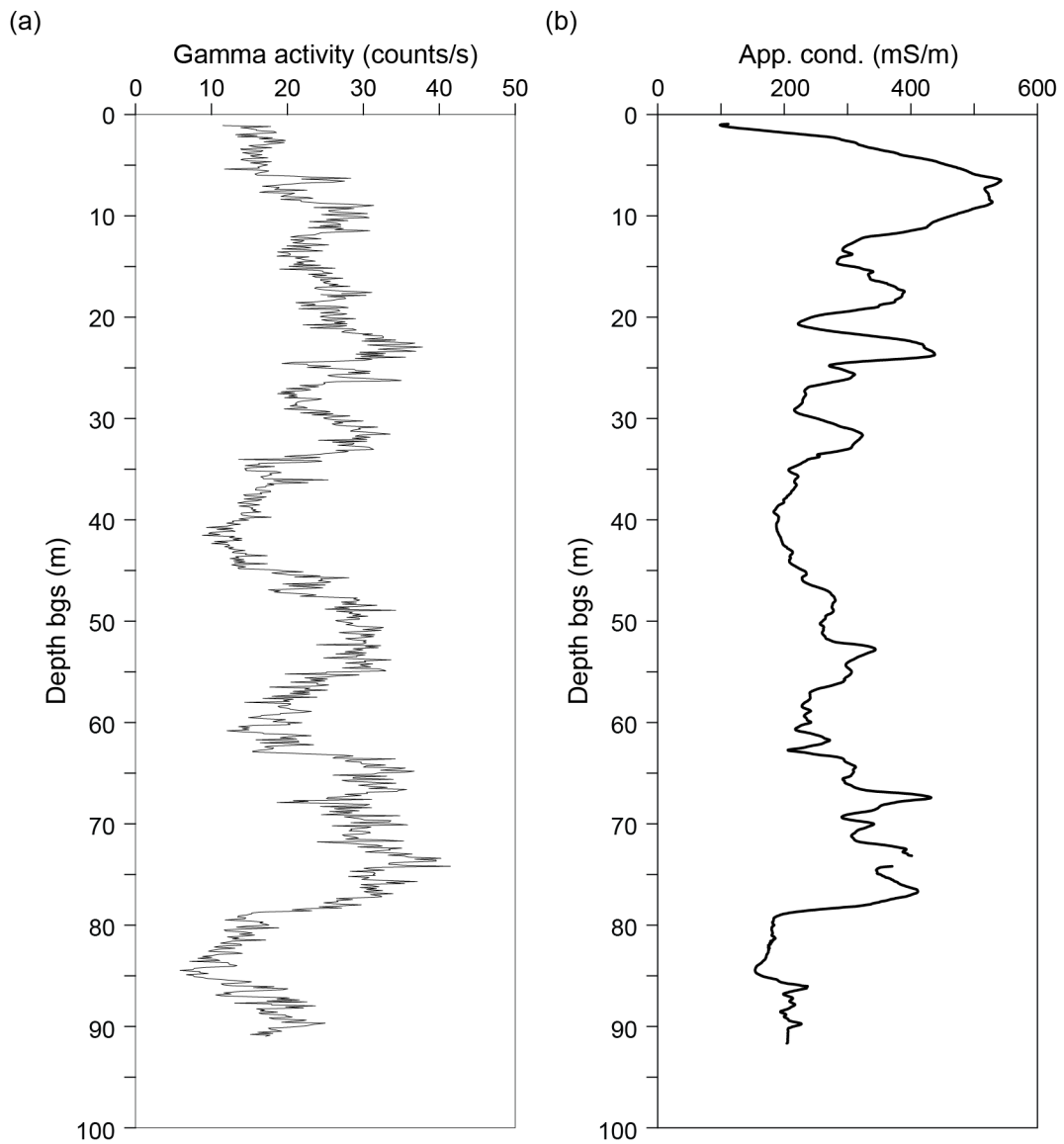


Figure A2. Natural gamma and apparent conductivity logs from water well PH02 (fig. 13). The well was logged on February 16, 2016.

PH03
Elevation: 3.71 m NAVD88 (BEG 2016 lidar survey)
Lat. 28.45090° N; Lon. 96.45591° W

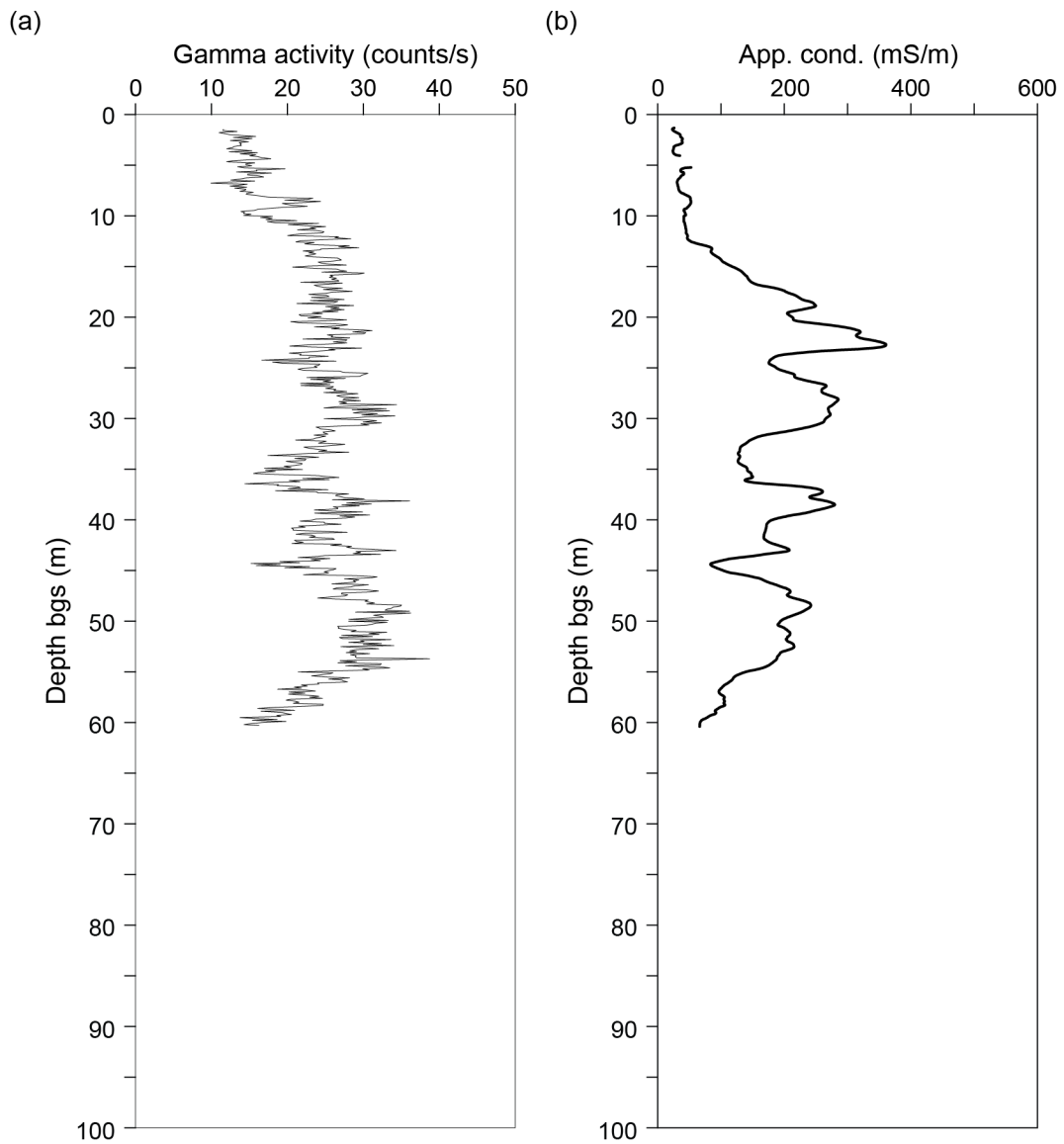


Figure A3. Natural gamma and apparent conductivity logs from water well PH03 (fig. 13). The well was logged on February 17, 2016.

PH04
Elevation: 4.32 m NAVD88 (BEG 2016 lidar survey)
Lat. 28.45580° N; Lon. 96.46777° W

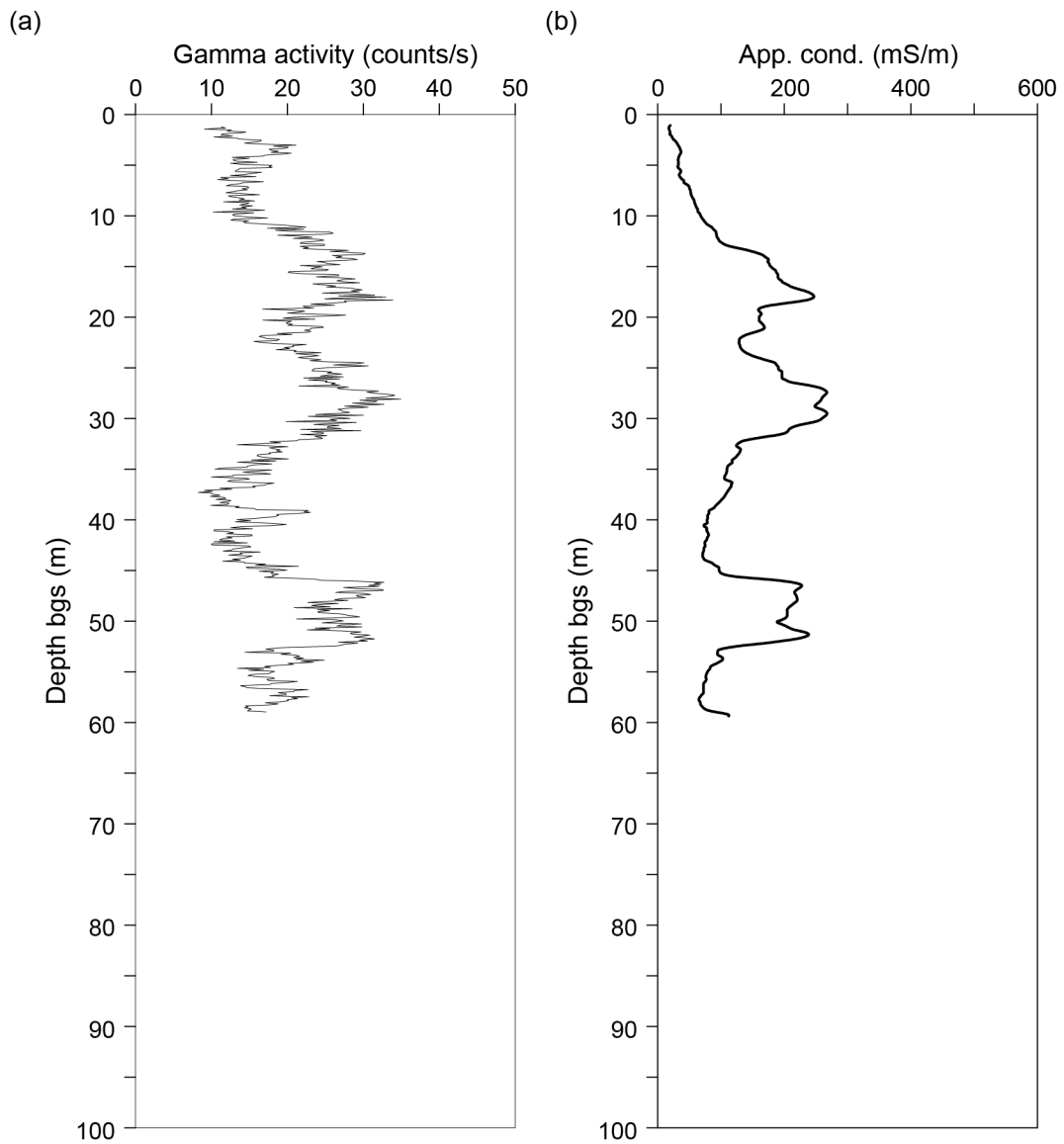


Figure A4. Natural gamma and apparent conductivity logs from water well PH04 (fig. 13). The well was logged on February 17, 2016 and January 10, 2018.

PH05
Elevation: 2.16 m NAVD88 (BEG 2016 lidar survey)
Lat. 28.46530° N; Lon. 96.42224° W

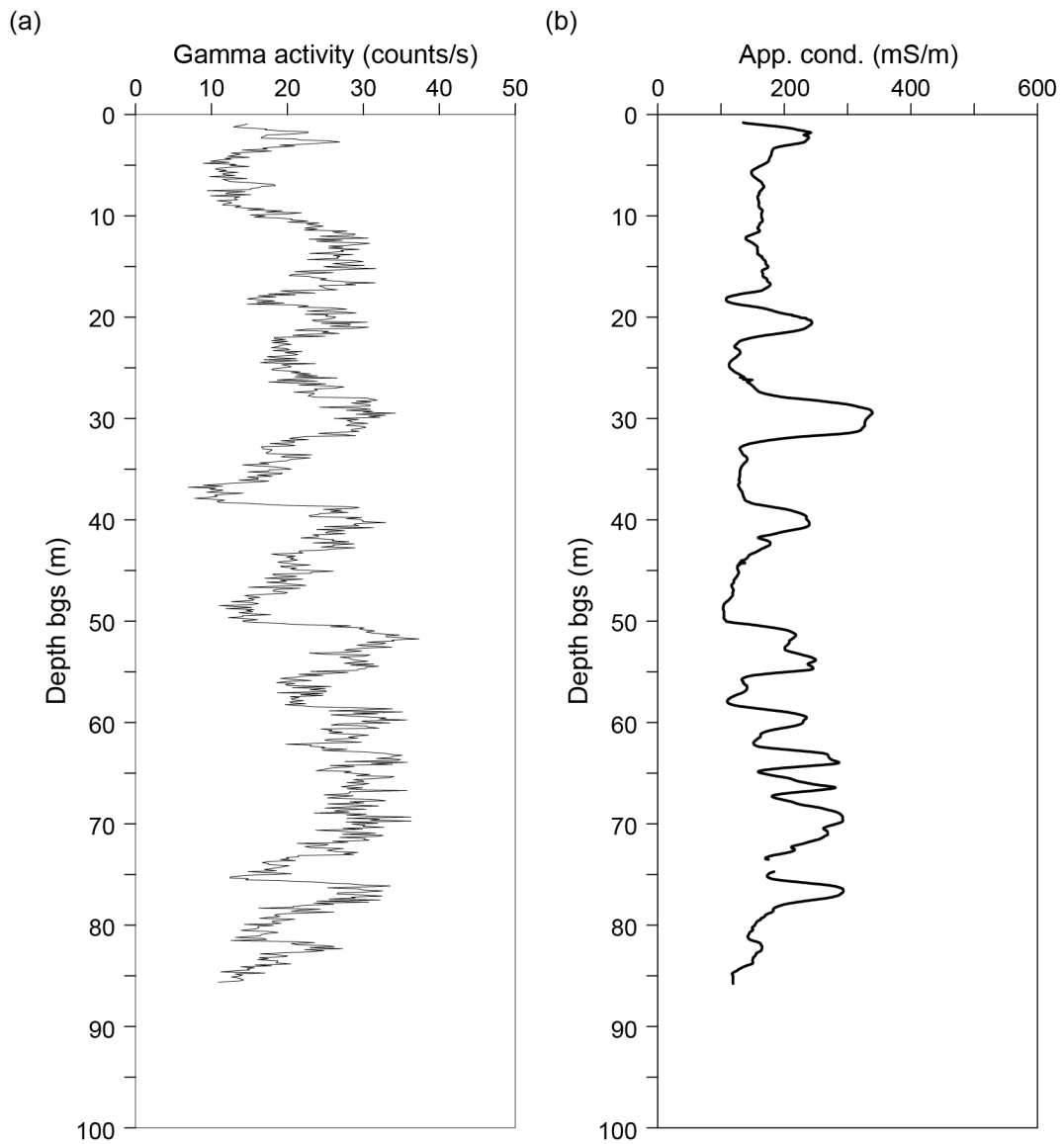


Figure A5. Natural gamma and apparent conductivity logs from water well PH05 (fig. 13). The well was logged on February 18, 2016 and January 9, 2018.

PH06
Elevation: 4.43 m NAVD88 (BEG 2016 lidar survey)
Lat. 28.44681° N; Lon. 96.50630° W

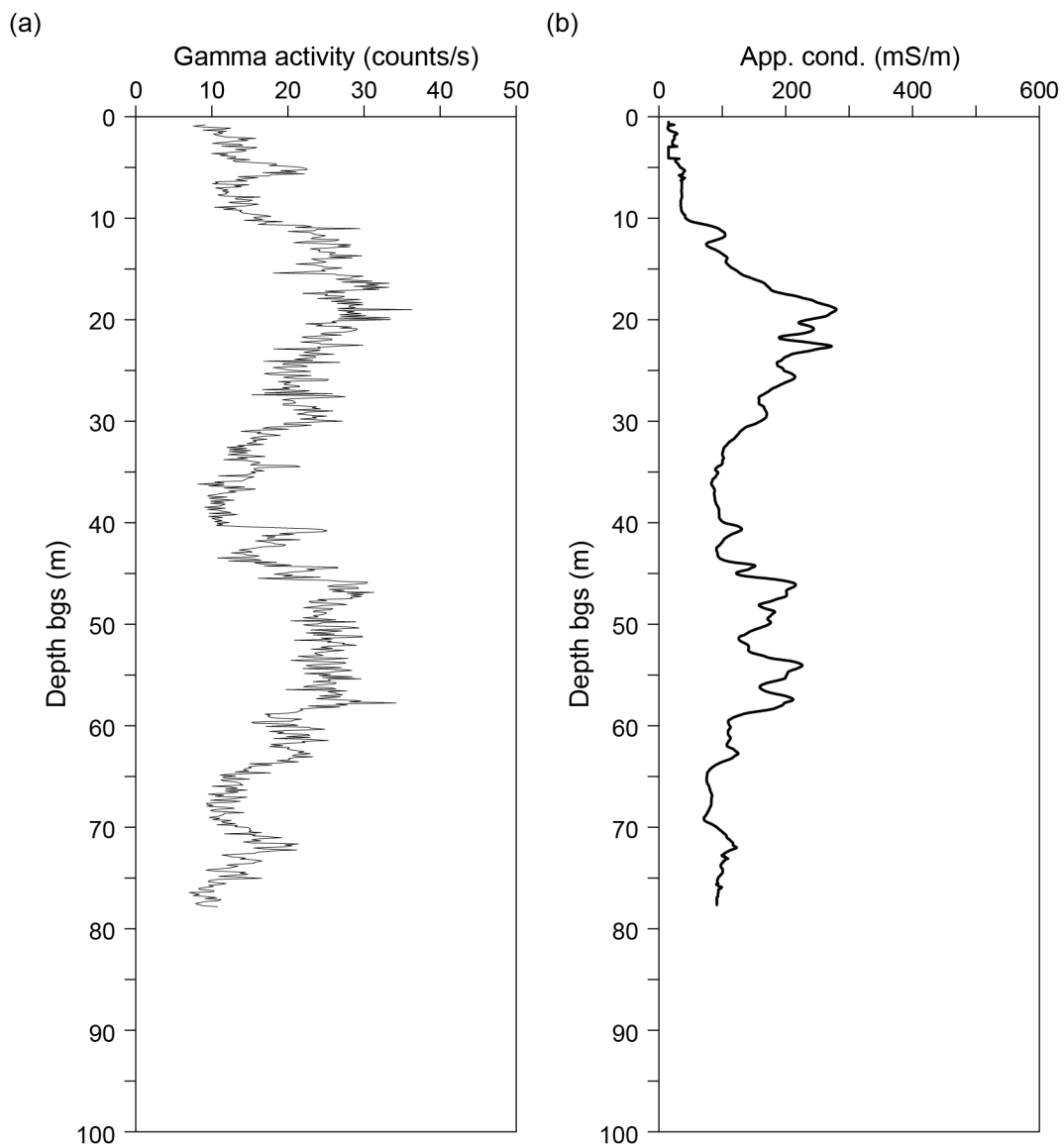


Figure A6. Natural gamma and apparent conductivity logs from water well PH06 (fig. 13). The well was logged on February 19, 2016 and January 10, 2018.

PH07
Elevation: 2.49 m NAVD88 (BEG 2016 lidar survey)
Lat. 28.49355° N; Lon. 96.49488° W

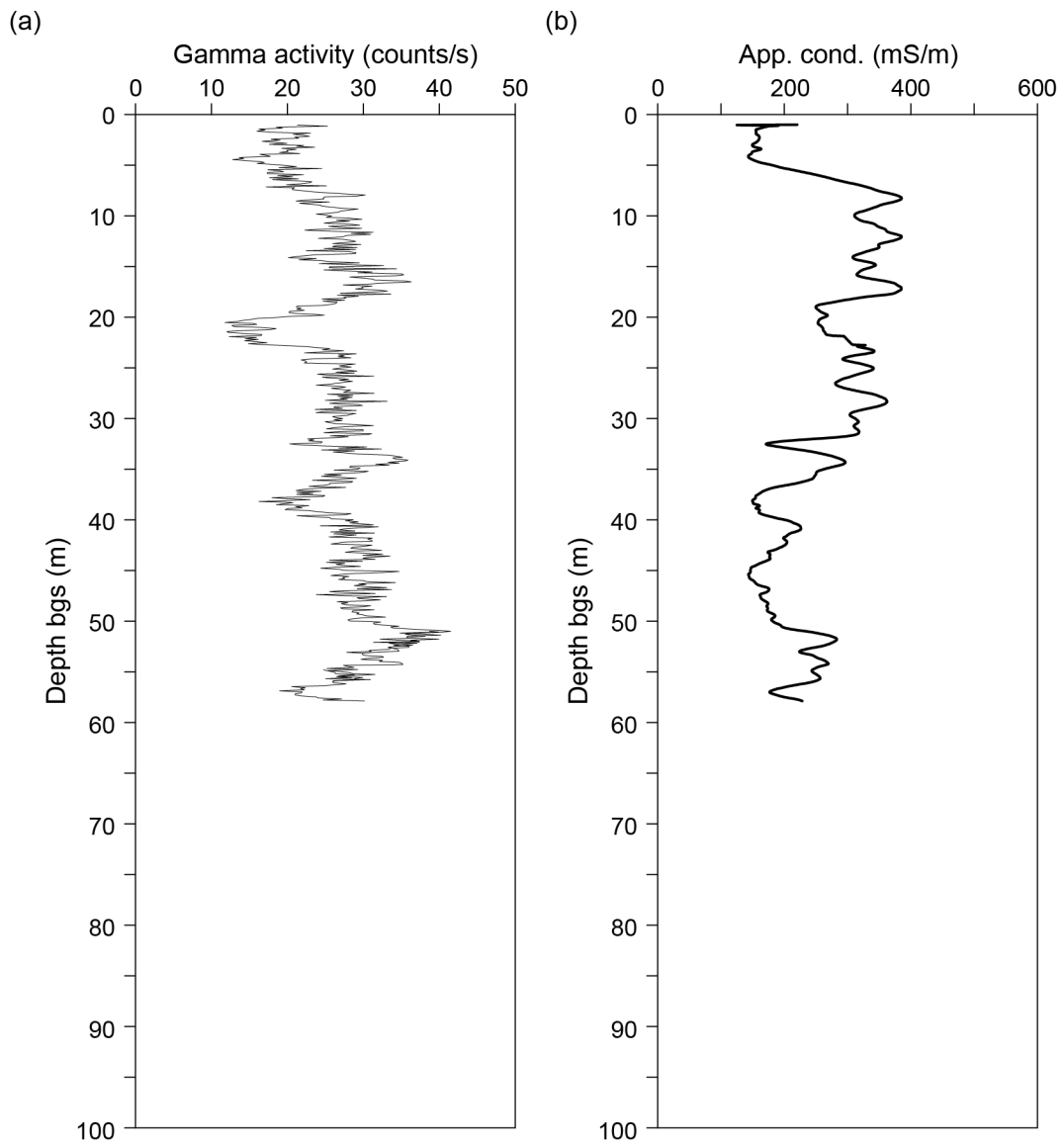


Figure A7. Natural gamma and apparent conductivity logs from water well PH07 (fig. 13). The well was logged on May 17, 2016.

PH08
Elevation: 4.89 m NAVD88 (BEG 2016 lidar survey)
Lat. 28.45769° N; Lon. 96.48898° W

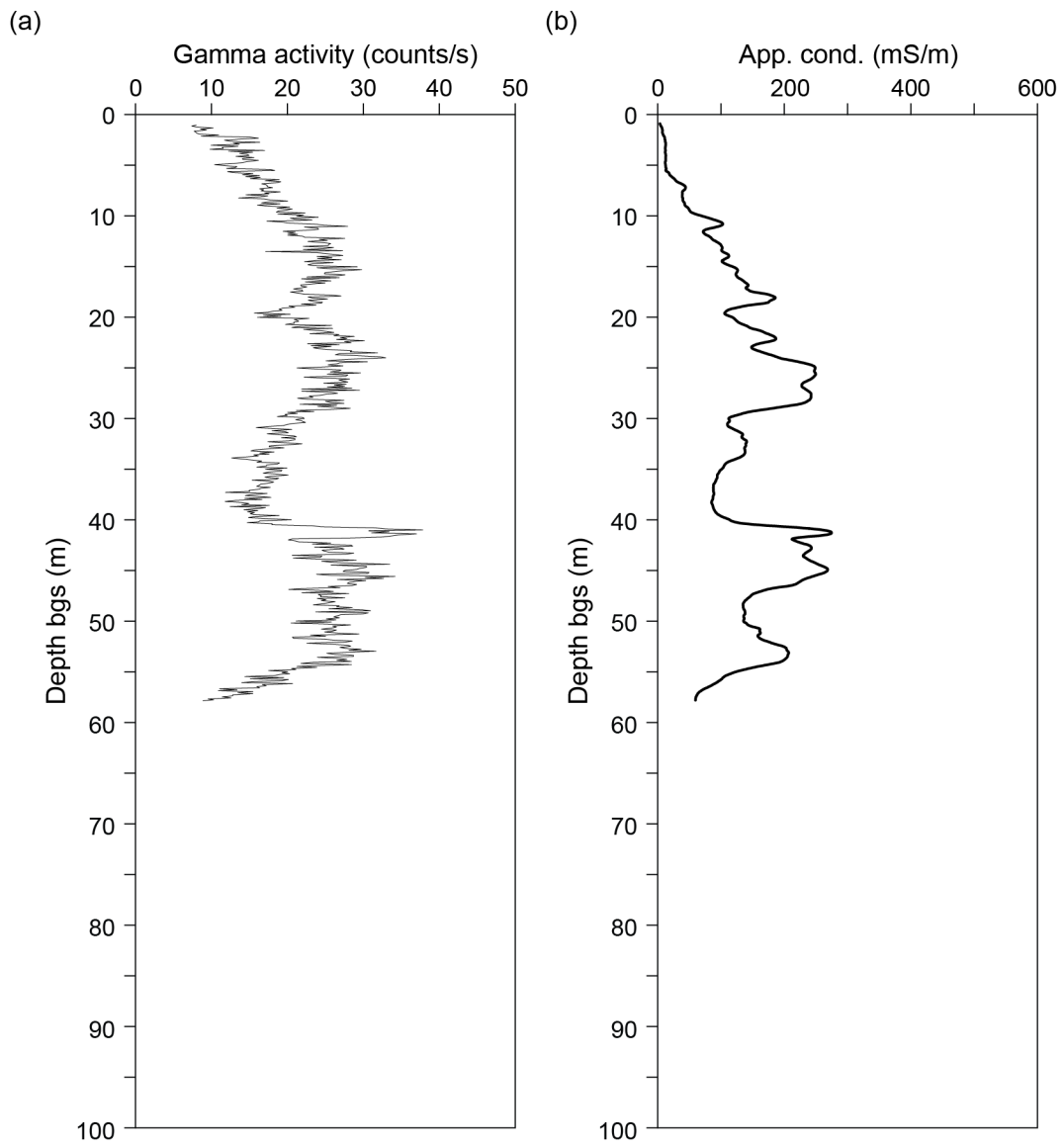


Figure A8. Natural gamma and apparent conductivity logs from water well PH08 (fig. 13). The well was logged on May 17, 2016.

PH09
Elevation: 1.83 m NAVD88 (BEG 2016 lidar survey)
Lat. 28.47980° N; Lon. 96.50990° W

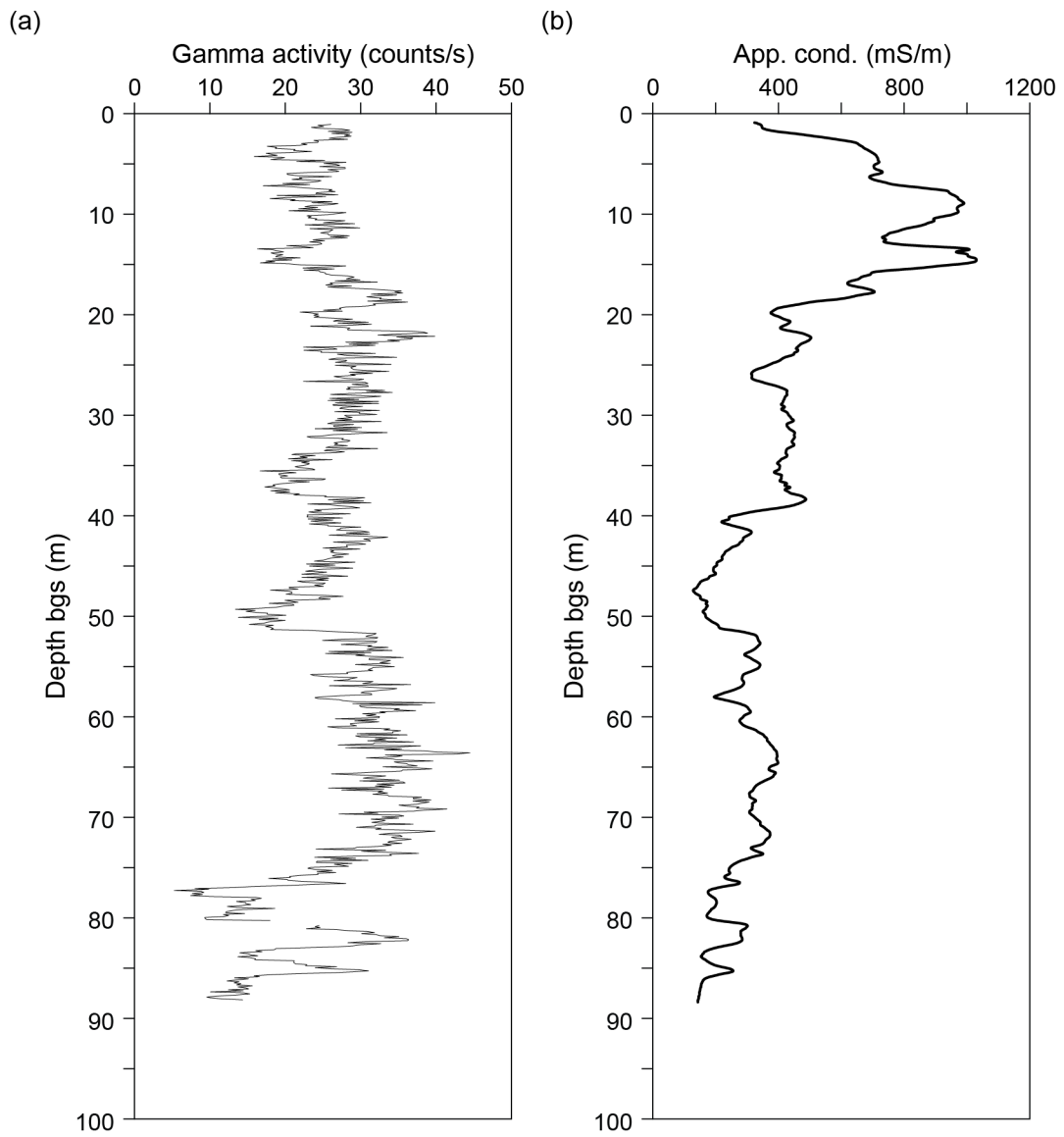


Figure A9. Natural gamma and apparent conductivity logs from water well PH09 (fig. 13). The well was logged on May 18, 2016.

PH10
Elevation: 1.59 m NAVD88 (BEG 2016 lidar survey)
Lat. 28.46430° N; Lon. 96.52297° W

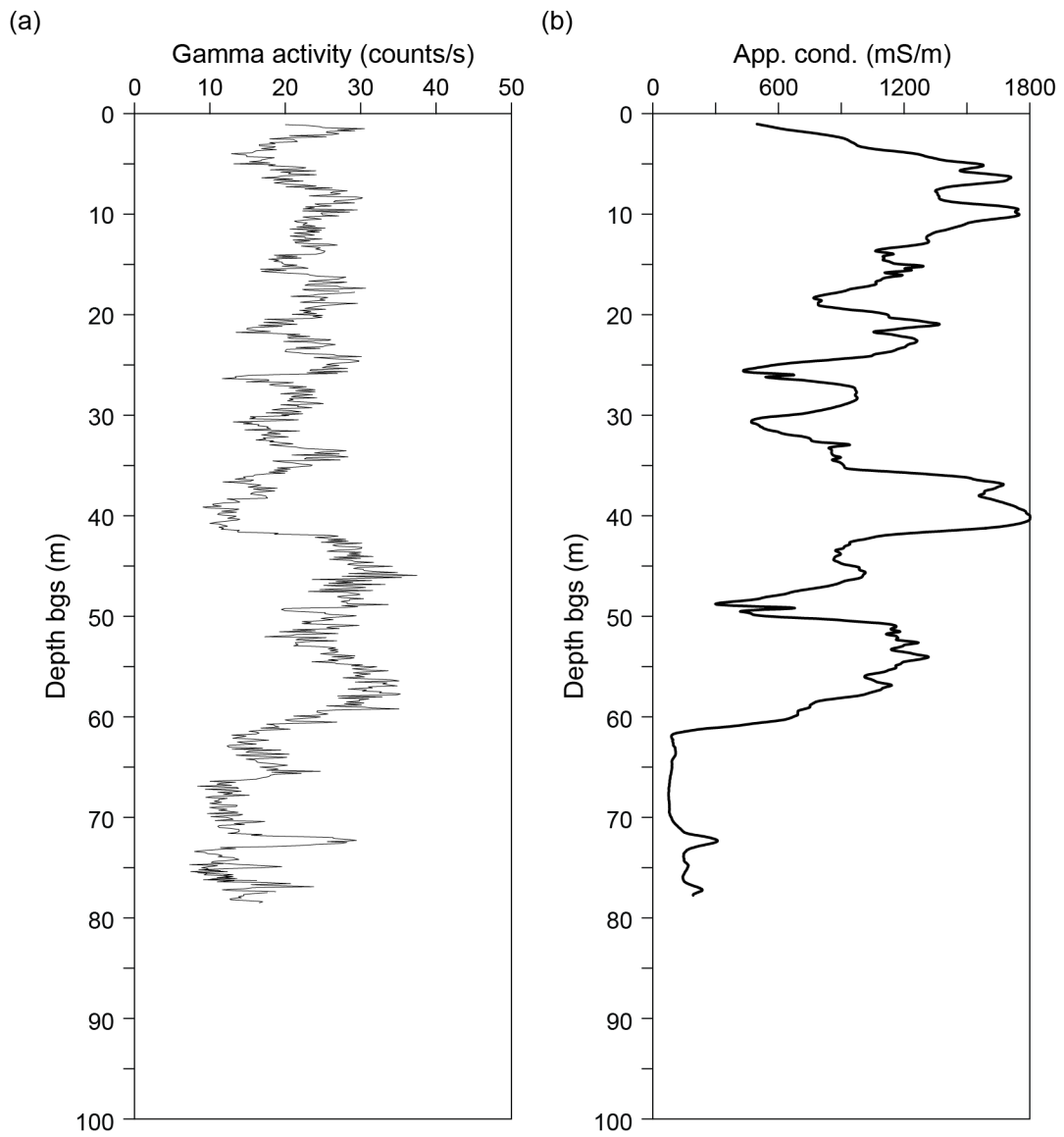


Figure A10. Natural gamma and apparent conductivity logs from water well PH10 (fig. 13). The well was logged on December 6, 2016.

PH11
Elevation: 2.96 m NAVD88 (BEG 2016 lidar survey)
Lat. 28.43289° N; Lon. 96.46915° W

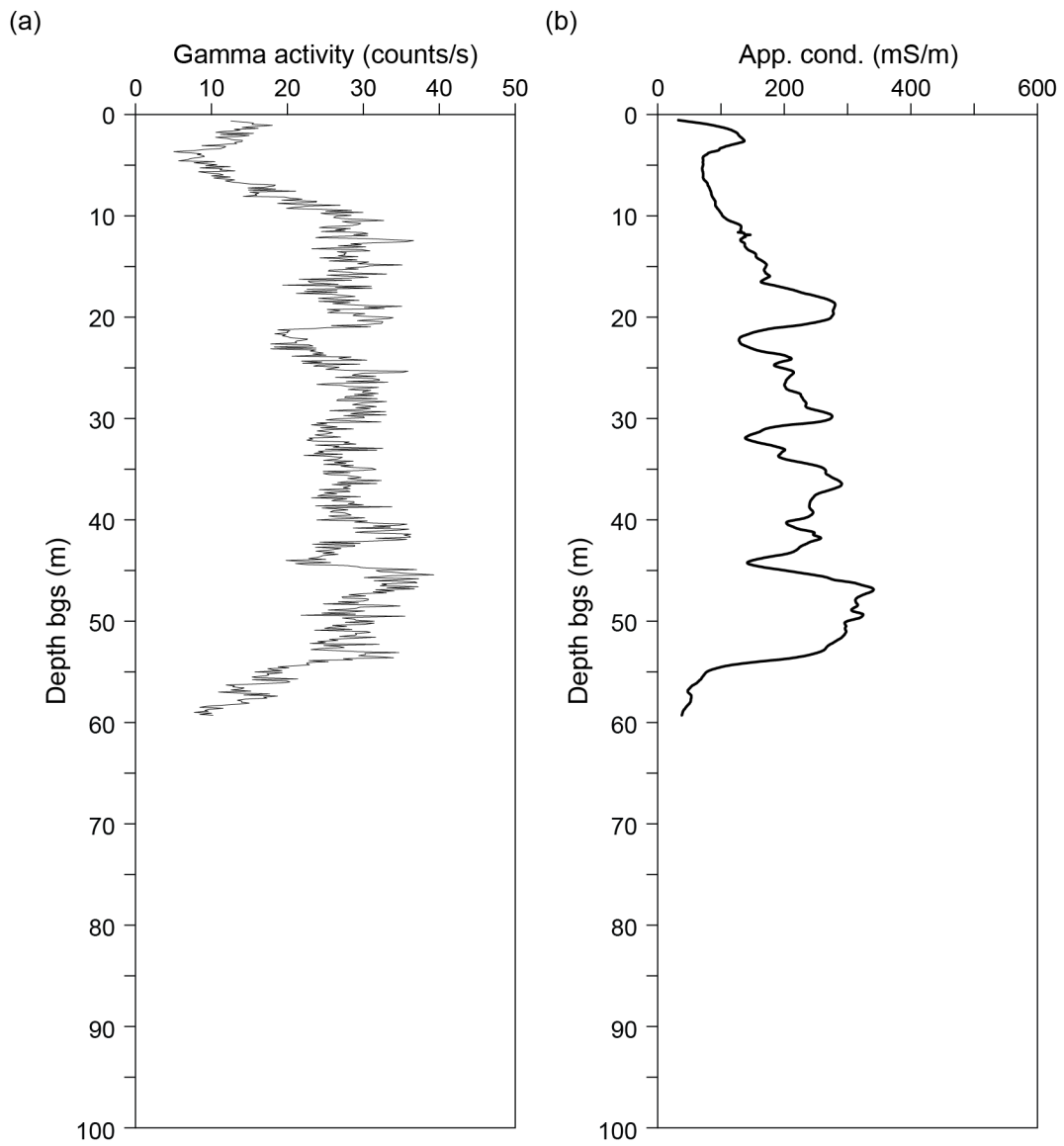


Figure A11. Natural gamma and apparent conductivity logs from water well PH11 (fig. 13). The well was logged on April 25, 2017.

PH12
Elevation: 3.49 m NAVD88 (BEG 2016 lidar survey)
Lat. 28.43686° N; Lon. 96.46721° W

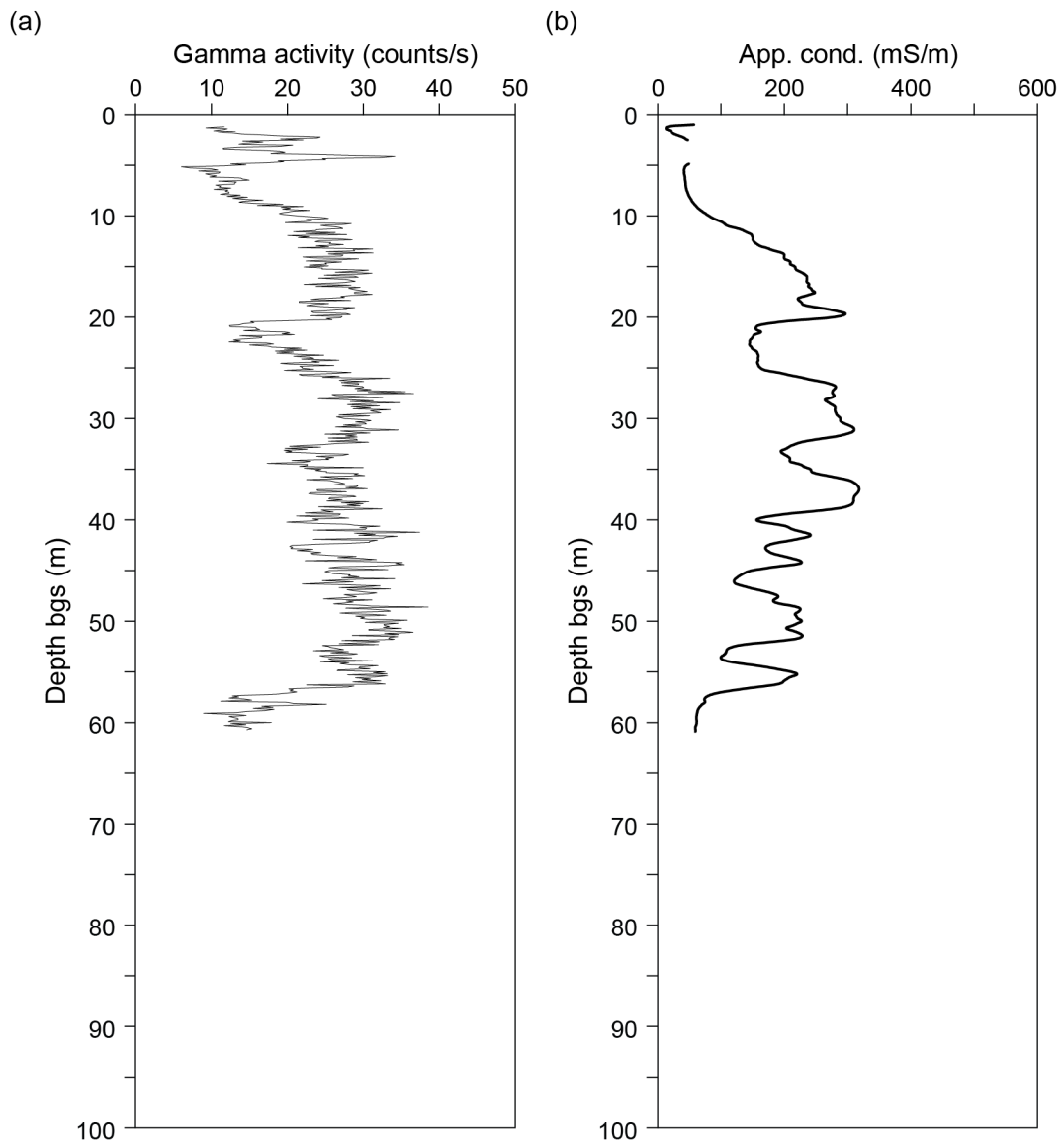


Figure A12. Natural gamma and apparent conductivity logs from water well PH12 (fig. 13). The well was logged on April 26, 2017.

PH13
Elevation: 3.24 m NAVD88 (BEG 2016 lidar survey)
Lat. 28.44271° N; Lon. 96.46067° W

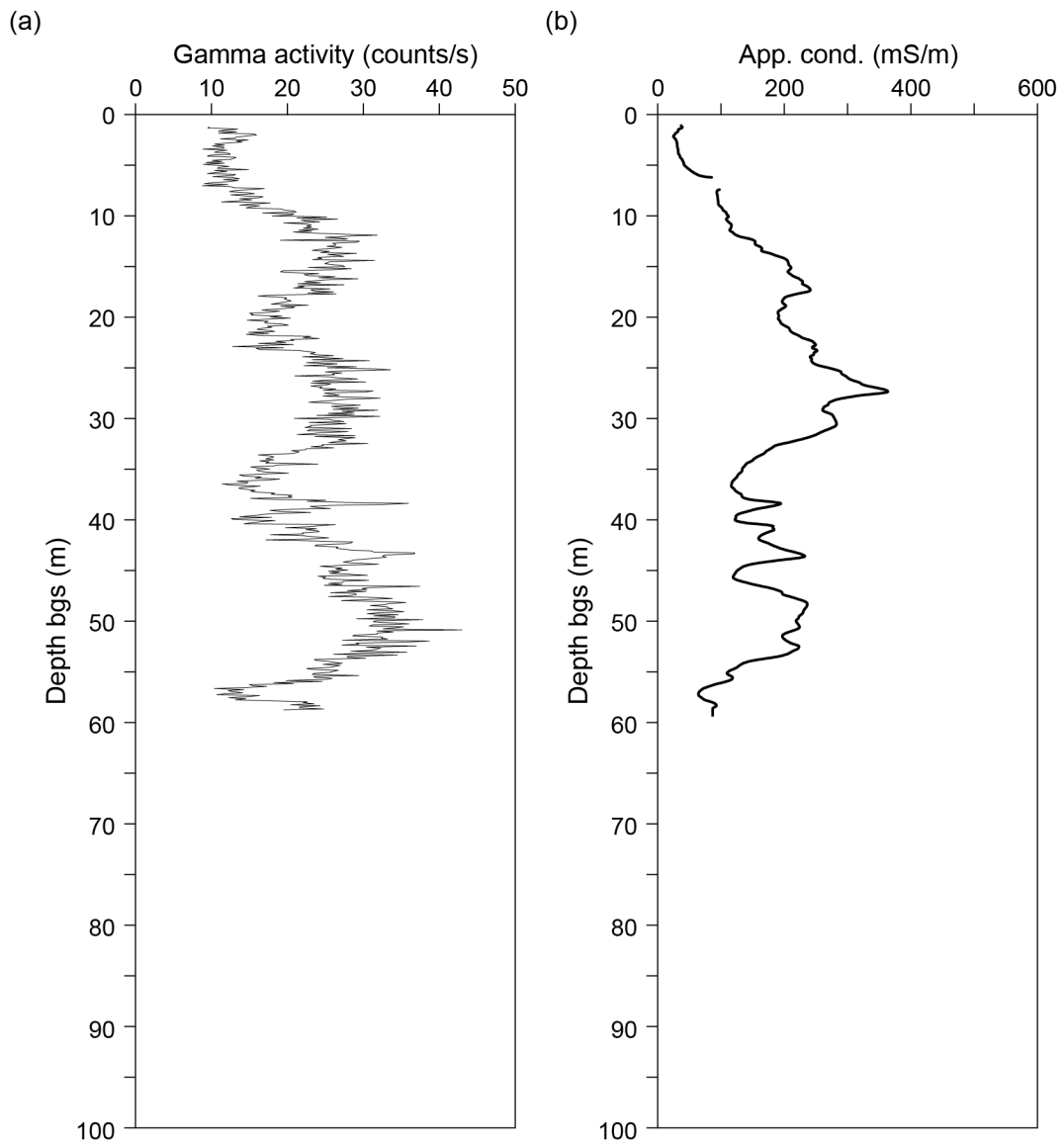


Figure A13. Natural gamma and apparent conductivity logs from water well PH13 (fig. 13). The well was logged on April 26, 2017.

PH14
Elevation: 3.64 m NAVD88 (BEG 2016 lidar survey)
Lat. 28.44611° N; Lon. 96.46095° W

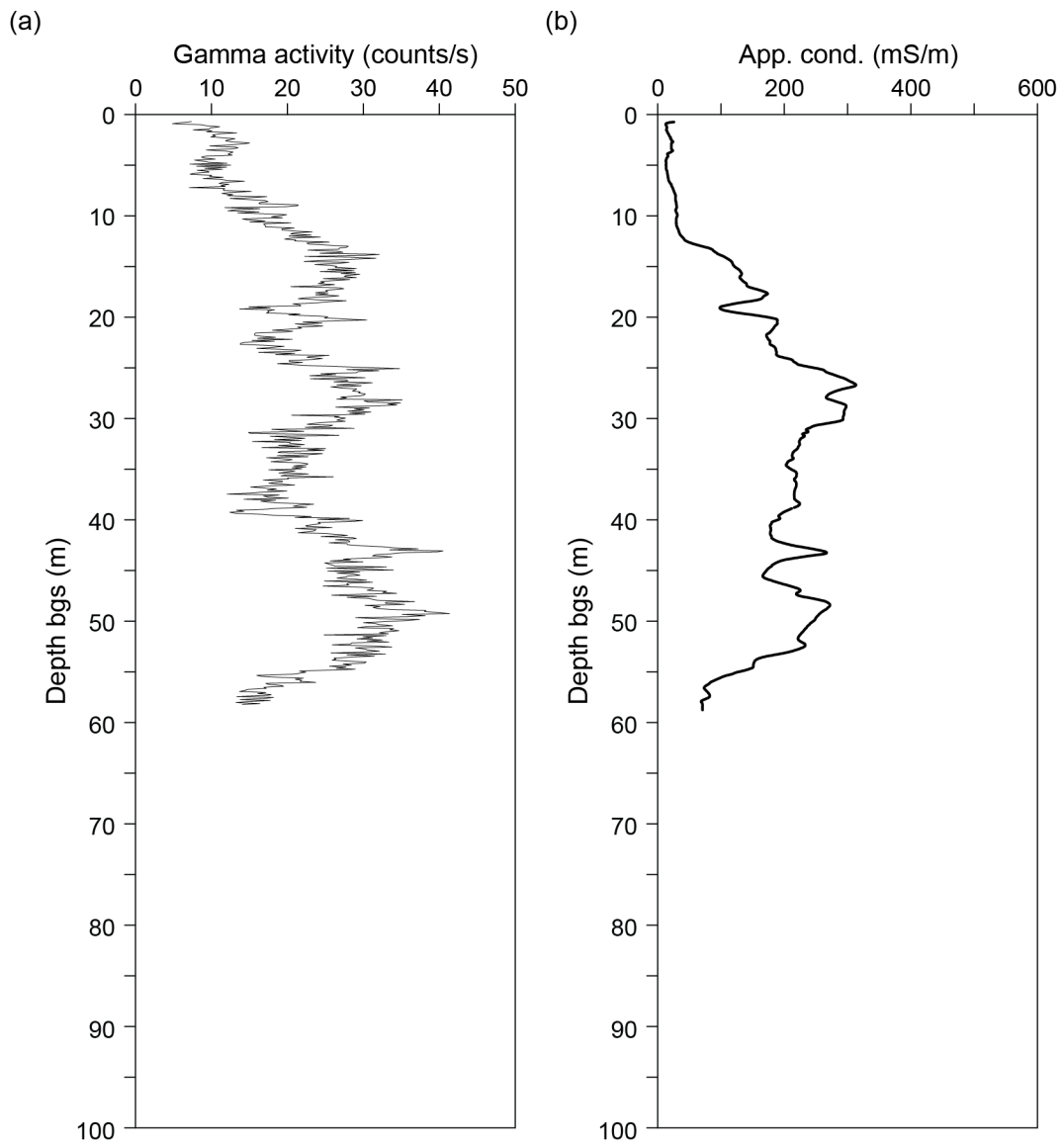


Figure A14. Natural gamma and apparent conductivity logs from water well PH14 (fig. 13). The well was logged on April 26, 2017.

PH15
Elevation: 2.61 m NAVD88 (BEG 2016 lidar survey)
Lat. 28.50143° N; Lon. 96.47635° W

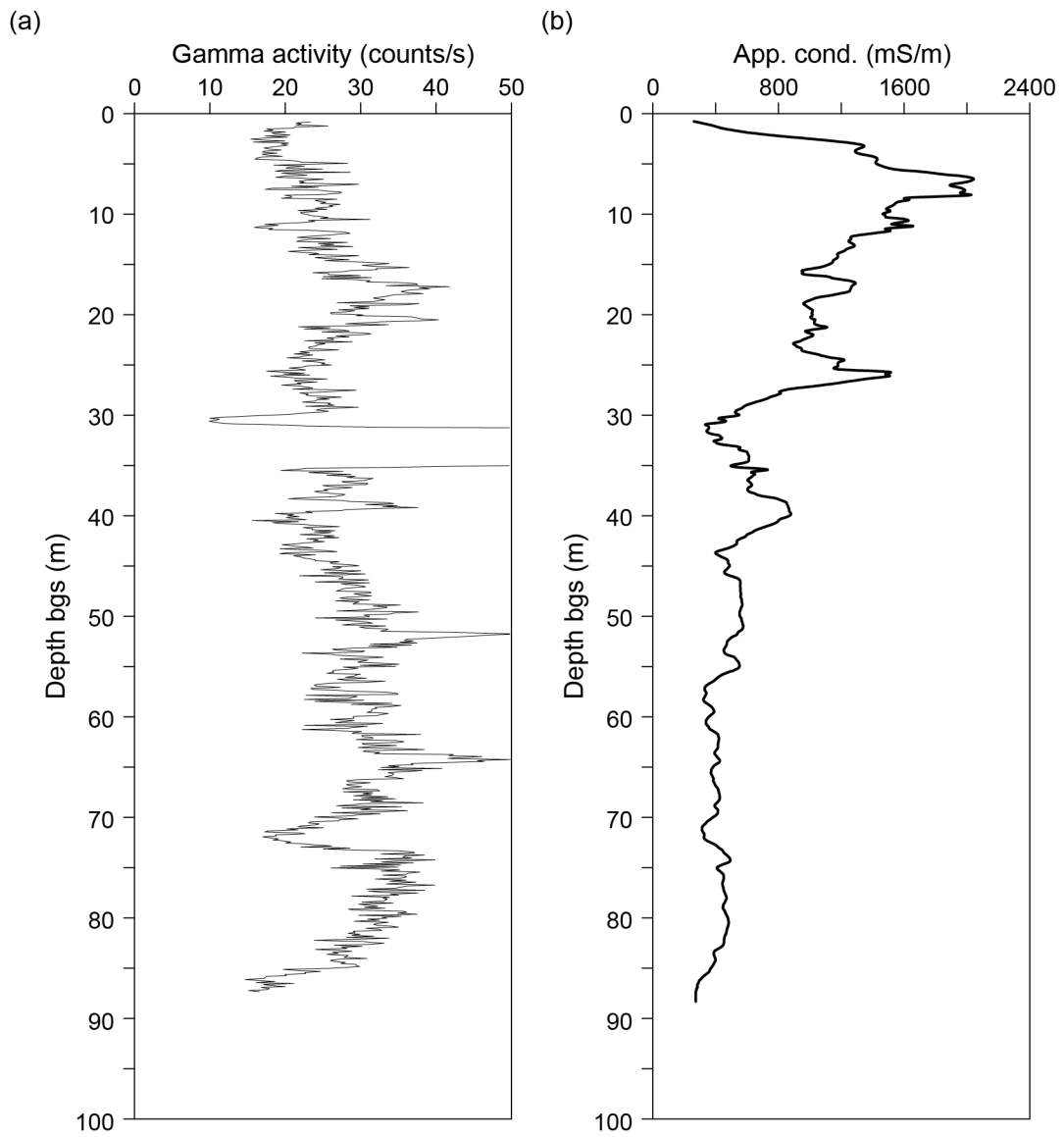


Figure A15. Natural gamma and apparent conductivity logs from water well PH15 (fig. 13). The well was logged on April 27, 2017.

PH16
Elevation: 1.15 m NAVD88 (BEG 2016 lidar survey)
Lat. 28.47553° N; Lon. 96.51126° W

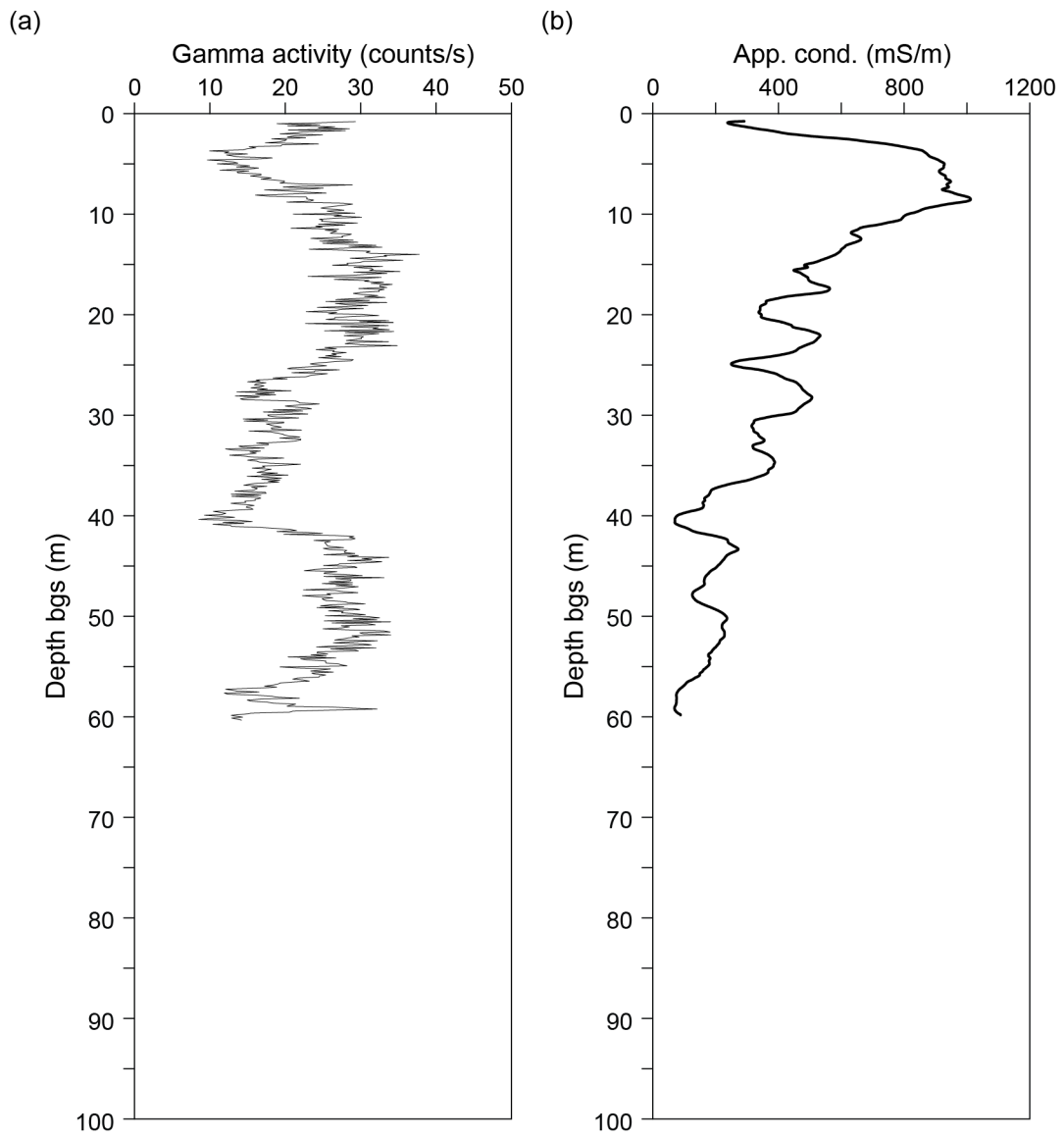


Figure A16. Natural gamma and apparent conductivity logs from water well PH16 (fig. 13). The well was logged on April 27, 2017.

PH17
Elevation: 2.51 m NAVD88 (BEG 2016 lidar survey)
Lat. 28.45815° N; Lon. 96.52424° W

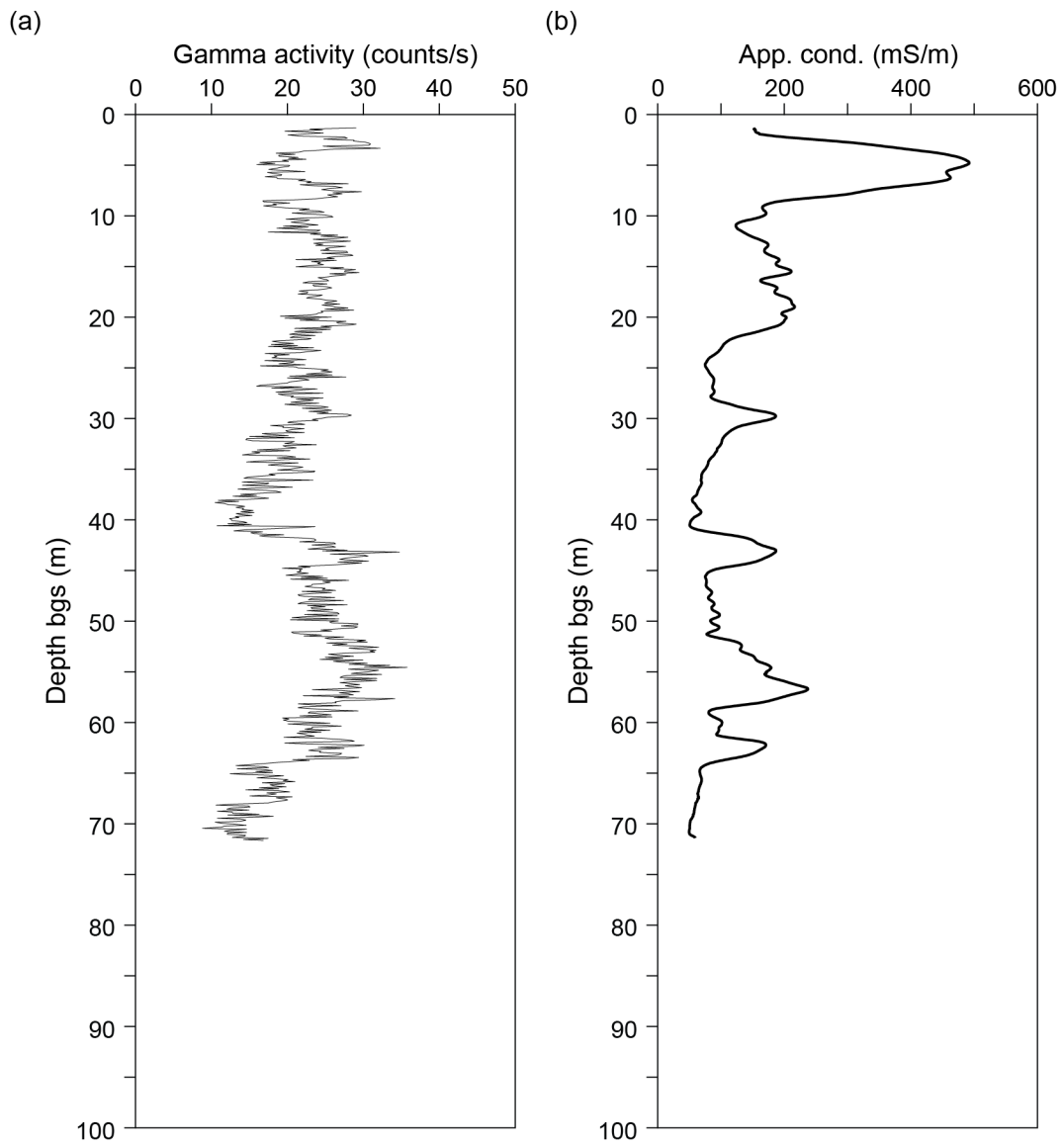


Figure A17. Natural gamma and apparent conductivity logs from water well PH17 (fig. 13). The well was logged on May 14 and 15, 2018.

PH18
Elevation: 1.61 m NAVD88 (BEG 2016 lidar survey)
Lat. 28.47479° N; Lon. 96.51703° W

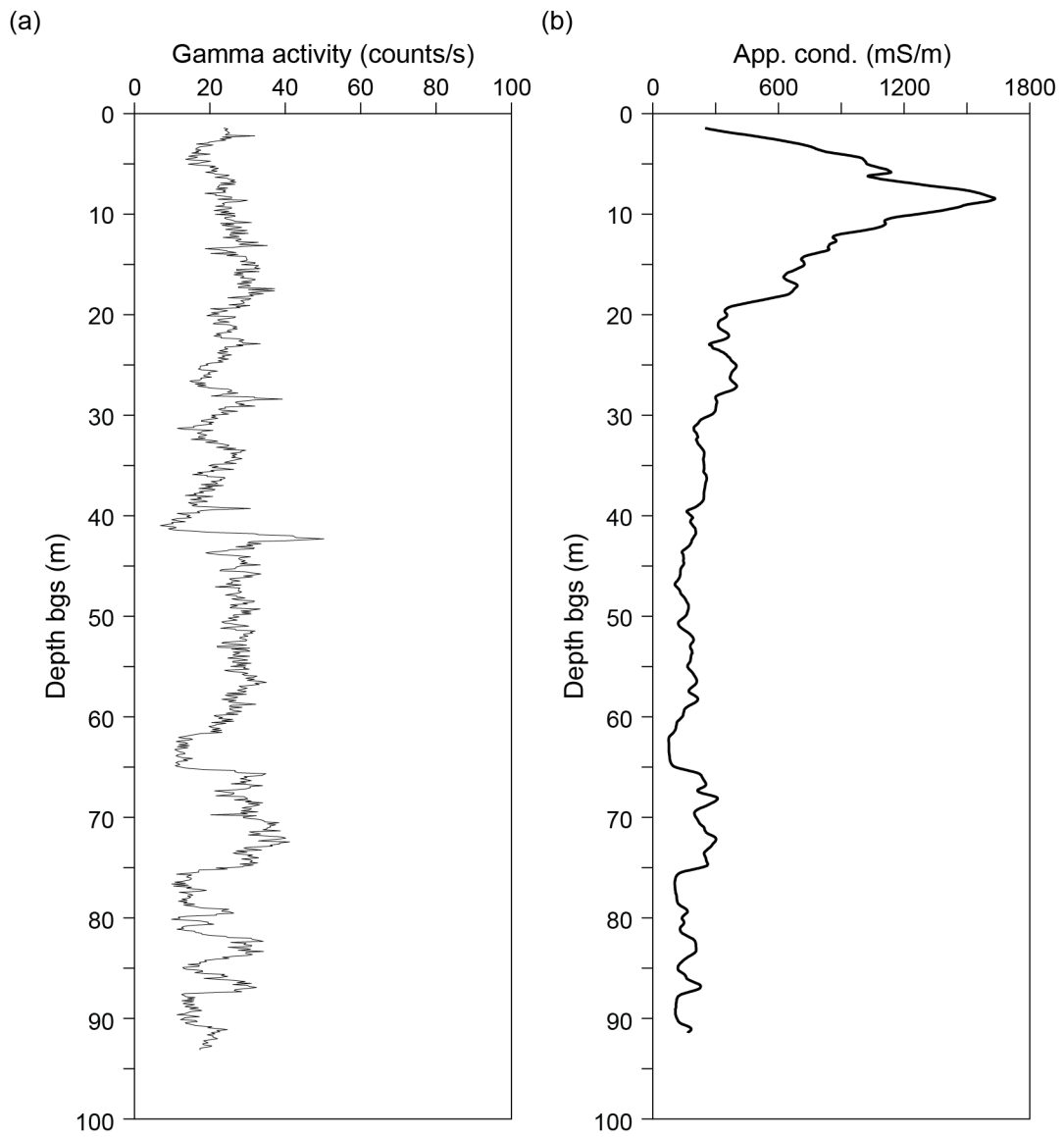


Figure A18. Natural gamma and apparent conductivity logs from water well PH18 (fig. 13). The well was logged on May 15, 2018.

PH19
Elevation: 2.26 m NAVD88 (BEG 2016 lidar survey)
Lat. 28.49593° N; Lon. 96.49339° W

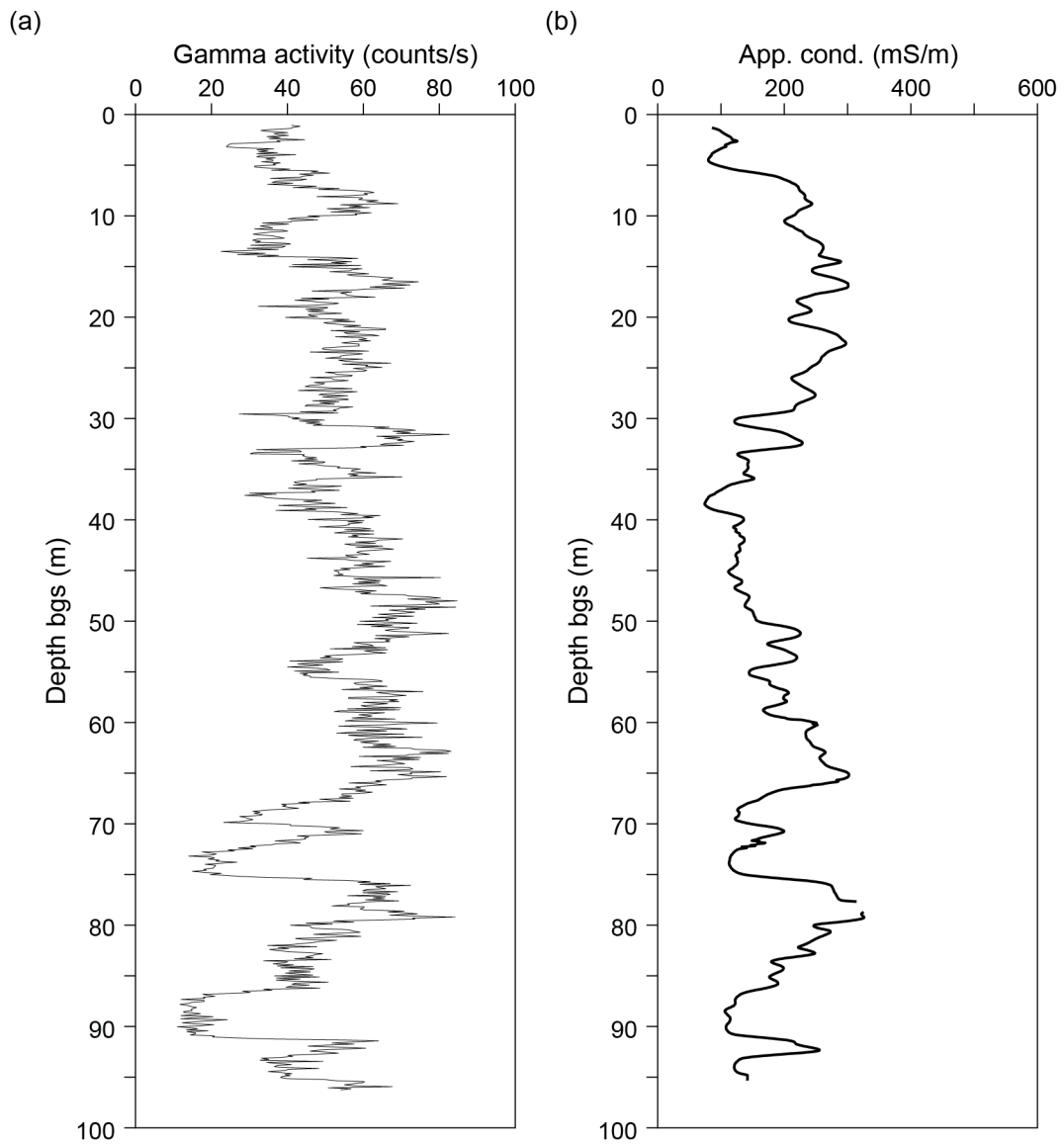


Figure A19. Natural gamma and apparent conductivity logs from water well PH19 (fig. 13). The well was logged on May 15 and 17, 2018.

Appendix B: Time-domain Electromagnetic Induction Soundings

Time-domain electromagnetic sounding locations on and near Powderhorn Ranch (fig. 13). All soundings were acquired using a WalkTEM instrument, a square or circular transmitter loop with a 160-m perimeter length, high- and low-moment transmitter pulses, and low-frequency (RC-200) and high-frequency (RC-5) receiver antennas located at the center of the transmitter loop. Locations of the center of the loop were determined using a GPS receiver. Elevations were extracted at the center of the sounding from the high-resolution DEM (fig. 3) constructed from the 2016 BEG airborne lidar survey of Powderhorn Ranch. TDEM sounding data were processed using SPIA software (Aarhus University) to produce best-fit conductivity profiles (figs. B1 through B8).

Sounding	Date (YYYYMMDD)	Longitude (deg. W)	Latitude (deg. N)	Elevation (m)	Transmitter loop type	Transmitter area (m²)
POC-01	20151111	96.46443	28.49616	2.7	square	1600
POC-02	20151111	96.47218	28.49620	2.6	square	1600
POC-03	20151112	96.46909	28.46604	4.4	square	1600
POC-04	20160404	96.45416	28.43469	4.1	square	1600
POC-05	20160405	96.49403	28.46701	2.8	square	1600
POC-06	20160405	96.49656	28.43101	3.0	square	1600
POC-07	20160405	96.47753	28.44645	4.0	square	1600
SNE-03	20170125	96.53859	28.43158	3.9	circle	2037

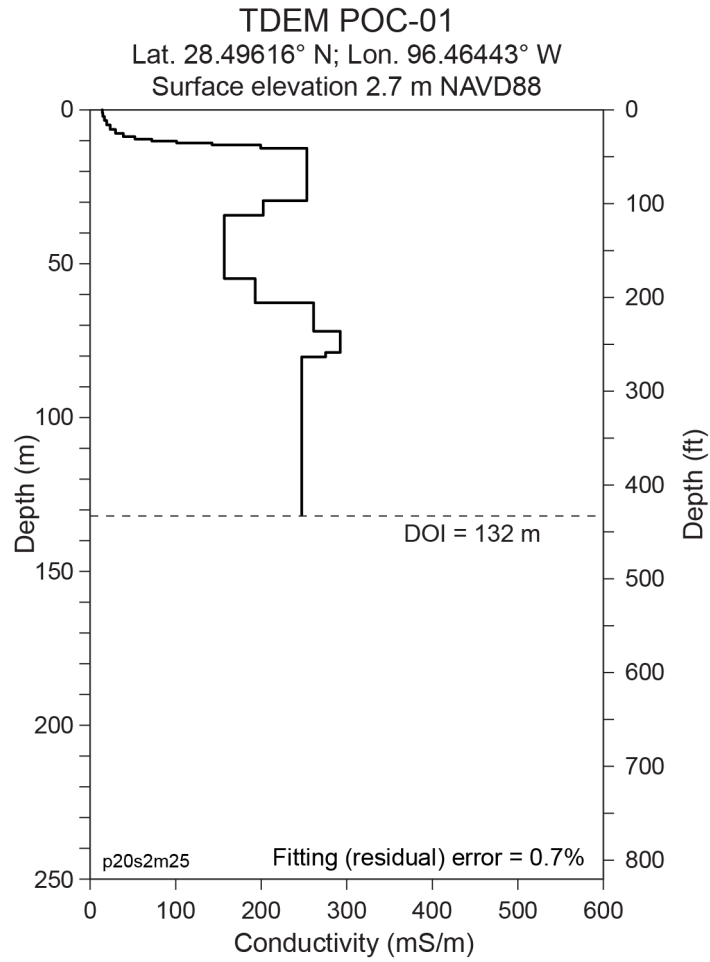


Figure B1. Subsurface electrical conductivity model constructed from time-domain electromagnetic induction (TDEM) sounding POC-01 (fig. 13).

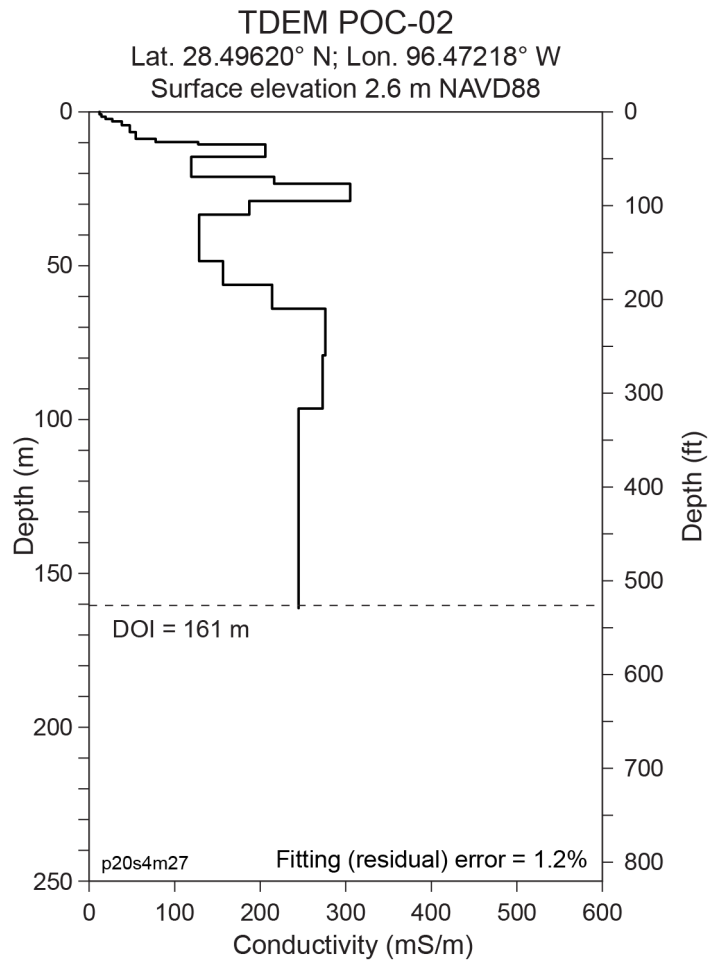


Figure B2. Subsurface electrical conductivity model constructed from TDEM sounding POC-02 (fig. 13).

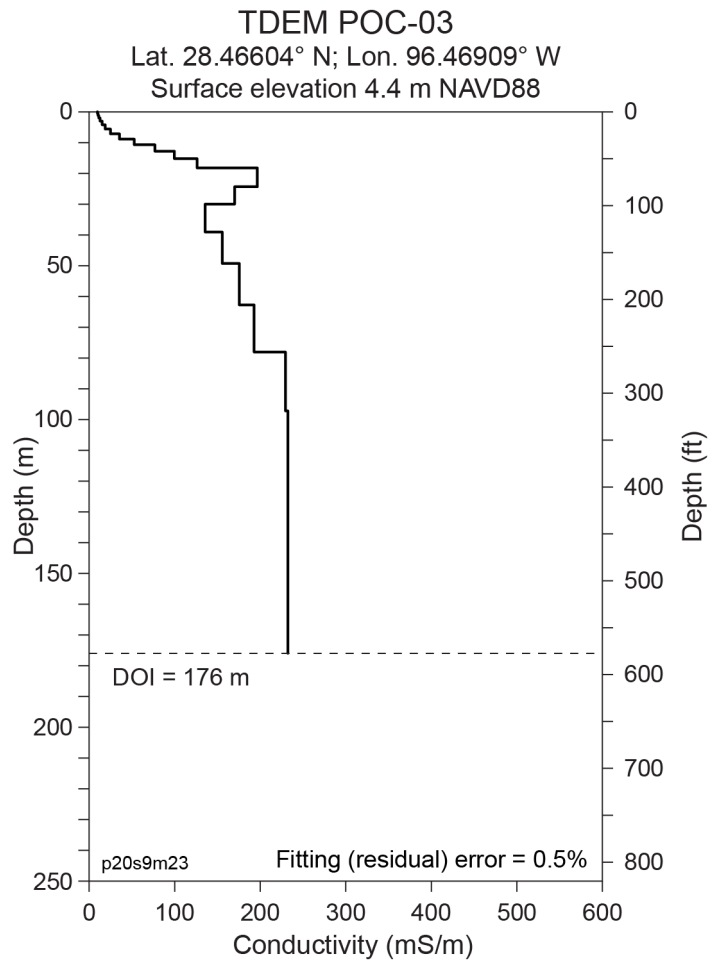


Figure B3. Subsurface electrical conductivity model constructed from TDEM sounding POC-03 (fig. 13).

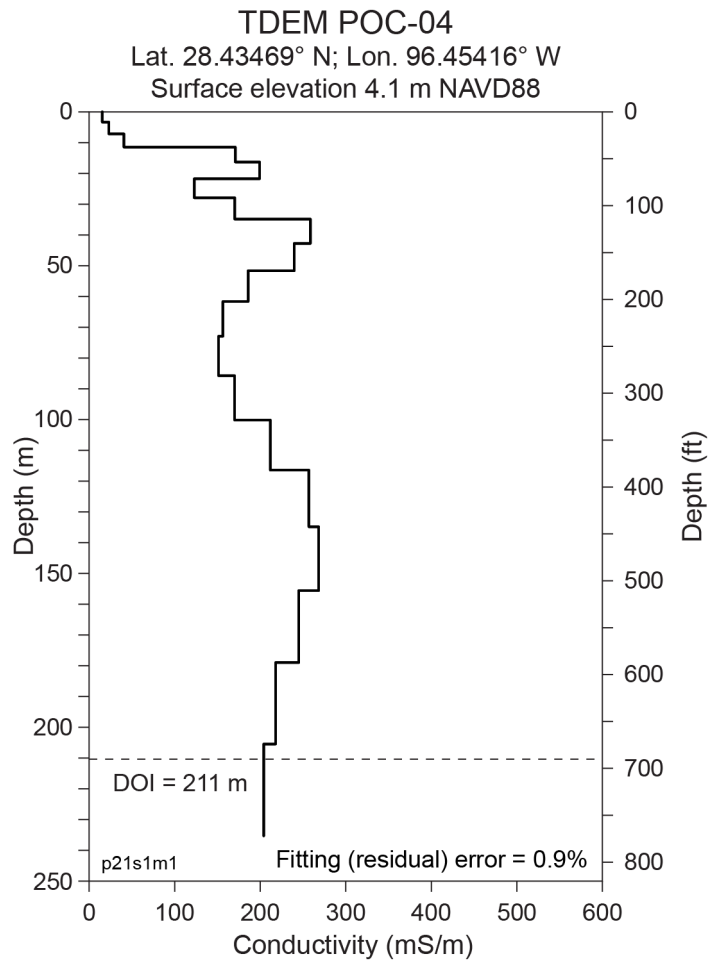


Figure B4. Subsurface electrical conductivity model constructed from TDEM sounding POC-04 (fig. 13).

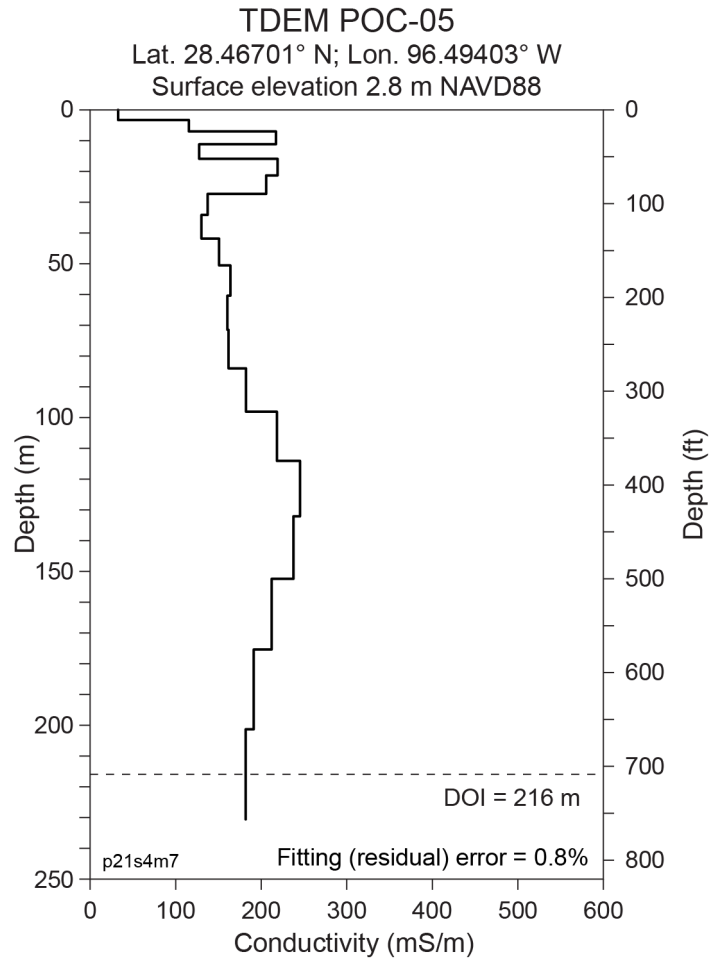


Figure B5. Subsurface electrical conductivity model constructed from TDEM sounding POC-05 (fig. 13).

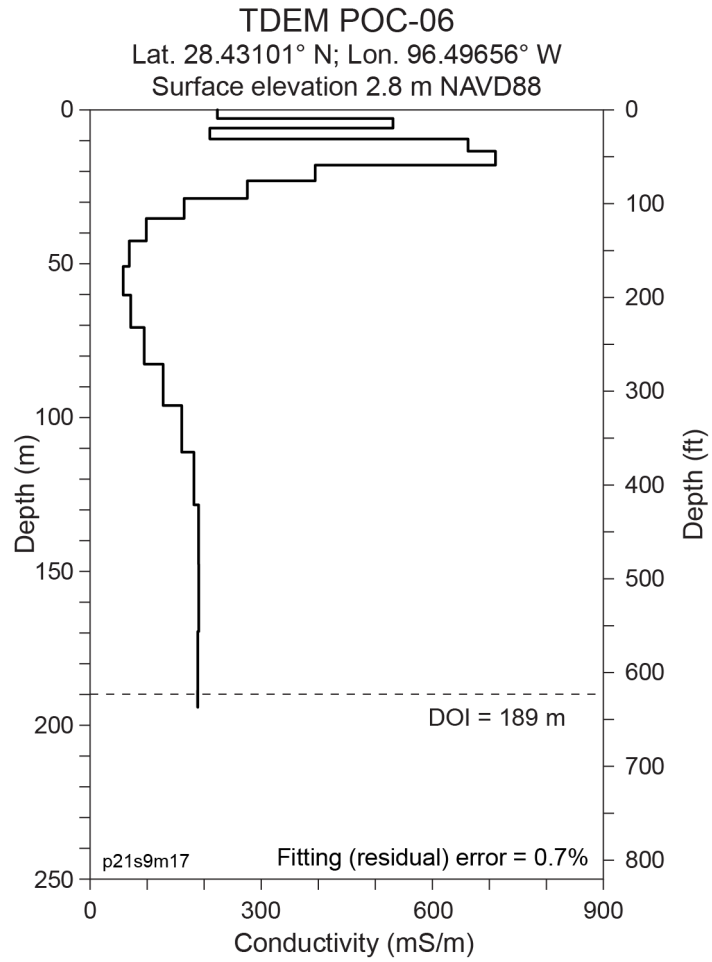


Figure B6. Subsurface electrical conductivity model constructed from TDEM sounding POC-06 (fig. 13).

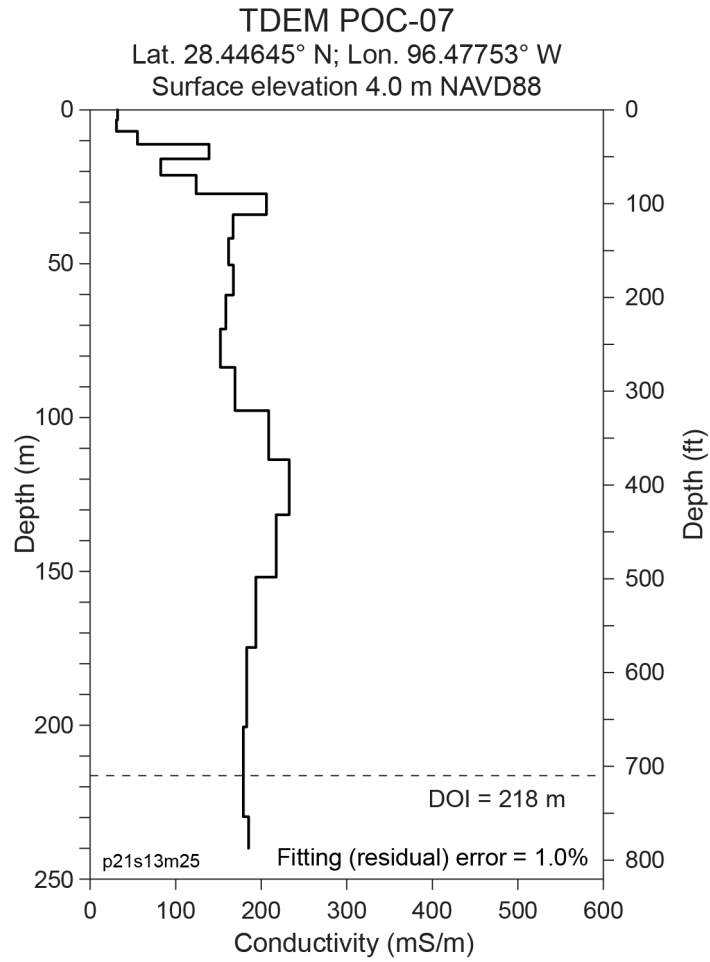


Figure B7. Subsurface electrical conductivity model constructed from TDEM sounding POC-07 (fig. 13).

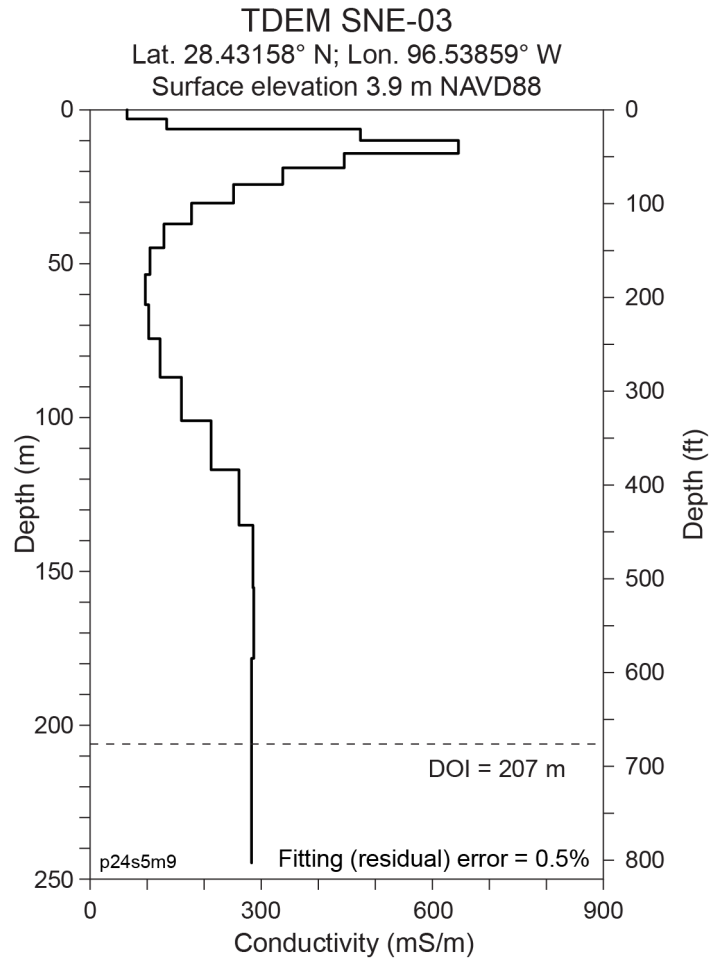


Figure B8. Subsurface electrical conductivity model constructed from TDEM sounding SNE-03 (fig. 13).